UNIVERSITÉ DU QUÉBEC À RIMOUSKI

VARIATIONS DE HAUTE FRÉQUENCE DU CHAMP MAGNÉTIQUE TERRESTRE AU COURS DE L'HOLOCÈNE DANS L'EST ET L'ARCTIQUE CANADIEN

Thèse présentée

dans le cadre du programme de doctorat en océanographie

en vue de l'obtention du grade de docteur ès sciences

PAR

© FRANCESCO BARLETTA

Juillet 2010

UNIVERSITÉ DU QUÉBEC À RIMOUSKI
Service de la bibliothèque

Avertissement

La diffusion de ce mémoire ou de cette thèse se fait dans le respect des droits de son auteur, qui a signé le formulaire « *Autorisation de reproduire et de diffuser un rapport, un mémoire ou une thèse* ». En signant ce formulaire, l'auteur concède à l'Université du Québec à Rimouski une licence non exclusive d'utilisation et de publication de la totalité ou d'une partie importante de son travail de recherche pour des fins pédagogiques et non commerciales. Plus précisément, l'auteur autorise l'Université du Québec à Rimouski à reproduire, diffuser, prêter, distribuer ou vendre des copies de son travail de recherche à des fins non commerciales sur quelque support que ce soit, y compris l'Internet. Cette licence et cette autorisation n'entraînent pas une renonciation de la part de l'auteur à ses droits moraux ni à ses droits de propriété intellectuelle. Sauf entente contraire, l'auteur conserve la liberté de diffuser et de commercialiser ou non ce travail dont il possède un exemplaire.

Dans l'ensemble, si varié, des sciences géophysiques, le champ magnétique terrestre tient une grande place, tant par son importance propre que par ses relations qu'il présente avec beaucoup des phénomènes physiques du Globe, intérieur et extérieur, et du Soleil. Pourtant, ce géant est presque ignoré du public cultivé qui ne connaît de lui et, encore, assez mal, que son action directrice sur la boussole; ce manque de considération va d'ailleurs jusqu'aux physiciens du magnétisme eux-mêmes, qui ne lui accordent le plus souvent qu'une place de pauvre dans leur cours ou dans leurs traités.

Émile Thellier (1904-1987)

«Da un punto di vista intellettuale, e anche morale, è un brutto segno in un giovane se si trova subito a proprio agio nel traffico delle relazioni umane, e se vi si sente a casa sua, come se avesse fatto un tirocinio preventivo: questo è sintomo di volgarità. Invece, in quest'ambito, un comportamento perplesso, interdetto, maldestro e bizzarro, è segno di indole nobile».

Arthur Schopenhauer (1788-1860)

REMERCIEMENTS

Je remercie tout d'abord mon épouse Lise, mes enfants, Jérôme et Rebecca ainsi que toute ma famille de l'Italie, ma belle-famille et les amis pour leur soutien pendant tout le déroulement du doctorat. Je remercie également mon directeur de thèse le Dr. Guillaume St-Onge, Jacques « Bouton » Labrie et les collaborateurs Dr. James E.T. Channell, Dr. Joseph Stoner, Dr. Stephanie Brachfeld, Dr. André Rochon, Dr. Anne de Vernal et le Dr. Claude Hillaire-Marcel. Un merci au GEOTOP, l'ISMER et la Fondation canadienne pour les sciences du climat et de l'atmosphère (FCSCA) pour le soutien financier. Je remercie les membres de l'INGV : Leonardo Sagnotti, Jaume Dinarès-Turrell, Fabio Speranza, Aldo Winkler et le prof. Pietro Dominici. Je suis très reconnaissant au Prof. Jean-Claude Brêthes pour son aide et ses conseils.

RÉSUMÉ

Plusieurs séquences sédimentaires marines ont été prélevées pendant les missions CASES (*Canadian Arctic Shelf Exchange Study*) en 2004 et HOTRAX (*Healy-Oden Trans-Arctic Expedition*) en 2005 dans les mers de Beaufort et Chukchi respectivement, ainsi que pendant la mission du N/R Coriolis II dans l'estuaire maritime et le golfe du St-Laurent afin 1) de déterminer le comportement du champ magnétique terrestre (CMT) pendant l'Holocène dans l'ouest de l'Arctique canadien et l'est du Canada, 2) d'évaluer les forces et les faiblesses des nouveaux modèles numériques du CMT au cours de l'Holocène et 3) d'explorer la possibilité d'utiliser ces modèles pour dater des séquences sédimentaires prélevées dans l'Arctique canadien.

Les séquences sédimentaires prélevées dans les mers de Beaufort et de Chukchi ont permis de reconstruire les variations d'intensité et d'orientation de haute résolution du champ magnétique terrestre couvrant la quasi-totalité des dernières 10 000 ans. Au cours de l'Holocène, la déclinaison et l'inclinaison magnétique des deux séquences étudiées peuvent être corrélées entre elles, avec des enregistrements paléomagnétiques lacustres ou volcaniques de l'ouest de l'Amérique du Nord à des échelles de temps au moins séculaires. Les variations de paléointensité relative des deux carottes analysées sont également cohérentes avec des enregistrements des variations du dipôle géomagnétique, confirmant ainsi l'origine géomagnétique de ces variations et suggérant leur nature dipolaire.

En ce qui concerne l'Est canadien (estuaire et golfe du St-Laurent), nous avons fourni une première compilation paléomagnétique (*paleomagnetic stack*) à l'Holocène en utilisant les données paléomagnétiques provenant de six séquences sédimentaires marines précédemment datées à l'aide de la méthode de datation au radiocarbone (^{14}C). Au cours de l'Holocène, l'inclinaison et la déclinaison magnétique peuvent être corrélées, à des échelles au moins séculaires, à des enregistrements lacustres ou volcaniques de l'Amérique du Nord ainsi que de l'Islande et l'Europe du Nord suggérant une origine géomagnétique à l'échelle hémisphérique. Par ailleurs, les variations de la paléointensité relative de l'Est canadien sont similaires aux variations dipolaires du CMT dérivées à partir d'enregistrements de paléointensité absolue et indiquent ainsi la prédominance des variations dipolaires au cours des derniers 10 000 ans en Amérique du Nord.

Les estimations fournies grâce au modèle en harmonique sphérique CALS7k.2 (*Continuous Archeomagnetic and Lake Sediment 7k years model, version 2*) se sont révélées assez satisfaisantes en ce qui concerne la reproduction des courbes de déclinaison et d'inclinaison magnétique dans les deux régions d'étude au cours des derniers ~7000 ans. Cependant, les estimations de la paléointensité locale produite par le modèle CALS7k.2 semblent être moins précises par rapport aux estimations de paléodirection. En effet, la banque de données de paléointensité utilisée pour construire le modèle est fortement concentrée dans les régions de l'Europe où le nombre d'artéfacts (*e.g.*, céramiques, poterie etc.) est plus élevé. Par conséquent, les estimations de paléointensité en Amérique du Nord seraient fortement affectées par la distribution spatiale hétérogène de la banque de données et par les hypothèses à la base de la procédure d'inversion utilisée pour construire le modèle.

ABSTRACT

Several long sedimentary sequences were recovered from the Beaufort and Chukchi Seas as part of the CASES (Canadian Arctic Shelf Exchange Study) and HOTRAX (Healy-Oden Trans-Arctic Expedition) programs in 2004 and 2005, respectively as well as with the R/V *Coriolis II* from the St. Lawrence Estuary and Gulf in order to 1) reconstruct changes in Earth's magnetic field during the Holocene in the Western Canadian Arctic and Eastern Canada, 2) determine the strengths and the weaknesses of the recent Holocene numerical models of the geomagnetic field and 3) explore the possibility of using these models as a new dating tool for sedimentary sequences from the Canadian Arctic.

Two sedimentary sequences from the Western Canadian Arctic provided changes in both direction and intensity of the geomagnetic field during the last 10 000 years. Several centennial- to millennial-scale Holocene declination and inclination features can be correlated in both cores, with other high-resolution western North American lacustrine and volcanic paleomagnetic records and with records of changes in Earth's dipole moment, supporting the geomagnetic origin of these features and implying that they are associated with changes in Earth's dipole moment.

Regarding Eastern Canada, a new high-resolution Holocene paleomagnetic secular variation (PSV) and relative paleointensity (RPI) stack was constructed using u-channel paleomagnetic data from six radiocarbon-constrained marine sedimentary sequences raised along the main axis of the Laurentian Channel. Centennial- to millennial-scale declination and inclination features of the eastern Canadian stack can be correlated, within the dating uncertainties, with other Holocene North American, Icelandic and European PSV records, suggesting a common geomagnetic origin possibly hemispheric in character.

Both magnetic inclination and declination data from the two analyzed geographical regions are consistent with the time-varying spherical harmonic model of the geomagnetic field CALS7k.2 (Continuous Archeomagnetic and Lake Sediment 7k years model, version 2) during the last ~7000 years. In addition, the eastern Canadian Holocene RPI stack reveals similar millennial and even centennial time-scale variations consistent with some virtual axial dipole moment (VADM) reconstructions derived from absolute paleointensity data as well as with North American lacustrine RPI records. Accordingly, these results suggest that the Holocene paleomagnetic secular variation in North America is significantly driven by large-scale (> 5000 km) geomagnetic field changes at these timescales.

Nevertheless, significant discrepancies exist between the millennial-scale RPI reconstructions and the local magnetic induction field as expected from the CALS7k.2 model. These differences are likely due to the heterogeneous spatial distribution of the actual paleointensity database used to constrain the CALS7k.2 model, as well as with the inversion procedure used to fit the model with the background dataset.

TABLE DES MATIÈRES

LISTE DES TABLEAUX

LISTE DES FIGURES

LISTE DES ABRÉVIATIONS

CODE	SIGNIFICATION
AD	*Anno Domini*
AF	Alternative Field
AGM	Alternating Gradient Magnetometer
AMS	Accelerator Mass Spectrometry
ARM	Anhysteretic Remanent Magnetization
BP	Before Present
Cal BP	Calendar Year Before Present
CALS7k	Continuous Archeomagnetic and Lake Sediment 7k years model
CASES	Canadian Arctic Shelf Exchange Study
CAT-scan	Computerized Axial Tomography
ChRM	Characteristic Remanent Magnetization
CMT	Champ Magnétique Terrestre
DC	Direct Current
Dec	(Magnetic) Declination
DM	Dipole Moment
FENNOSTACK	Inclination and Declination data Stacks for Fennoscandia
GAD	Geocentric Axial Dipole
Hc	Coercive Force
Hcr	Coercivity of Remanence
HOTRAX	Healy-Oden Trans-Arctic Expedition
Inc	(Magnetic) Inclination
IRM	Isothermal Remanent Magnetization
k_{ARM}	Anhysteretic Susceptibility
k_{LF}	Low-field Magnetic Susceptibility
MAD	Maximum Angular Deviation
MD	Multi Domain
MDF	Median Destructive Field
Mrs	Remanence Saturation
Ms	Magnetization Saturation
MSCL	Multi Sensor Core Logger
NRM	Natural Remanent Magnetization
PC	Piston Core
PCA	Principal Component Analysis
PNM	Pôle Nord Magnétique
PSD	Pseudo Single Domain
PSV	Paleomagnetic Secular Variation
PSVL	Paleomagnetic Secular Variation from Lava Flows
RPI	Relative Paleointensity Proxy
SD	Single Domain
SIRM	Saturation Isothermal Remanent Magnetization
TWC	Trigger Weight Core
VADM	Virtual Axial Dipole Moment
VPDB	Vienna Pee-Dee Belemnite

INTRODUCTION GÉNÉRALE

Le champ magnétique terrestre (CMT) a été le premier des champs physiques à être décrit en 1600 par W. Gilbert (*e.g.*, Stern, 2002). Aujourd'hui, nous savons que l'origine de la partie fondamentale du CMT est liée aux processus magnétohydrodynamiques qui ont lieu dans le noyau externe terrestre (*e.g.*, Merrill *et al.*, 1996). Une contribution essentielle aux connaissances actuelles sur le magnétisme terrestre a été fournie grâce aux mesures directes effectuées depuis les quatre derniers siècles (la variation séculaire historique; *e.g.*, Jackson *et al.*, 2000) et le vertigineux développement de la science du paléomagnétisme depuis les années soixante. Il est maintenant bien établi que le CMT d'origine interne peut varier à des échelles temporelles allant de quelques années jusqu'à l'âge de la Terre (*e.g.*, Merrill *et al.*, 1996). Notamment, les variations d'orientation et de paléointensité du CMT obtenues à partir de l'aimantation rémanente naturelle des sédiments ont été primordiales pour fournir une preuve irréfutable des inversions de polarité magnétique du CMT au cours des derniers 160 millions d'années (Merrill *et al.*, 1996). Malgré le fait que ce dernier phénomène soit actuellement bien établi à l'échelle globale, très peu d'information existe sur la variabilité spatio-temporelle du CMT durant les périodes de polarité constante. Par exemple, si nous focalisons sur la période de l'Holocène, la plupart des enregistrements paléomagnétiques proviennent de lacs en milieu continental (*e.g.*, Korte *et al.*, 2005a). En Amérique du Nord, des études paléomagnétiques ont montré une dérive occidentale (*westward drift*) des composantes angulaires (*e.g.*, Creer, 1981; Verosub *et al.*, 1986) au cours de la plupart de l'Holocène souvent associée au déplacement des sources non-dipolaires du CMT localisées à l'interface noyau-manteau. Par contre, Lund (1996) en analysant la variation séculaire paléomagnétique an

Amérique du Nord au cours derniers 12000 ans n'a pas observé cette dérive occidentale mettant en doute ces premiers résultats. En effet, selon des études successives, les différences observées dans les enregistrements paléomagnétiques lacustres en Amérique du Nord serait plutôt dues aux incertitudes de la chronologie basée sur la datation au radiocarbone (^{14}C) de sédiment brut qu'à une possible origine géomagnétique (Hagstrum et Champion, 2002; St-Onge *et al.*, 2003). Par ailleurs, la rareté de données de haute résolution de paléointensité a été un autre facteur limitant d'une description complète du comportement du CMT en Amérique du Nord au cours de l'Holocène. De plus, des modèles numériques récents du CMT à l'Holocène (Korte et Constable, 2006) suggèrent des variations séculaires du dipôle géomagnétique. Cette hypothèse pourrait avoir des répercussions importantes pour les reconstructions de l'activité solaire à partir des données de taux de production des isotopes cosmogéniques tels que le ^{14}C et ^{10}Be (*e.g.*, St-Onge *et al.*, 2003; Snowball et Muscheler, 2007) ainsi que, selon des théories récentes, d'une possible influence directe des fluctuations séculaires du CMT sur le climat (*e.g.*, Usoskin et Kovaltsov, 2008). Également, si les informations concernant le comportement du CMT au cours de l'Holocène en Amérique du Nord sont assez fragmentaires aucune information n'est actuellement disponible pour l'Arctique canadien. Par exemple, aucun des enregistrements contenus dans la banque de données des modèles en harmoniques sphériques du CMT en Amérique du Nord ne dépasse la latitude de 51° N (Korte *et al.*, 2005a). La question à propos de la validité de ces modèles mathématiques dans la région de l'Arctique canadien demeure ainsi ouverte. Notamment, l'efficacité de ces modèles, si démontrée, pourrait aider à la datation de sédiments arctiques holocène à travers la technique de la datation paléomagnétique. En fait, la technique traditionnelle de datation

au radiocarbone s'est révélée assez limitée dans ces régions à cause de la rareté et des problèmes de préservation du matériel pour la datation (*e.g.*, Ledu *et al.*, 2008). Par ailleurs, une autre difficulté est liée à la correction des âges radiocarbones due à la variabilité spatio-temporelle de l'effet de réservoir régional (ΔR) qui est souvent inconnu dans les régions arctiques (*e.g.*, Darby *et al.*, 2009).

Or, dans cette thèse de doctorat, nous toucherons en partie les sujets précédemment exposés. Particulièrement, nous tenterons de répondre aux trois questions fondamentales suivantes : 1) quel a été le comportement du CMT pendant l'Holocène dans l'Ouest de l'Arctique canadien et l'Est du Canada ? 2) Les modèles numériques du CMT reproduisent-ils les variations séculaires à millénaires du CMT ? 3) Est-il possible d'utiliser les modèles numériques récents en harmoniques sphériques du CMT pour dater des séquences sédimentaires prélevées dans l'Arctique canadien ?

Pour répondre à ces questions, nous utiliserons plusieurs séquences sédimentaires marines prélevées pendant les missions *Canadian Arctic Shelf Exchange Study* (CASES) en 2004 et *Healy-Oden Trans-Arctic Expedition* (HOTRAX) en 2005 dans les mers de Beaufort et Chukchi respectivement (Tableau 1), ainsi que celles recueillies pendant la mission du N/R Coriolis II dans l'estuaire maritime et le golfe du St-Laurent (Est canadien; Tableau 2).

Cette thèse est rédigée en anglais sous forme d'articles scientifiques. Ces articles suivent la forme exigée par les revues scientifiques dans lesquelles les articles ont été soumis. Mis à part le premier article qui a déjà été publié en 2008, les deux autres ont été acceptés pour publication avec les titres suivants :

1) Barletta, F., St-Onge, G., Channell, J.E.T., Rochon, A., Polyak., L., Darby, D.A., 2008. High-resolution paleomagnetic secular variation and relative paleointensity records from the western Canadian Arctic: implication for Holocene stratigraphy and geomagnetic field behaviour. *Canadian Journal of Earth Sciences*, 45, 1265-1281.

2) Barletta, F., St-Onge, G., Stoner, J.S., Lajeunesse, P., Locat, J. (Sous presse). A high-resolution Holocene paleomagnetic secular variation and relative paleointensity stack from eastern Canada. *Earth and Planetary Science Letters*, doi: 10.1016/j.epsl.2010.07.038.

3) Barletta, F., St-Onge, G., Channell, J.E.T., Rochon, A. (Sous presse). Dating of Holocene Western Canadian Arctic sediments by matching paleomagnetic secular variation to a geomagnetic field model. *Quaternary Science Reviews,* doi: 10.1016/j.quascirev.2010.05.35.

Étant le premier auteur de ces trois articles, j'ai rédigé la première version des articles, réalisé la grande partie des analyses, traité et interprété la majorité des données. Les co-auteurs ont notamment joué un rôle essentiel pour la supervision en laboratoire, l'organisation, la préparation et le choix des sites d'échantillonnage des séquences sédimentaires utilisées pour cette thèse ainsi que pour l'acquisition et l'interprétation d'une partie des données concernant la chronostratigraphie et les propriétés physiques des sédiments. Par ailleurs, la combinaison des différentes compétences des co-auteurs a été primordiale durant la révision des articles scientifiques tant au niveau de la forme que du

contenu scientifique. Finalement, trois articles issus de mon travail de doctorat et dont je suis co-auteur ont été publiés dans les revues *Global and Planetary Change* et *Paleoceanography* et ont été inclus dans les références bibliographiques.

CHAPITRE 1

HIGH-RESOLUTION PALEOMAGNETIC SECULAR VARIATION AND RELATIVE PALEOINTENSITY RECORDS FROM THE WESTERN CANADIAN ARCTIC: IMPLICATION FOR HOLOCENE STRATIGRAPHY AND GEOMAGNETIC FIELD BEHAVIOUR

1.1 Abstract

Two piston cores recovered from the Chukchi and the Beaufort Seas document Arctic Holocene geomagnetic field behaviour and highlight the potential of secular variation and relative paleointensity as a regional chronostratigraphic tool. Several centennial- to millennial-scale Holocene declination and inclination features can be correlated in both cores, with other high-resolution western North American lacustrine and volcanic paleomagnetic records and with records of changes in Earth's dipole moment, supporting the geomagnetic origin of these features and implying that they are associated with changes in Earth's dipole moment.

Résumé

Deux carottes sédimentaires prélevées dans les mers de Beaufort et de Chukchi ont permis de reconstruire les variations d'intensité et d'orientation de haute résolution du champ magnétique terrestre au cours de l'Holocène afin de caractériser le comportement du champ géomagnétique dans l'Arctique ainsi que d'explorer la possibilité d'utiliser les variations du champ géomagnétique comme outil chronostratigraphique. Au cours de l'Holocène, la déclinaison et l'inclinaison magnétique des deux séquences étudiées peuvent être corrélées entre elles, avec des enregistrements paléomagnétiques lacustres ou

volcaniques de l'ouest de l'Amérique du Nord à des échelles de temps au moins séculaires. Les variations de paléointensité relative des deux carottes analysées sont également cohérentes avec des enregistrements des variations du dipôle géomagnétique, confirmant ainsi l'origine géomagnétique de ces variations et suggérant leur nature dipolaire.

1.2 Introduction

Our knowledge of historical secular variation in the Arctic is only limited to the last 200 years (Jonkers et al. 2002; Jackson et al. 2000). The Arctic geomagnetic field, as revealed by recent satellite data as well as ground-based measurements, is characterized by secular variation at a much higher rate than for the rest of the Earth (Hulot et al. 2002; Olson and Aurnou 1999). One of the most evident expressions of this behaviour can be seen in changes of the North Magnetic Pole (NMP) position. The first direct reading placed the NMP at Cape Adelaide (Canadian Arctic) in 1831. Successive determinations performed during the last century depicted a clear migration of the NMP towards the Arctic Ocean (Olsen and Mandea 2007). Recent observations from the Resolute Bay geomagnetic observatory (Canada) have detected a strong increase in NMP velocity since the 1970s, from 9 km yr^{-1} to 41 km yr^{-1} and to almost 60 km yr^{-1} in 2003 (Olsen and Mandea 2007), and the rate of change of the intensity has increased from 10 nT yr^{-1} to about 70 nT yr^{-1} during the last 50 years (Geological Survey of Canada, unpublished data). These recent changes suggest that the Arctic may be a vantage point to record rapid changes in Earth's magnetic field behaviour and to help determine the high frequency dynamics of Earth's magnetic field during the Holocene.

Spherical harmonic models of the geomagnetic field, based on global historical measurements, have estimated the position of the NMP over the last 400 yrs (e.g., Jackson et al. 2000), revealing that changes in the NMP position are consistent with the observations of the last century, whereas a new generation of time-varying spherical harmonic models, constrained by Holocene paleomagnetic data, have revealed that the rate of change of the dipole intensity could vary at the centennial timescale (Korte and

Constable 2006). Nevertheless, the lack of directional as well as intensity measurements in the Arctic is an important limitation to accurately assessing if the current accelerated Arctic secular variation is a persistent feature of the geomagnetic field.

The reconstruction of Earth's magnetic field behaviour beyond historical records can be achieved by study of geological materials like volcanic rocks and fired archaeological artefacts (e.g., Hagstrum and Champion 2002; Gallet et al. 2002; Genevey and Gallet 2003). The thermoremanent magnetization acquired by this type of material has the advantage of yielding absolute intensities (e.g., Dunlop and Özdemir 1997). However, due to the nature (lavas or artefacts) of these records, they are not continuous, often of low temporal resolution, and more or less absent in the Arctic. In contrast, the study of well-dated sedimentary sequences has proven to provide reliable, continuous and high resolution records of geomagnetic field variation during the Holocene at high latitudes (e.g., Snowball and Sandgren 2002; St-Onge et al. 2003; Snowball and Sandgren 2004; Snowball et al. 2007; Stoner et al. 2007). In this paper, we present two high resolution continuous Holocene paleomagnetic records from the western Canadian Arctic and discuss the potential of Arctic secular variation (direction and relative paleointensity) as a chronostratigraphic tool and assess geomagnetic field behaviour in the Arctic during the Holocene.

1.3 Geological setting

This study is based on the analysis of sediment cores collected on the slope of the continental shelf of the Chukchi Sea (410 m) and on the Mackenzie Shelf in the Beaufort Sea (218 m) (Fig. 1.1). Holocene postglacial sediments from the western Canadian

continental shelf are characterized by much higher sedimentation rates than in the Arctic central basins (Darby et al. 2006). Since the Bering Strait was flooded by marine waters at about 12 ka, Holocene sedimentation rates in the Hope Valley (southern Chukchi Sea, 53 m) have varied from 60 cm/kyr up to 200 cm/kyr and postglacial sediments are mainly composed of clays and silts (Keigwin et al. 2006).

Similar high sediment accumulation areas are also found on the Mackenzie Shelf. Modern sedimentation rates for the shelf sediments are estimated between 10-300 cm/kyr with higher sedimentation rates in the Mackenzie Trough (water depths comprised between 50 and 500 m; MacDonald et al. 1998). Holocene sediment inputs in the Mackenzie Delta and on the Shelf are mainly derived from the Mackenzie River. Most of the shelf is covered by Holocene marine mud predominantly in the clay-size range (Hill et al. 1991). Similarly, in the upper part of two piston cores collected in the Beaufort Sea and Amundsen Gulf, Scott et al. (2009) described fine-grained sediments with a mean grain size <6 μm, whereas Andrews and Dunhill (2004) described four Holocene sedimentary facies ranging from laminated olive grey mud containing dark grey laminations at the base, to faintly bioturbated mud, and similar but more bioturbated mud with greyish black laminations at the top of a core collected on the Beaufort Sea slope, west of the Mackenzie River delta. This core revealed an average sedimentation rate of 135 cm/kyr during the Holocene (Andrews and Dunhill 2004). Finally, the onset of deglaciation in the Beaufort Sea and Amundsen Gulf was estimated at 12.5 ka by the dating of a sedimentary unit rich in ice rafted debris (Scott et al. 2009). Because of the high sedimentation rates recently observed in cores from both the Chukchi and Beaufort Seas, these two areas thus present a

unique opportunity for the study of centennial- to millennial-scale geomagnetic field variations in the Arctic.

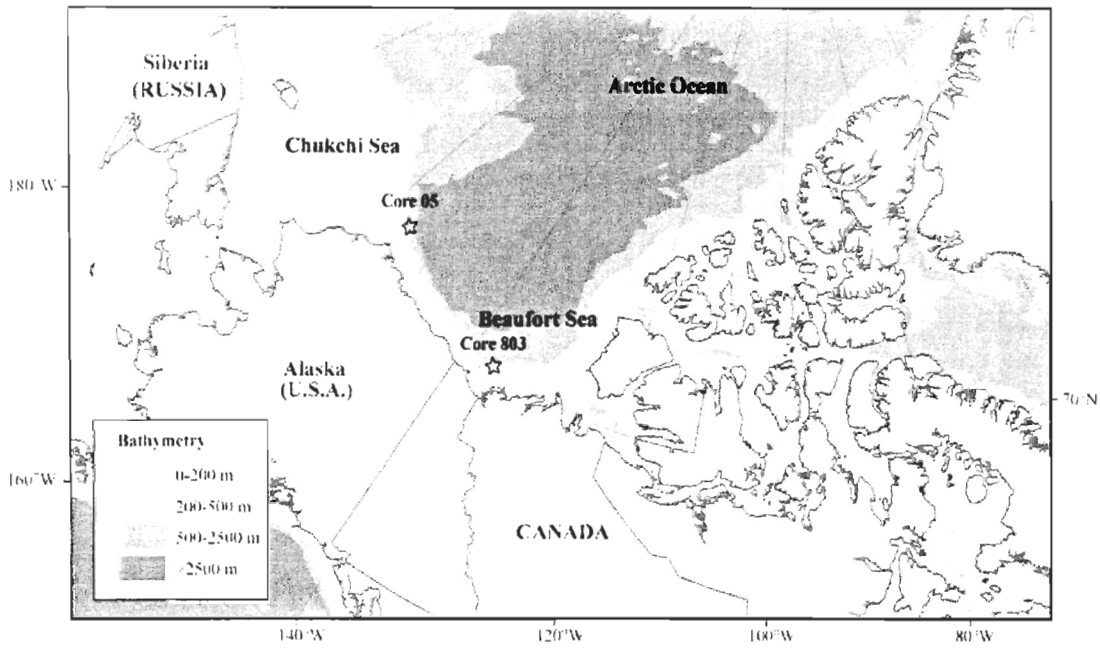

Fig. 1.1. Sampling location of piston cores HLY0501-05JPC (core 05) and 2004-804-803 (core 803).

1.4 Sampling and Methods

Piston core HLY0501-05JPC (hereinafter referred to as core 05) was collected on board the USCGC Healy with a companion trigger weight core in the Chukchi Sea margin at a water depth of 410 m as part of 2005 HOTRAX (Healy-Oden Trans Arctic Expedition) expedition (Table 1). Piston core 2004-804-803 (hereinafter referred to as core 803) and its companion trigger weight core were collected on board the CCGS Amundsen in the Beaufort Sea on the Mackenzie Shelf area at a water depth of 218 m during the 2004 CASES (Canadian Arctic Shelf Exchange Study) expedition (Table 1).

The core sections were cut and split on board. The core sections were described and sampled with u-channels (rigid u-shaped plastic liners with a square 2 cm cross-section and a length of 1.5 m). The first 95 cm of core 05 (section 1) was not sampled because the sediment was too soupy. The magnetic measurements were performed in a magnetically shielded laboratory at the University of Florida (Gainesville, USA).

Table 1.1. Coordinates of the sampling sites.

Core	Lat. (°N)	Long. (°W)	Water depth (m)	Length (cm)
HLY0501-05JPC	72°51.618'	158°25.26'	410	1648
2004-804-803	70°37.976'	135°52.815'	218	598

1.4.1 Magnetic susceptibility

The low-field volumetric magnetic susceptibility (k_{LF}) was measured at 1 cm intervals using a Sapphire Instruments susceptibility bridge installed on a track for the measurement of u-channels. The response function of magnetic susceptibility measurements is similar to that of the cryogenic magnetometer used for remanence measurements (4.5 cm; Thomas et al. 2003). K_{LF} essentially reflects the concentration of ferrimagnetic minerals such as magnetite, but is also strongly grain size dependent (e.g., Dunlop and Özdemir 1997).

1.4.2 Magnetic remanences

The natural remanent magnetization (NRM) was measured on u-channel samples using a 2-G Enterprises Model 760R cryogenic magnetometer at 1 cm intervals. However, due to the finite spatial resolution of the pick-up coils (half-width of the response function = 4.5 cm) some smoothing occurs (Weeks et al. 1993). The data from the upper and lower 4 cm of each u-channel were thus excluded because they are affected by an edge effect (i.e., the integration of 'no sediment' at the end and beginning of each u-channel). In order to isolate the characteristic remanent magnetization (ChRM), the NRM was measured and progressively demagnetized using stepwise peak alternating fields (AF) of 10-60 mT in 5 mT steps, 70 and 80 mT. Magnetic declination and inclination of the ChRM (labelled ChRM D and ChRM I, respectively) were calculated at 1 cm intervals using a least-square line-fitting procedure (Kirschvink 1980). Since the cores were not azimuthally oriented, the ChRM D profiles are relative. The ChRM D profiles were also corrected by rotating the mean declination of the entire core to North. The precision of the best-fit procedure was estimated by the maximum angular deviation (MAD; Kirschvink 1980). MAD values below 5^{o} were recently suggested for high quality marine u-channel data. Finally, the median destructive field (MDF_{NRM}) of the NRM (the value of the peak AF necessary to reduce the NRM intensity to half of its initial value) was calculated using the software developed by Mazaud (2005). The MDF_{NRM} is a coercivity and grain size dependent parameter useful to estimate magnetic mineralogy.

An anhysteretic remanent magnetization (ARM) was imparted using a 100 mT AF field with a 50 μT direct current (DC) biasing field. The ARM was measured and demagnetized at peak fields of 20, 25, 30, 35, 40, 45, 50, 55, 60 mT and 10, 20, 25, 30, 35,

40, 50, 60, 80 mT for cores 05 and 803, respectively. The ARM was also expressed as anhysteretic susceptibility (k_{ARM}) by normalizing the ARM with the biasing field. If magnetic mineralogy is principally controlled by pseudo-single domain magnetite, k_{ARM}/k_{LF} varies inversely with magnetic grain size (e.g., King et al. 1982). Two isothermal remanent magnetizations (IRMs) were imparted to the z axis of the u-channels with a DC pulse field of 0.3 T ($IRM_{0.3T}$) and 0.95 T (SIRM) using a 2-G Enterprise pulse magnetizer. Each IRM was then demagnetized and measured at peak AF of 0, 10, 20, 25, 30, 35, 40, 50, 60, 70, 80 mT and 0, 10, 20, 25, 30, 35, 40, 50, 60, 80 mT for cores 05 and 803, respectively. These IRMs were used to construct a pseudo S-ratio by dividing the $IRM_{0.3T}$ by the SIRM. Pseudo S-ratio values close to 1 are indicative of low coercivity minerals such as magnetite, whereas lower values are indicative of the presence of high coercivity minerals such as hematite. Finally, magnetite grain size was estimated by the k_{LF} versus SIRM diagram (Thompson and Oldfield 1986). Even though the later diagram is based on the use of pure magnetite for calibration, it is often used in paleomagnetism for the estimation of grain size (e.g., Gogorza et al. 2004; Sager and Hall 1990).

1.4.3 Hysteresis measurements

Hysteresis loops were performed on core 05 on small quantity of sediment taken at the base of each u-channel and in some selected intervals using a vibrating sample magnetometer system from Princeton Measurements Corporation. Hysteresis parameters including magnetization saturation (Ms), coercive force (Hc), saturation remanence (Mrs) and coercivity of remanence (Hcr) were extracted from the hysteresis data in order to characterize the magnetic mineralogy and grain size (Day et al. 1977).

1.4.4 Radiocarbon dating

The chronology of both cores were determined using accelerator mass spectrometry (AMS) ^{14}C measurements on six and four calcareous pelecypod shells for cores 05 and 803, respectively (Table 2). All radiocarbon ages were calculated using Libby's half-life (5568 yr) and corrected for natural and sputtering fractionation ($\delta^{13}C$= -25 ‰ VPDB; Stuiver and Polach 1977). The conventional ^{14}C ages were calibrated using the on-line CALIB 5.0.2 software (Stuiver et al. 2005) and the Hughen et al. (2004) marine dataset. A regional reservoir correction (ΔR) of 400 years was applied to core 803 based on the average ΔR value derived from 5 dates realized on pelecypod shells collected prior to nuclear testing from the Amundsen Gulf (McNeely et al. 2006). In contrast, no regional reservoir correction was applied to core 05, as that core was raised from the slope in intermediate Atlantic-derived waters.

Table 1.2. Radiocarbon dates.

Core	Depth (cm)	Corr. depth (cm)[a]	Age (yr BP)[b]	Calibrated age (cal BP)[c]	Dated material	Lab number
803	50	108	1530 ± 40	693 (621-765)	*Yoldia myalis*	Beta-201958
803	274	332	3000 ± 40	2249 (2140-2358)	*Buccinum* sp.	Beta-201959
803	360	418	3540 ± 40	2928 (2800-3056)	Shell fragments	Beta-201960
803	550	608	4560 ± 40	4242 (4105-4378)	Shell fragments	Beta-201961
05	37	112	1930 ± 45	1477 (1358-1595)	*Thyasira* sp.	CAMS- 128414
05	484	559	4465 ± 40	4656 (4522-4789)	*Yoldia* sp.	CAMS- 128415
05	589	664	4820 ± 70	5091 (4891-5290)	*Thyasira* sp.	CAMS- 128416
05	689	764	5220 ± 40	5569 (5471-5667)	*Yoldia* sp.	CAMS- 128417
05	800	875	5885 ± 40	6303 (6212-6393)	*Portlandia* sp.	CAMS- 128418
05	880	955	6395 ± 45	6867 (6740-6993)	*Portlandia* sp. + *Thyasira* sp.	CAMS- 128419

[a]Depth corrected for the missing sediment (see text for details). [b]All ages were measured by the AMS method using Libby's half-life (5568 yr) and corrected for natural and sputtering fractionation ($\delta^{13}C$ = -25‰ VPDB). The statistical uncertainty of the age determination is given as one standard deviation (Stuiver and Polach 1977). [c]Calibrated using the on-line CALIB 5.0.2 software (Stuiver et al. 2005) using the Hughen et al. (2004) marine dataset. Regional reservoir correction (ΔR) for cores 05 and 803 is 0 and 400 yr, respectively. The first and last ages, in parentheses, represent the 2-σ cal age range.

The two age models were constructed using a linear fit between the available calibrated ages on a composite depth scale corrected for missing sediments due to the piston coring process (Fig. 1.2). For core 05, the comparison of the attenuated gamma ray count measurements from the piston and trigger weight cores reveals that about 75 cm of sediment was lost during piston coring (Fig. 1.3a). An analogous estimate was made for core 803 using both the magnetic susceptibility and wet bulk density profiles, revealing that about 58 cm of sediments was missing in the piston core (Fig. 1.3b). For core 05, the age model was only constructed for Unit 1 (see below), as the sedimentation rates in the sediments of unit 2 are currently unknown and could be much higher as this unit was deposited in a glacial/deglacial environmental setting (see below).

1.5 Results

Core 05

1.5.1 Lithology

From 0 to 1315 cm (lithological unit 1; Fig. 1.4a), core 05 consists of olive grey (5Y 4/2) to dark olive grey mud (5Y 3/2) with the presence of iron sulphides (speckles, diffuse laminae). From 1315 to 1723 cm (lithological unit 2), the sediment is characterized by a succession of dark olive grey (5Y 3/2) to very dark grey (2.5Y 3/2) greyish brown (2.5Y 4/2) mud with disseminated sand layers and ice-rafted debris (IRD). The available ^{14}C dates and the presence of IRD in unit 2 indicate that units 1 and 2 correspond to postglacial and glacial/deglacial sediments, respectively.

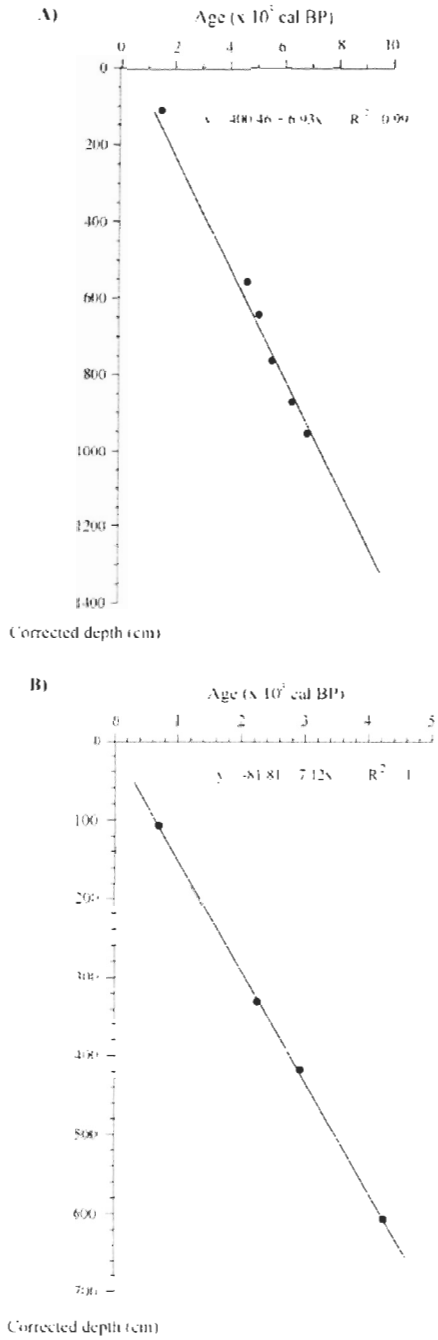

Fig. 1.2. Age model for cores A) 05 and B) 803. The depths were corrected for the missing sediments associated with piston coring (see text for details). Errors bars are the 2-σ ranges associated with the calibrated ages.

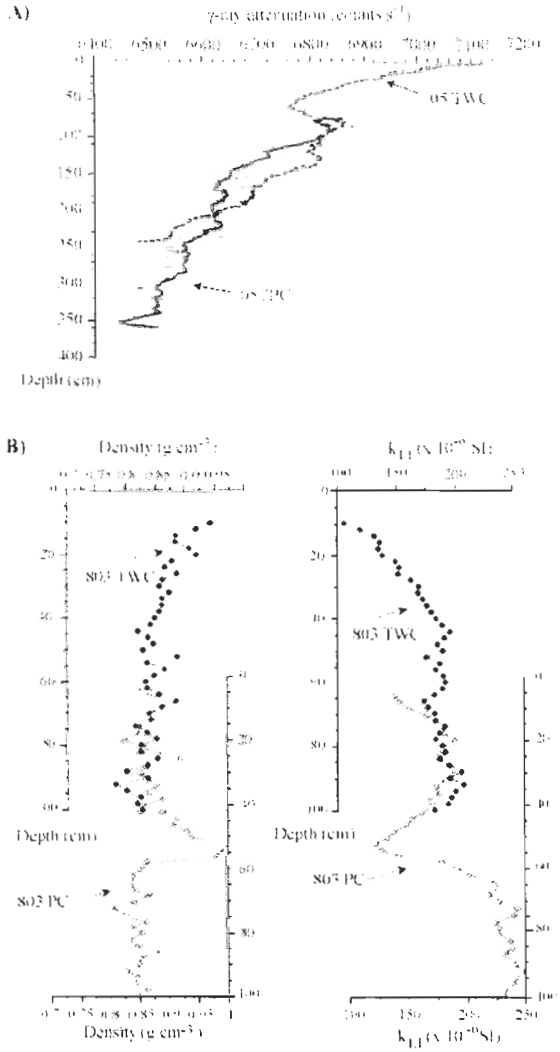

Fig. 1.3. Core top correlation. A) Correlation of gamma ray attenuation counts between core 05 piston (PC) and trigger weight (TWC) cores (red thick and blue dotted curves are smoothed data). The correlation between the piston and trigger weight cores indicates that the first 75 and 58 cm are missing from cores 05 and 803, respectively. B) Correlation of wet bulk density (left graphs) and whole core low-field volumetric magnetic susceptibility (k_{LF}) profiles (right graphs) from core 803 piston (PC) and trigger weight (TWC) cores. Core 803 data was acquired on board the ice-breaker CGCS Amundsen using a GEOTEK MSCL. The density data were not properly calibrated on board and therefore represent only relative changes.

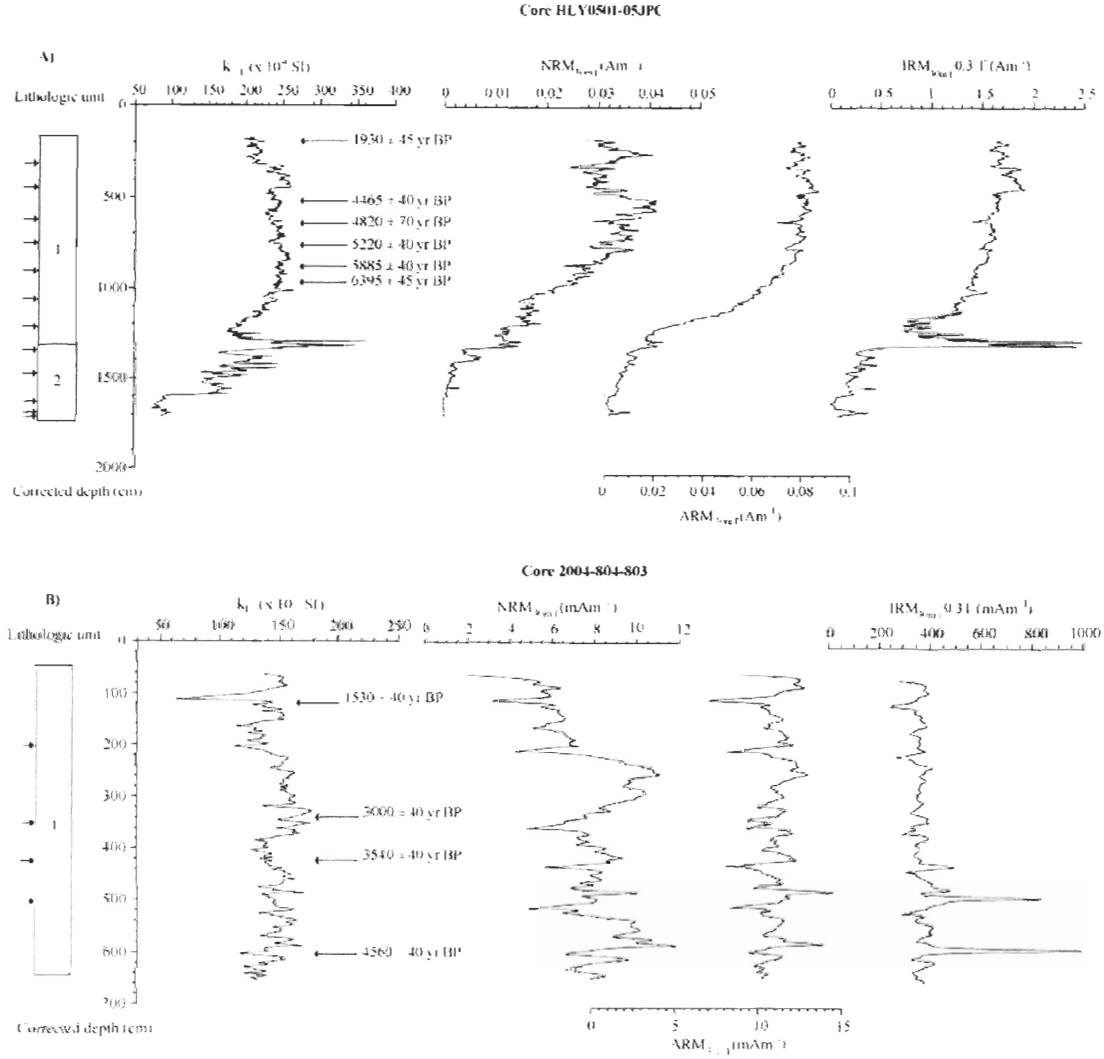

Fig. 1.4. Magnetic properties of cores A) 05 and B) 803. Illustrated are low-field volumetric magnetic susceptibility (k_{LF}), natural remanent magnetization (NRM), anhysteretic remanent magnetization (ARM) and isothermal remanent magnetization diagrams after an AF demagnetization of 30 mT. Also illustrated are the lithological units (1 and 2), the radiocarbon dates (uncorrected conventional ^{14}C dates) and section breaks (black arrows).

1.5.2 Magnetic properties

k_{LF} values of core 05 range from 200 to 250 (x 10^{-6} SI) within lithologic unit 1 (Fig. 1.4a). In lithological unit 2, k_{LF} values reveal more variations and range from 80 to 300 (x 10^{-6} SI), consistent with mineralogical and grain size variations observed during visual description of the core. Aside from the first 800 cm, where NRM is relatively constant (about 0.03 Am^{-1}, after the 30 mT demagnetization step), a long-term downcore decreasing trend is observed. The same long-term downcore decreasing trend is observed in the ARM and IRM profiles, consistent with a diminution of the ferrimagnetic concentration downcore (Fig. 1.4a).

Vector end-point orthogonal projection diagrams (Zijderveld 1967) reveal that the measured NRM is characterized by two magnetic components (Fig. 1.5a). A soft magnetic component (viscous magnetization) with a coercivity spectrum in the 0-20 mT AF range and a stable, well-defined, magnetic component in the 25-80 mT AF range. The characteristic component magnetization (ChRM) was isolated using ten demagnetization steps between 25 mT and 80 mT. The component inclinations (ChRM I) fluctuate around the expected inclination (I_{GAD}) calculated at the sampling site using a geocentric axial dipole (GAD) model (Fig. 1.6a). Aside from lithologic unit 2, where the ChRM is poorly defined, downcore MAD values are lower than 2°, indicative of very well-defined ChRM.

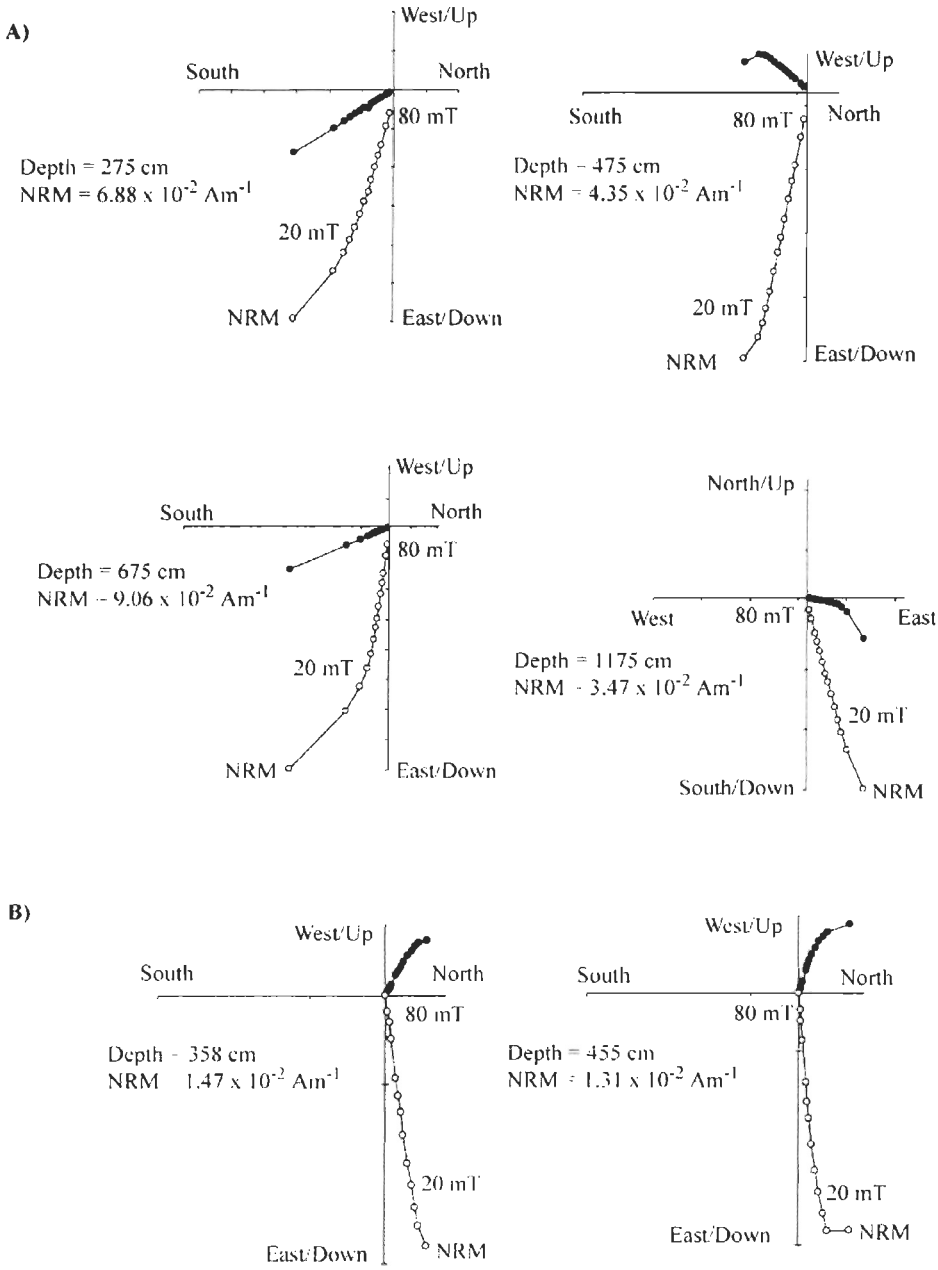

Fig. 1.5. Typical vector end-point orthogonal projection diagrams for cores A) 05 and B) 803. One division on the intensity scales corresponds to 0.01 Am^{-1}.

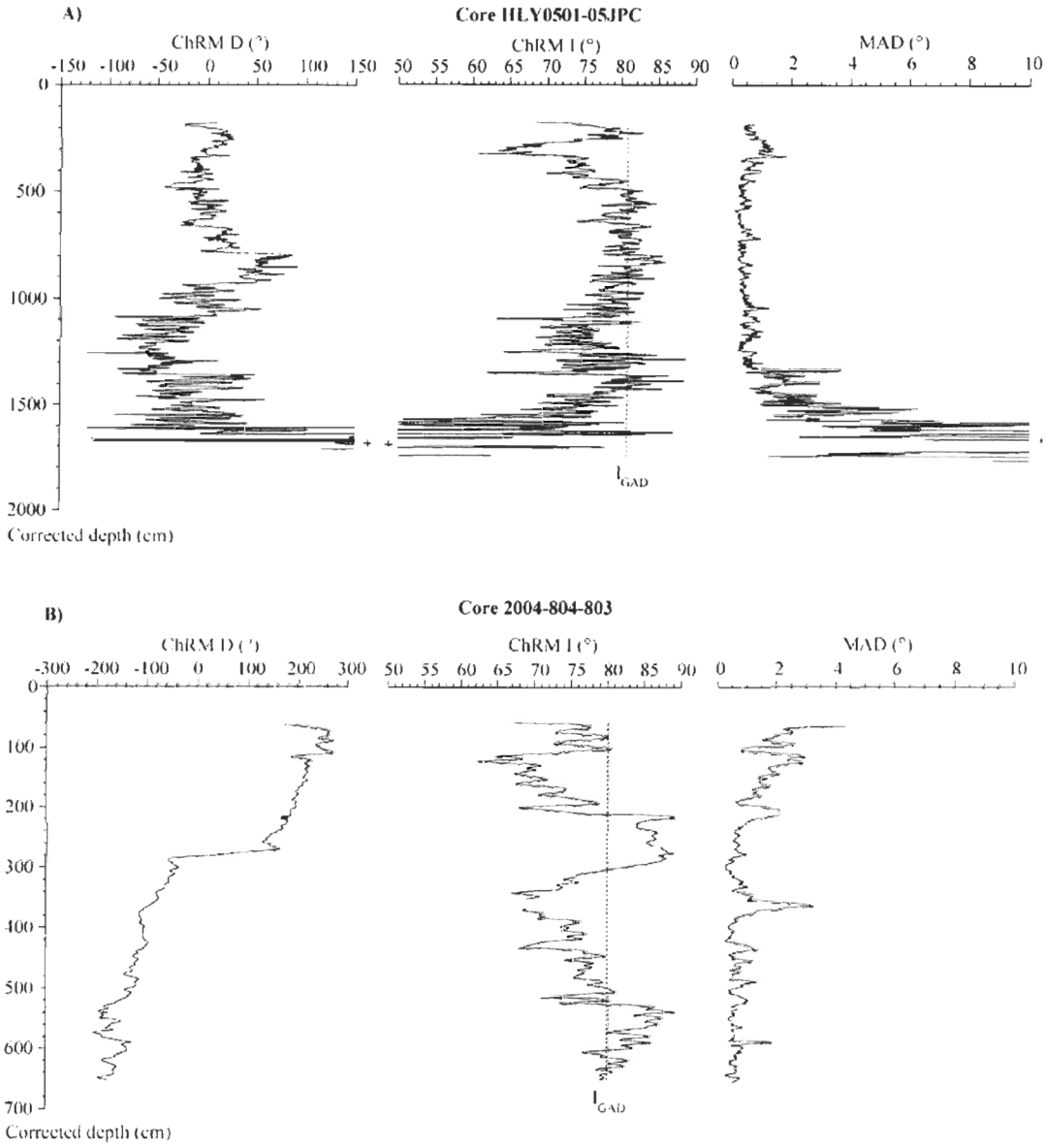

Fig. 1.6. Characteristic remanent magnetization (ChRM) declination (D) and inclination (I), as well as the corresponding maximum angular deviation values (MAD) of cores A) 05 and B) 803. The dashed vertical lines represent the expected inclination (I_{GAD}) according to a geocentric axial dipole (GAD).

MDF_{NRM} values fluctuate between 13.7 and 56 mT, with an average of 29.40 ± 8.03 mT (Fig. 1.7a). Such an average and range are typical of magnetite. The k_{LF} versus SIRM diagram is compatible with the presence of magnetite in the 1-16 μm grain size range (Fig. 1.8a). Downcore variations of the grain size dependent ratio k_{ARM}/k_{LF} depict a decreasing trend compatible with an increasing magnetite grain size (Fig. 1.7a). A submicron magnetite grain size from 319 cm to 1215 cm, as well as multi domain (MD) magnetite grain size (> 16 μm) below 1605 cm is observed (Fig. 1.8a). Coarse MD magnetite grains are inefficient carriers of a stable detrital remanent magnetization (DRM) (e.g., Dunlop and Özdemir 1997).

All the studied samples fall in the pseudo-single domain region (PSD) for magnetite (Fig. 1.9a; Day et al. 1977). Aside from lithologic unit 2, pseudo S-ratio values are close to 1, indicative of low coercivity minerals such as magnetite (Fig. 1.7a). In summary, the magnetic mineralogy and grain size of lithologic unit 1 is compatible with the presence of PSD magnetite, whereas the magnetic mineralogy and grain size of lithologic unit 2 is compatible with coarse MD magnetite.

The hysteresis loops indicate saturation fields well below 200 mT and coercivities typical of magnetite (Fig. 1.9b). In addition, all loops are characterized by a paramagnetic component. However, an almost linear relationship between the measured magnetic moment M and the applied magnetic field H with no hysteresis loop is observed in some intervals of lithological unit 2 indicating that the magnetic behaviour of such samples is dominated by the paramagnetic fraction. For this reason, we will now only focus on the upper unit (postglacial sediments) of core 05 (unit 1).

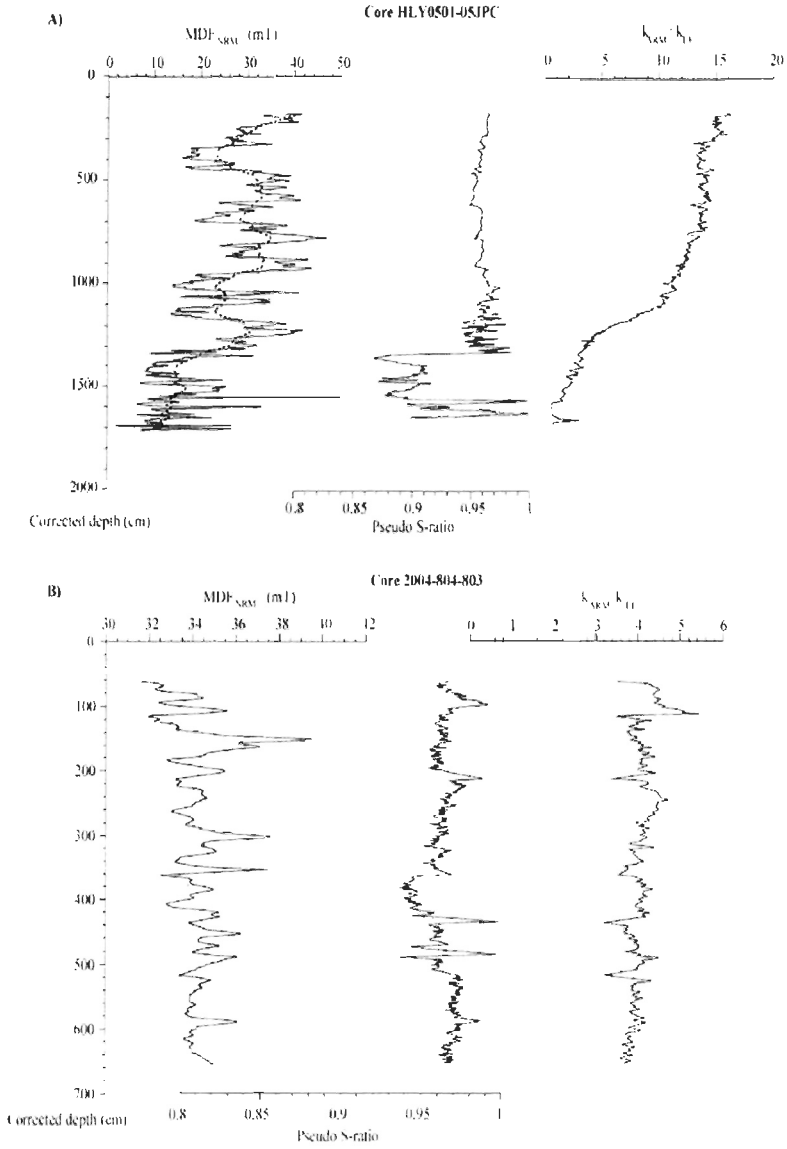

Fig. 1.7. Median destructive field of the NRM (MDF_{NRM}), pseudo S-ratio and k_{ARM}/k_{LF} of cores A) 05 and B) 803. The dashed curve in the MDF_{NRM} diagram represents smoothed data.

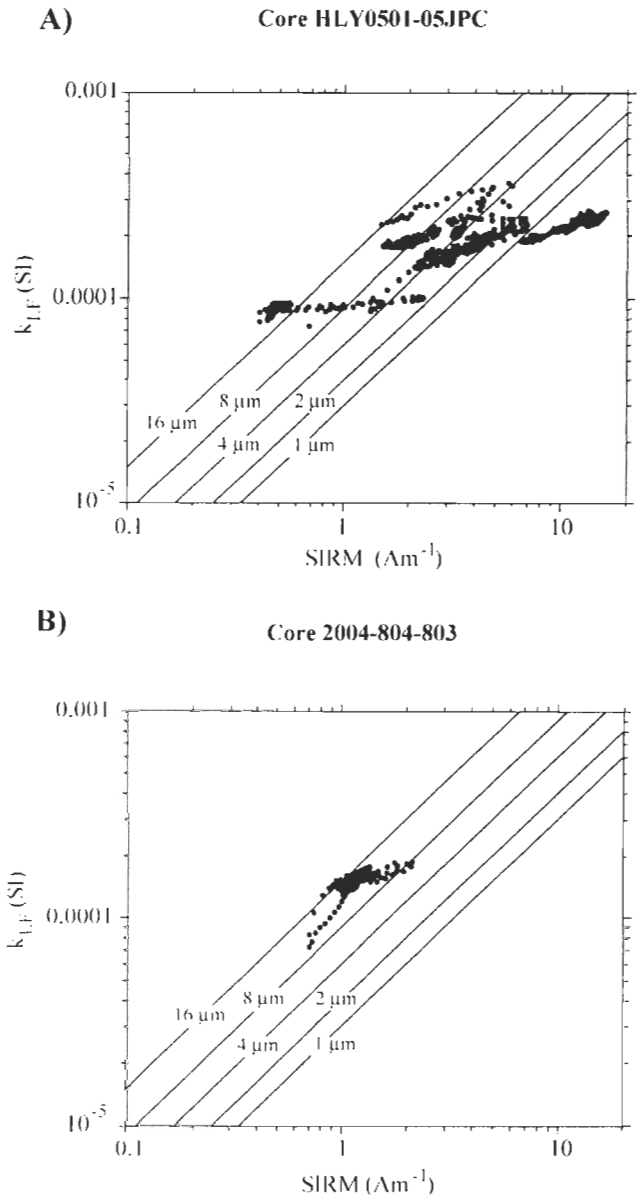

Fig. 1.8. Magnetic susceptibility versus saturated isothermal remanenent magnetization (SIRM) diagram (Thompson and Oldfield 1986) for cores A) 05 and B) 803.

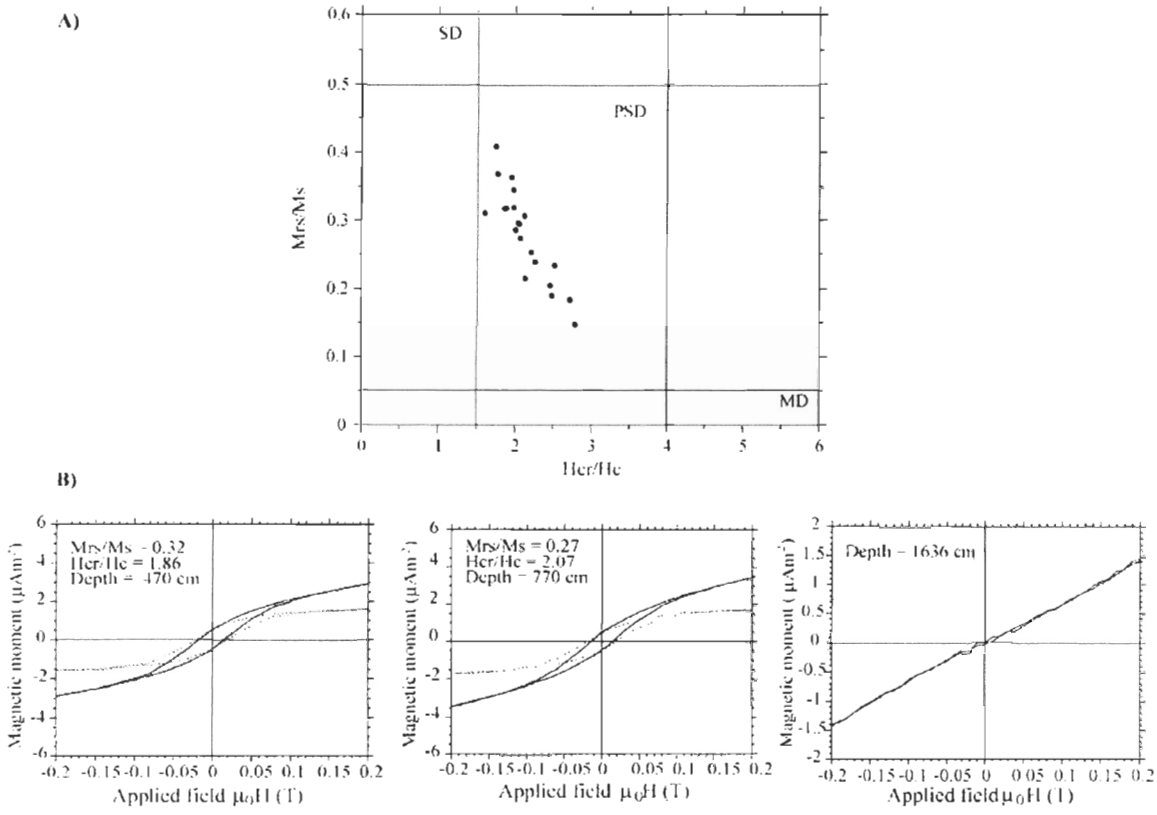

Fig. 1.9. Magnetic grain size and mineralogy for core 05. A) Day plot (Day et al. 1977) and B) Hysteresis loops of three selected depths. Dotted curves represent hysteresis loops after slope correction.

Core 803

1.5.3 Lithology

The top 88 cm consists of faintly bioturbated olive grey mud (5Y 4/1). From 88 to 113 cm, an alternation of dark olive grey (5Y 3/2) to olive grey (5Y 4/1) mud is observed, whereas the rest of the core (113 to 658 cm) is characterized by olive grey mud (5Y 4/1) with a variable degree of bioturbation. Occasional black horizons and laminations are also observed along the entire core. The available ^{14}C dates and very similar sedimentary facies

below 113 cm indicate that the entire core is composed of postglacial sediments (lithological unit 1; Fig. 1.4b).

1.5.4 Magnetic properties

k_{LF} values of core 803 are relatively constant (about 150 $x10^{-6}$ SI) along the entire core (Fig. 1.4b). Variations of magnetic concentration-dependent parameters like NRM, ARM and IRM are below one order of magnitude along the entire core (Fig. 1.4b).

As for core 05, the NRM of core 803 is characterized by a viscous, low-coercivity magnetization easily removed by the application of a 20 mT peak AF (Fig. 1.5b). A stable, well-defined ChRM was isolated using 11 magnetization steps from 20 to 80 mT. The characteristic component inclinations fluctuate around the calculated I_{GAD} and MAD values are lower than 2° (Fig. 1.6b), again indicative of a very well-defined ChRM (e.g., Kirschvink 1980). The MDF_{NRM} values are between 31.5 and 41.9 mT with an average of 34.35 ± 1.22 mT, whereas pseudo S-ratios vary close to 1 (Fig. 1.7b). These results are compatible with the presence of magnetite as the principal carrier of the ChRM.

As revealed from the K_{LF} versus SIRM diagram, the magnetic mineralogy is characterized by PSD magnetite in the 8-16 μm grain size range (Fig. 1.8b). Downcore variations of k_{ARM}/k_{LF} depict uniform grain size variations (Fig. 1.7b).

1.6 Relative paleointensity (RPI) determination

The standard technique employed to derive a RPI proxy record is to normalize the measured NRM by a magnetic concentration-dependent parameter like ARM, IRM or k_{LF}

in order to compensate for the variable ferrimagnetic concentration (Tauxe 1993). The use of ARM as a normalizer has been justified both on an empirical and theoretical basis by King et al. (1983) and was successfully used in numerous studies (e.g., Channell 2006; Stoner et al. 2003), whereas the use of IRM and k_{LF} as a normalizer necessitates careful evaluation (e.g., Valet 2003). In order to assess the reliability of a RPI proxy, some pre-established criteria must be satisfied (Tauxe 1993). According to Tauxe (1993) and more recently by Stoner and St-Onge (2007), the NRM must be characterized by a strong, stable, single component magnetization with MAD values lower than 5°, whereas the measured NRM must be a DRM carried by magnetite in the PSD (1-15 μm) grain size range. In addition, magnetite concentration variations of more than one order of magnitude should be avoided (Tauxe 1993).

The previous sections have shown that the postglacial sediments of both cores are characterized by a strong, stable and single component magnetizations with MAD values generally lower than 5°. Variations of concentration-dependent parameters like k_{LF} and ARM of both cores are well below one order of magnitude (Figs. 1.10b, 1.10d). The magnetic data of the postglacial sediments also indicate that the NRM is primarily carried by low coercivity minerals such as magnetite in the PSD size range, thus respecting the above set of criteria. In order to construct a relative paleointensity proxy, we first calculated the average of NRM/ARM and NRM/IRM over the 30-45 mT AF range and then divided each mean by the standard deviation. As revealed from the orthogonal projections (Fig. 1.5), this AF window falls inside the AF range of the isolated and stable ChRM. The two calculated RPI proxy records display very similar pattern (r^2 =0.80 and 0.93 for cores 803 and 05, respectively), suggesting that the ARM and IRM activate the

same magnetic assemblages (Figs. 1.10a, 1.10c). The standard deviation of each proxy is comparable. Although the two methods of normalization yield essentially the same intensity records, we have chosen ARM as the preferred normalizer. According to Levi and Banerjee (1976), the use of ARM as a normalizer offers the advantage of dealing with single-or PSD grains of magnetite whereas IRM can also activate a large fraction of magnetic grains that do not carry the NRM.

1.7 Discussion

1.7.1 Western North American comparison

The Holocene paleomagnetic inclination records of cores 803 and 05 show similar features with one and the other, as well as with several Holocene PSV records from the western North America (Fig. 1.11). The different nature of these records [marine: cores 803 and 05, lacustrine: Fish Lake (Verosub et al. 1986) and Grandfather Lake (Geiss and Banerjee 2003), volcanic rocks: PSVL compilation (Hagstrum and Champion 2002)] further corroborates the geomagnetic origin of the signal in cores 803 and 05, as well as the ΔR used for both cores. The two most prominent magnetic inclination minima are observed at around 1000 (magnetic feature I-1) and 2500 cal BP (magnetic feature I-2) in all examined records. Similarly, a magnetic inclination minimum is observed around 8500 cal BP (magnetic feature I-3) in three high latitude western North American records, Grandfather Lake (Alaska), Fish Lake (Oregon) and core 05 (Chukchi Sea).

Fig. 1.10. Relative paleointensity proxies of cores A) 05 and C) 803. Note the strong similarities of both proxies (NRM/ARM and NRM/IRM). Also illustrated are changes in concentration-dependent magnetic susceptibility (k_{LF}) and anhysteretic remanent magnetization (ARM) for cores B) 05 and D) 803. Arrows indicate the maximum variability.

Core HLY0501-05JPC

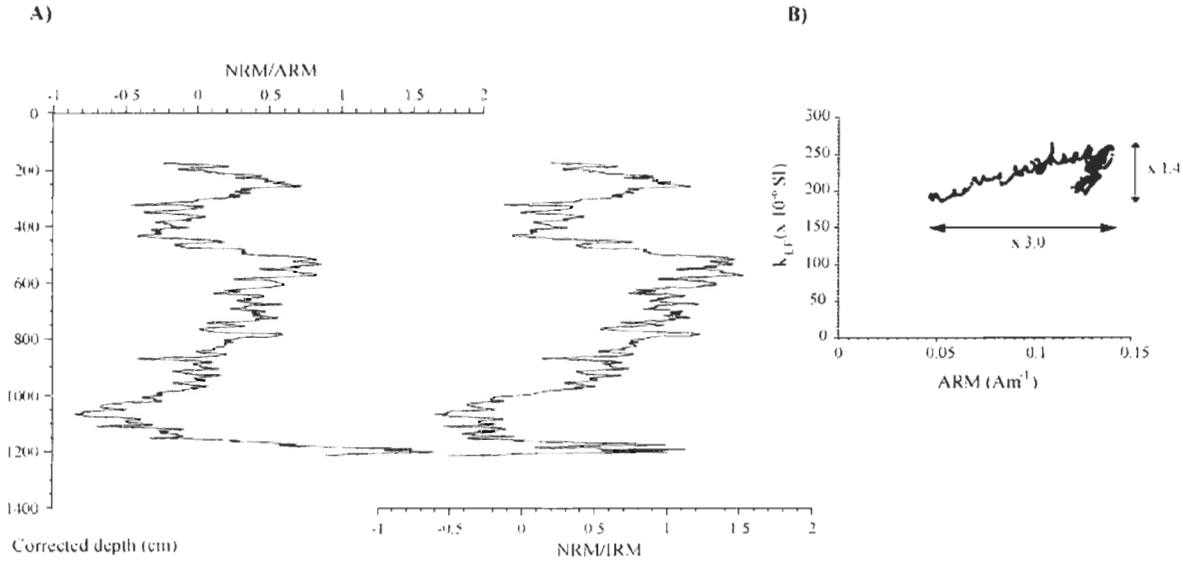

Core 2004-804-803

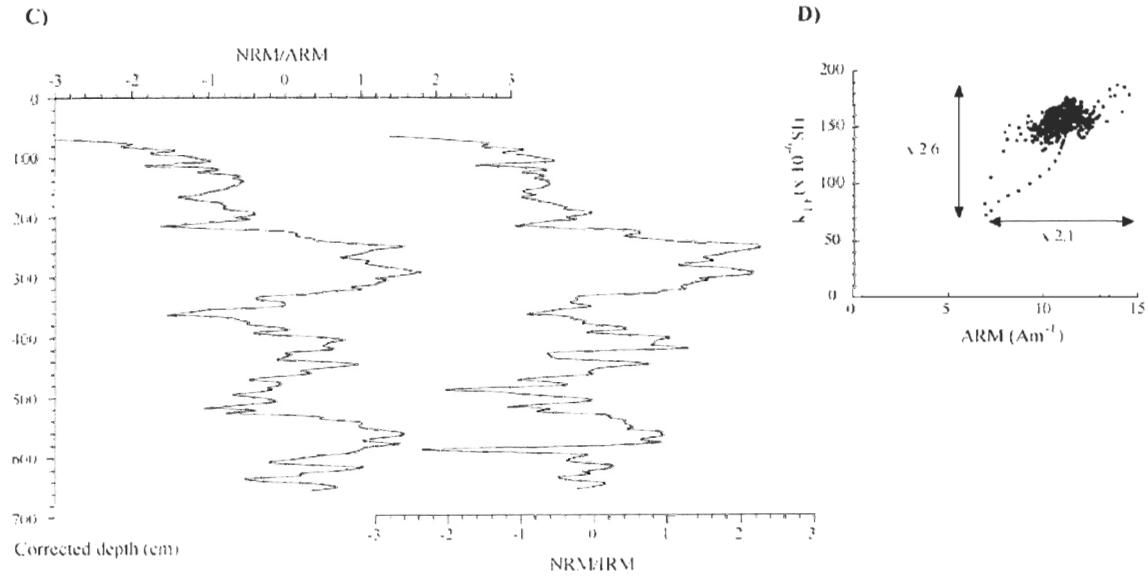

Fig. 1.11. Western North American inclination (left graphs) and declination (right graphs) comparison for the last 9000 cal BP. Correlative inclination features I-1, I-2 and I-3 are presented (see text for details). Illustrated are cores 05 and 803 (this study), the western United States PSVL volcanic compilation (Hagstrum and Champion 2002), Grandfather Lake (Alaska; Geiss and Banerjee 2003) and Fish Lake (Oregon, USA; Verosub et al. 1986). Fish Lake data were calibrated using the Stuiver et al. (1998) radiocarbon calibration curve (Verosub, K., pers. comm.). The continuous red curves in the inclination figures represent weighted functions. Note that the inclination and declination scales are not identical.

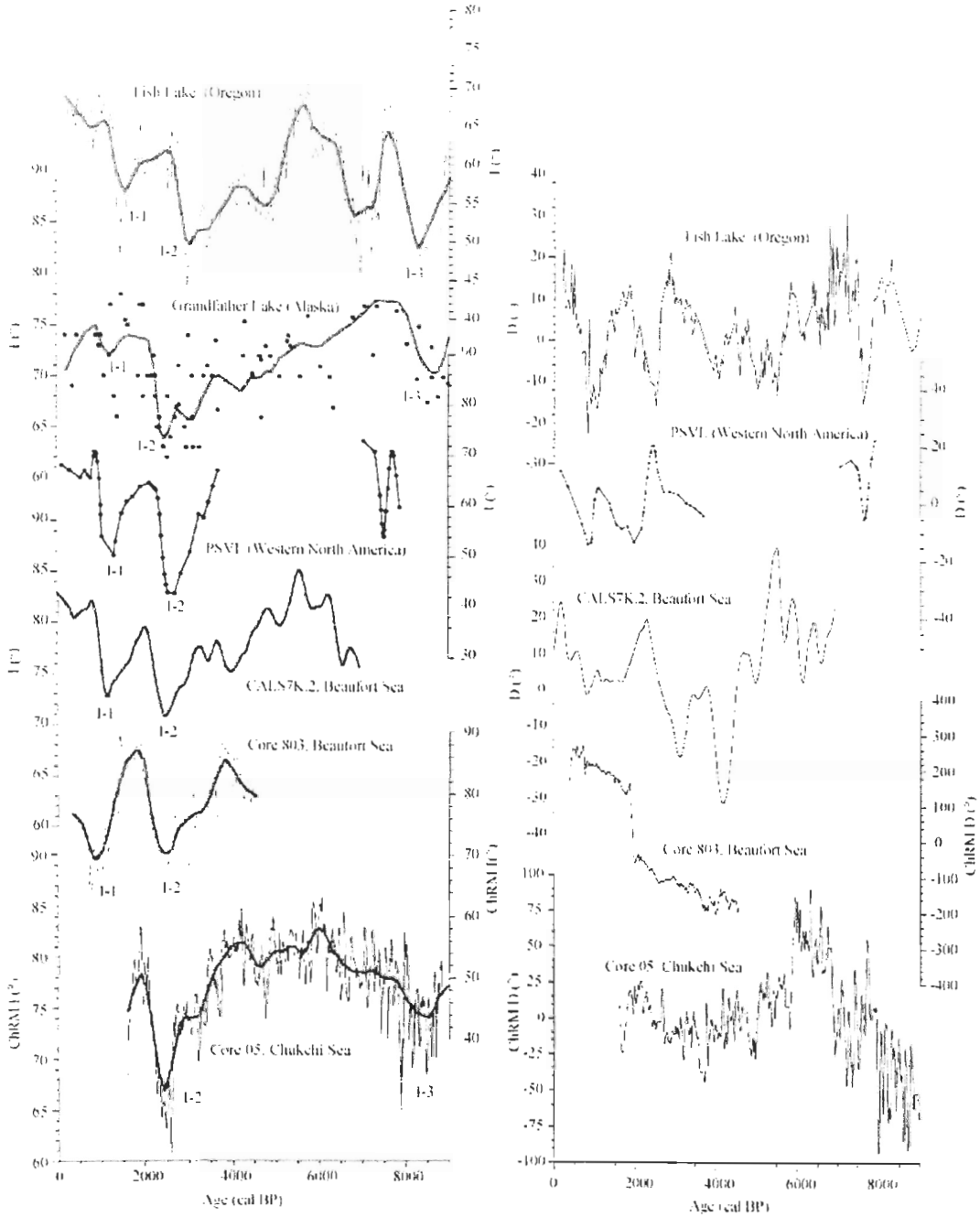
Fish Lake (Oregon)
Grandfather Lake (Alaska)
PSVL (Western North America)
CALS7K.2, Beaufort Sea
Core 803, Beaufort Sea
Core 05, Chukchi Sea
I-1
I-2
I-3
T (°C)
ChRM D (°)
Age (cal BP)
0
2000
4000
6000
8000

The most striking feature in the declination record is the abrupt one observed in core 803 around 1850 cal BP (Fig. 1.11), although the steep inclination at this level means that the shift in declination in less dramatic than it appears in the declination plot. This feature does not occur at a section break and does not result from a sampling artefact (e.g., hole in the u-channel, etc.) or a major lithological change. On the other hand, it is not apparent in core 05 and should thus be treated with caution at this stage. Excluding this sharp declination change, comparison of cores 803 and 05 declination records depict millennial to centennial-scale variability from 2000 to 4500 cal BP, where the two records can be directly compared (Fig. 1.12). In addition, some common centennial-scale declination features can also be clearly detected from 2000 to 2500 cal BP (Fig. 1.13; magnetic features D-1, D-2, D-3).

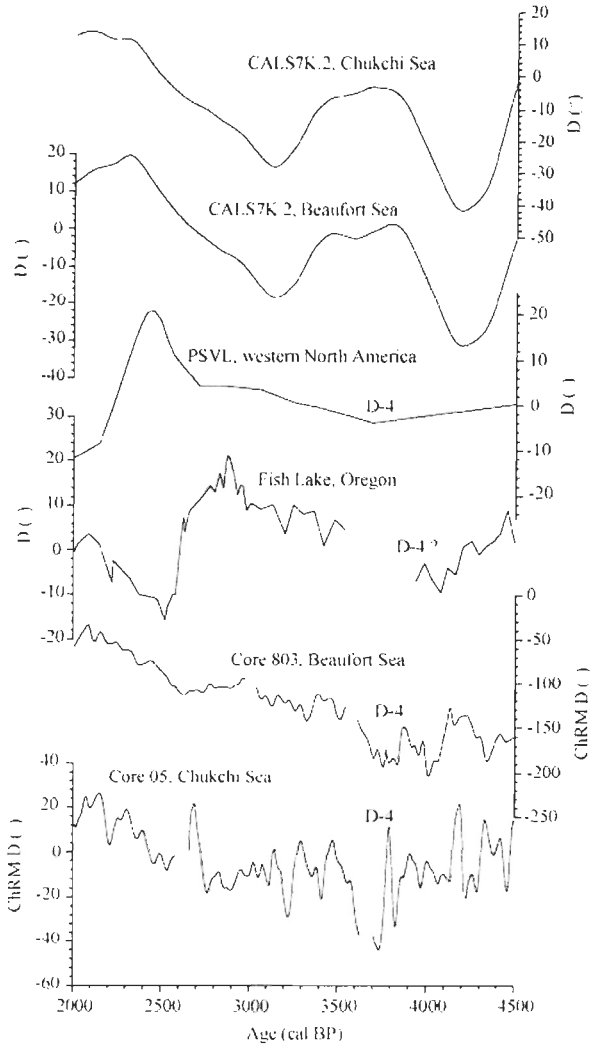

Fig. 1.12. Western North American declination comparison from 2000 to 4500 cal BP. Correlative declination feature D-4, is indicated (see text for details). Illustrated are cores 05 and 803 (this study), the western United States PSVL volcanic compilation (Hagstrum and Champion 2002), Fish Lake (Oregon, USA; Verosub et al 1986) and the CALS7K.2 declination output for cores 803 and 05. Fish Lake data were calibrated using the Stuiver et al. (1998) radiocarbon calibration curve (Verosub, K., pers. comm.). The model output was calculated by M. Korte using the CALS7K.2 model (Korte and Constable 2005a). Note that the declination scales are not identical.

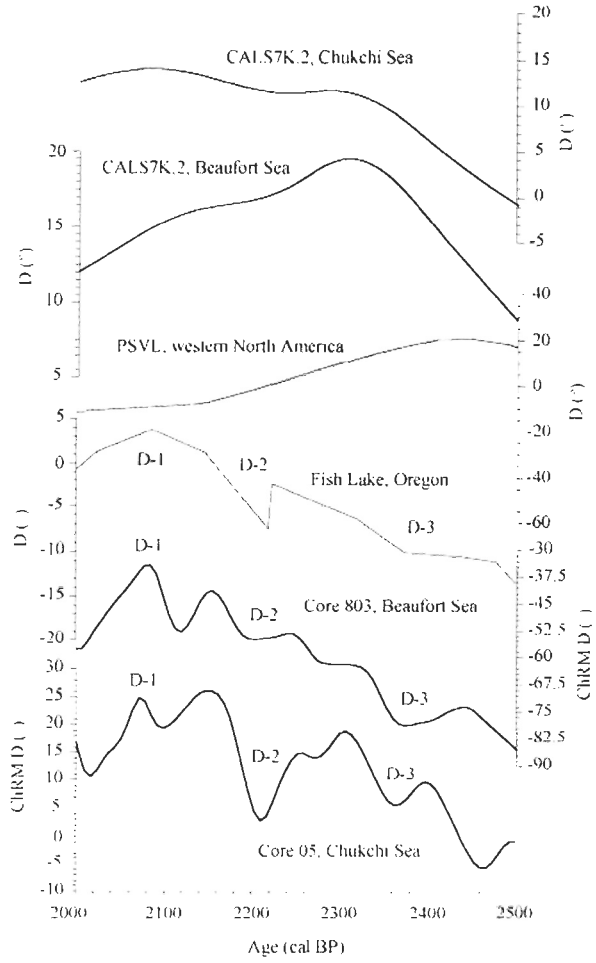

Fig. 1.13. Western North American declination comparison from 2000 to 2500 cal BP. Correlative declination features D-1, D-2 and D-3, are indicated (see text for details). Note that the declination scales are not identical.

The relative paleointensity (RPI) records of cores 05 and 803 reveal similar millennial-scale features for the last 4500 cal BP, as well as higher frequency centennial-scale fluctuations (Fig. 1.14). Unfortunately, no high-resolution continuous Holocene RPI records from the Arctic are currently available for comparison purposes. Nonetheless, between 3500 and 8500 cal BP, the RPI proxy records of cores 05 and 803 are consistent with the global dipole moment compilations of Ohno and Hamano (1993) and McElhinny and Senanayake (1982) although, as suggested by Dunai (2001), very high dipole moment values for the earliest part of the Ohno and Hamano (1993) synthetic record may be an artefact of poor data replication. Discrepancies are nonetheless observed between the RPI records and the global dipole moment estimate of McElhinny and Senanayake (1982) for the last 3500 cal BP, but could be the result of an important European bias in the database used for the reconstruction. For example and as pointed out by Ohno and Hamano (1993), this bias seems particularly true between 2500 and 3500 cal BP when the dipole axis was tilted towards the European region. Consequently, the millennial-scale relative paleointensity features of cores 05 and 803 may reflect global dipole moment variations. Because of the paucity of Arctic RPI records, it is impossible to assess the dipolar nature of the centennial-scale features, although recent geomagnetic models have implied that changes in the intensity of the dipole moment can occur at the centennial timescale (Korte and Constable 2006).

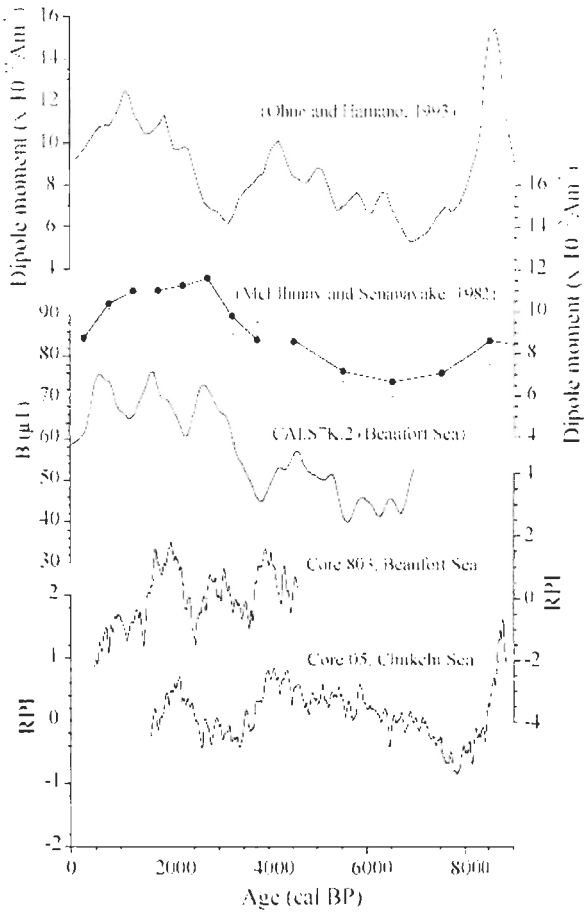

Fig. 1.14. Relative paleointensity (RPI) records of cores 05 and 803. Also illustrated are the synthetic record of Ohno and Hamano (1993), the global-dipole moment reconstruction based on archeomagnetic data of McElhinny and Senanayake (1982) and the CALS7K.2 intensity output for core 803. The model output was calculated by M. Korte using the CALS7K.2 model (Korte and Constable 2005a). Error bars are 95% confidence limits. Note that the RPI scales are not identical.

1.7.2 Comparison with geomagnetic model output

The inclination record calculated for the sampling site of both cores using the time-varying paleomagnetic model CALS7K.2 (Korte and Constable 2005c) are very consistent with cores 05 and 803 inclination records, notably for the last 3000 cal BP (Fig. 1.11). Several large centennial to millennial-scale features are clearly recognizable and further support the reliability of both inclination records as well as the age models. Nevertheless, the paleointensity and the declination records calculated with CALS7K.2 model show more discrepancies with the variations recorded in the sedimentary records (Figs. 1.12, 1.13). The paleointensity records used in the model are mainly distributed in central Europe (Korte and Constable 2005b). Model-derived paleointensity records are thus strongly biased towards the central Europe dataset. Overestimates of the non-dipole components of the geomagnetic field for pre-historic times, as discussed by Valet et al. (2008), could explain the observed discrepancies between magnetic declination record and CALS7K.2 prediction. In addition, only 5 declination datasets were used to constrain the model for North America, with none of them being above 50° N (Korte et al. 2005c).

1.7.3 Implications for Arctic chronostratigraphy

Distinctive magnetic inclination and declination features of cores 05 and 803 can be correlated over more than 3000 km to the western North American volcanic secular variation compilation of Hagstrum and Champion (2002) to the sedimentary record from Fish Lake, Oregon (Verosub et al. 1986), and the RPI records of both cores are consistent

with changes in Earth's dipole moment at the millennial timescale, at least from 3500 to 8500 cal BP. These results open the possibility to use both Holocene PSV and RPI records as a new regional chronostratigraphical tool in the western Canadian Arctic. For example, distinctive inclination lows were observed at 1000, 2500 and 8500 cal BP (Fig 1.11); distinctive declination features at 2060, 2200, 2360 and 3560 cal BP (Figs. 1.12, 1.13); distinctive RPI highs at 2000, 4000 and 8500 cal BP (Fig. 1.14). Comparison with similar eastern Arctic paleomagnetic records is nonetheless necessary prior to the use of such paleomagnetic features for stratigraphic correlation on a larger spatial scale.

1.8 Conclusions

Cores 803 and 05 provide the first continuous Holocene high-resolution PSV and RPI records for the western Canadian Arctic. Similar centennial-to millennial-scale Holocene magnetic declination and inclination features can be correlated in both cores and with other high-resolution western North American lacustrine and volcanic records. In addition, the RPI records of cores 803 and 05 reveal consistent millennial-scale fluctuations compatible with changes in Earth's dipole moment. These results also highlight the potential use both Holocene PSV and RPI records for chronostratigraphy purposes in the western Canadian Arctic.

1.9 Acknowledgements

We are in debt to the captain, officers, crew and scientists on board the USCGC Healy and CCGS Amundsen for the recovery of cores 05 and 803, respectively. We wish to thank Dr.

C. E. Geiss and an anonymous reviewer for their constructive reviews to improve the manuscript as well as Dr. K. Verosub for sharing his data and Dr. M. Korte for providing the CALS7K.2 model outputs for cores 05 and 803. This study was supported by the Canadian Arctic Shelf Exchange Study (CASES), the Polar Climate Stability Network and by NSERC Special opportunity (International Polar Year) and Discovery grants to G. St-Onge and A. Rochon. This is GEOTOP contribution number 2008-0024.

1.10 References

Andrews, J.T., and Dunhill, G. 2004. Early to mid-Holocene Atlantic water influx and deglacial meltwater events, Beaufort Sea slope, Arctic Ocean. Quaternary Research, **61**: 14-21.

Channell, J.E.T. 2006. Late Brunhes polarity excursions (Mono Lake, Laschamp, Iceland Basin and Pringle Falls) recorded at ODP Site 919 (Irminger Basin). Earth and Planetary Science Letters, **244**: 378-393.

Darby, D.A., Polyak, L., and Bauch, H.A. 2006. Past glacial and interglacial conditions in the Arctic Ocean and marginal seas – a review. Progress in Oceanography, **71**: 129-144.

Day, R., Fuller, M., and Schmidt, V.A. 1977. Hysteresis properties of titanomagnetites; grain size and compositional dependence. Physics of the Earth and Planetary Interiors, **13**: 260-267.

Dunai, T.J. 2001. Influence of secular variation of the geomagnetic field on production rates of in situ produced cosmogenic nuclides. Earth and Planetary Science Letters, **193**: 197-212.

Dunlop, D.J., and Özdemir, Ö. 1997. Rock Magnetism: Fundamentals and Frontiers. Cambridge University Press, Cambridge and New York.

Gallet, Y., Genevey, A., and Le Goff., M. 2002. Three millennia of directional variation of the Earth's magnetic field in western Europe as revealed by archeological artefacts. Physics of the Earth and Planetary Interiors, **131**: 81-89.

Geiss, C.E., and Banerjee, S.K. 2003. A Holocene-late Pleistocene Geomagnetic Inclination Record from Grandfather Lake, SW Alaska. Geophysical Journal International, **153**: 497-507.

Genevey, A., and Gallet, Y. 2003. Eight thousand years of geomagnetic field intensity variations in the eastern Mediterranean. Journal of Geophysical Research, **108**: 1-18.

Gogorza, C.S.G., Lirio, J.M., Nunez, H., Chaparro, M., Bertorello, H.R., and Sinito, A.M. (2004). Paleointensity studies on Holocene-Pleistocene sediments from lake Escondido, Argentina. Physics of the Earth and Planetary Interiors, **145**: 219-238.

Hagstrum, J.T., and Champion, D.E. 2002. A Holocene paleosecular variation record from 14C-dated volcanic rocks in western North America. Journal of Geophysical Research, **107**: 1-14.

Hill, P.R.B., Blasco, S.M., Harper, J.R., and Fissel, D.B. 1991. Sedimentation on the Canadian Beaufort Shelf. Continental Shelf Research, **11**: 821-842.

Hughen, K.A., Baillie, M.G.L., Bard, E., Bayliss, A., Beck, J.W., Bertrand, C.J.H., Blackwell, P.G., Buck, C.E., Burr, G.S., Cutler, K.B., Damon, P.E., Edwards, R.L., Fairbanks, R.G., Friedrich, M., Guilderson, T.P., Kromer, B., McCormac, F.G., Manning, S., Bronk Ramsey, C., Reimer, P.J., Reimer, R.W., Remmele, S., Southon, J.R., Stuiver, M., Talamo, S., Taylor, F.W., van der Plicht, J., and Weyhenmeyer, C.E.

2004. Marine04 Marine radiocarbon age calibration, 0-26 Cal Kyr BP. Radiocarbon, **46**: 1059-1086.

Hulot, G., Eymin, C., Langlais, B., Mandea, M. and Olsen, N. 2002. Small-scale structure of the geodynamo inferred from Oersted and Magsat satellite data. Nature, **416**: 620-623.

Jackson, A., Jonkers, A.R.T., and Walker, M. 2000. Four centuries of geomagnetic secular variation from historical records. Philosophical Transactions of the Royal Society A, **358**: 957-990.

Jonkers, A.R.T., Jackson, A., and Murray, A. 2002. Four centuries of geomagnetic data from historical records. Reviews of Geophysics, **41**: 1-74.

Keigwin, L.D., Donnelly, J.P., Cook, M.S., Driscoll, N.W., and Brigham-Grette, J. 2006. Rapid sea-level rise and Holocene climate in the Chukchi Sea. Geology, **34**: 861-864.

King, J.W., Banerjee, S.K., Marvin, J.A., and Özdemir, Ö. 1982. A comparison of different magnetic methods for determining the relative grain size of magnetite in natural materials: some results from lake sediments. Earth and Planetary Science Letters, **59**: 404-419.

King, J.W., Banerjee, S.K., and Marvin, J. 1983. A new rock magnetic approach to selecting sediments for geomagnetic intensity studies: Application to paleointensity for the last 4000 years. Journal of Geophysical Research, **88**: 5911-5921.

Kirschvink, J.L. 1980. The least-squares line and plane and the analysis of paleomagnetic data. Geophysical Journal of the Royal Astronomical Society, **62**: 699-718.

Korte, M., and Constable, C.G. 2005a. Continuous geomagnetic field models for the past 7 millennia: 2. CALS7K. Geochemistry Geophysics Geosystems, **6**: 1-18.

Korte, M., and Constable, C.G. 2005b. The geomagnetic dipole moment over the last 7000 years-new results from a global model. Earth and Planetary Science Letters, **236**: 348-358.

Korte, M., Genevey, A., Constable, C.G., Frank, U., and Schnepp, E. 2005c. Continuous geomagnetic field models for the past 7 millennia: 1. A new global data compilation. Geochemistry Geophysics Geosystems, **6**: 1-28.

Korte, M., and Constable, C.G. 2006. Centennial to millennial geomagnetic secular variation. Geophysical Journal International, **167**: 1-10.

Levi, S., and Banerjee, S.K. 1976. On the possibility of obtaining relative paleointensities from lake sediments. Earth and Planetary Science Letters, **29**: 219-226.

MacDonald, R.W., Solomon, S.M., Cranston, R.E., Welch, H.E., Yunker, M.B., and Gobeil, C. 1998. A sediment and organic carbon budget for the Canadian Beaufort Shelf. Marine geology, **144**: 255-273.

Mazaud, A. 2005. User-friendly software for vector analysis of the magnetization of long sediment cores. Geochemistry Geophysics Geosystems, **6**: 1-8.

McElhinny, M.W., and Senanayake, W.E. 1982. Variations in the geomagnetic dipole 1: the past 50,000 years. Journal of Geomagnetism and Geoelectricity, **34**: 39-51.

McNeely, R., Dyke, A.S., and Southon, J.R. 2006. Canadian marine reservoir ages, preliminary data assessment. Geological Survey Canada, Open File 5049.

Ohno, M., and Hamano, Y. 1993. Global analysis of the geomagnetic field; time variation of the dipole moment and the geomagnetic pole in the Holocene. Journal of Geomagnetism and Geoelectricity, **45**: 1455-1466.

Olsen, N., and Mandea, M. 2007. Will the Magnetic North Pole move to Siberia? Eos, **88**: 293-294.

Olson, P., and Aurnou, J. 1999. A polar vortex in the Earth's core. Nature, **402**: 170-173.

Sager, W.W., and Hall, S.T. 1990. Magnetic properties of black mud turbitides from ODP LEG 116, distal Bengal Fan, Indian Ocean. *In* Cohran, J.R., Stow, D.A.V. et al. Proceedings of the Ocean Drilling Program, Scientific Results, vol. **116**: 317-336.

Scott, D.B., Schell, T., St-Onge, G., Rochon, A., Blasco, S. 2009. Foraminiferal assemblage changes over the last 15,000 years on the Mackenzie/Beaufort Sea slope and Amundsen Gulf, Canada : implication for past sea-ice conditions. Paleoceanography, **24**: PA2219, doi: 10.1029/2007PA001575.

Snowball, I., and Sandgren, P. 2002. Geomagnetic field variations in northern Sweden during the Holocene quantified from varved lake sediments and their implications for cosmogenic nuclide production rates. The Holocene, **12**: 517-530.

Snowball, I., and Sandgren, P. 2004. Geomagnetic field changes in Sweden between 9000 and 450 cal BP: extending the record of "archaeomagnetic jerks" by means of lake sediments and the pseudo-Thellier technique. Earth and Planetary Science Letters, **227**: 361-376.

Snowball, I., Zillén, L., Ojala, A., Saarinen, T., and Sandgren, P. 2007. FENNOSTACK and FENNORPIS: Varve dated Holocene palaeomagnetic secular variation and relative palaeointensity stacks for Fennoscandia. Earth and Planetary Science Letters, **255**: 106-116.

Stoner, J.S., Channell, J.E.T., Howell, D.A., and Charles, C. 2003. A 580 kyr paleomagnetic record from the sub-Antarctic South Atlantic (ODP Site 1089). Journal of Geophysical Research Letters, **108**: 1-19.

Stoner, J.S., Jennings, A., Kristjansdottir, G.B., Dunhill, G., Andrews, J.T., and Hardardottir, J. 2007. A paleomagnetic approach toward refining Holocene radiocarbon based chronologies: Paleoceanographic records from North Iceland (MD99-2269) and East Greenland (MD99-2322) margins. Paleoceanography, **22**: 1-23.

Stoner, J.S., and St-Onge, G. 2007. Magnetic stratigraphy in paleoceanography: reversals, excursions, paleointensity and secular variation. *In* Proxies in Late Cenozoic Paleoceanography. *Edited by*: C. Hillaire-Marcel and A. de Vernal (Eds.), Elsevier, pp. 99-137.

St-Onge, G., Stoner, J.S., and Hillaire-Marcel, C. 2003. Holocene paleomagnetic records from the St. Lawrence Estuary: centennial- to millennial-scale geomagnetic modulation of cosmogenic isotopes. Earth and Planetary Science Letters, **209**: 113-130.

Stuiver, M., and Polach, H.A. 1977. Discussion: Reporting of 14C data. Radiocarbon, **19**: 355-363.

Stuiver, M., P.J., Reimer, E., Bard, J.W., Beck, G.S., Burr, K.A., Hughen, B., Kromer, G., McCormac, van der Plicht, J., and Spurk, M. 1998. INTCAL98 Radiocarbon Age Calibration, 24000-0 cal BP. Radiocarbon, **40:** 1041-1083.

Stuiver, M., Reimer, P.J., and Reimer, R.W. 2005. CALIB 5.0. Available from http://radiocarbon.pa.qub.ac.uk/calib/.

Tauxe, L. 1993. Sedimentary records of relative paleointensity: theory and practice. Reviews of Geophysics, **31**: 319-354.

Thomas, R., Guyodo, Y., and Channell, J.E.T. 2003. U-channel track for susceptibility measurements. Geochemistry Geophysics Geosystems, **1050** doi:10.1029/2002GC000454.

Thompson, R., and Oldfield, F. 1986. Environmental Magnetism. Allen & Unwin, London, United Kingdom.

Valet, J.-P. 2003. Time variations in geomagnetic intensity. Reviews of Geophysics, **41** doi:10.1029/2001RG000104.

Valet, J.-P., Herrero-Bervera, E., LeMouël, J.-L., and Plenier, G. 2008. Secular variation of the geomagnetic dipole during the past 2000 years. Geochemistry Geophysics Geosystems, **9**: 1-15.

Verosub, K., Mehringer, P. Jr., and Waterstraat, P. 1986. Holocene Secular Variation in Western North America: Paleomagnetic Record from Fish Lake, Harney County, Oregon. Journal of Geophysical Research, **91**: 3609-3623.

Weeks, R., Laj, C., Endignoux, L., Fuller, M., Roberts, A., Manganne, R., Blanchard, E., and Goree, W. 1993. Improvements in long-core measurement techniques: applications in palaeomagnetism and palaeoceanography. Geophysical Journal International, **114**: 651-662.

Zijderveld, J.D.A. 1967. AC demagnetization of rock: analysis of results. *In* Methods in Paleomagnetism. *Edited by*: Collinson, D.W., Creer, K.M., Runcorn, S.K. Elsevier, Amsterdam, pp. 254-286.

CHAPITRE 2

A HIGH-RESOLUTION HOLOCENE PALEOMAGNETIC SECULAR VARIATION AND A RELATIVE PALEOINTENSITY STACK FROM EASTERN CANADA

2.1 Abstract

A high-resolution Holocene paleomagnetic secular variation (PSV) and relative paleointensity (RPI) stack was constructed using u-channel paleomagnetic data from six radiocarbon-constrained marine sedimentary sequences raised along the main axis of the Laurentian Channel (eastern Canada), from its head to its mouth. Centennial- to millennial-scale declination and inclination features of the eastern Canadian stack can be correlated, within the dating uncertainties, with other Holocene North American, Icelandic and European PSV records, suggesting a common, possibly hemispheric in character, geomagnetic origin. Both magnetic inclination and declination of the eastern Canadian stack is generally consistent with the time-varying spherical harmonic model of the geomagnetic field CALS7k.2, notably during the last ~ 4000 cal BP. In addition, the eastern Canadian Holocene RPI stack reveals similar millennial and even centennial time-scale variations consistent with some virtual axial dipole moment (VADM) reconstructions derived from absolute paleointensity data as well as with North American lacustrine RPI records. Accordingly, these results suggest that the Holocene paleomagnetic secular variation in North America is significantly driven by large-scale (> 5000 km) geomagnetic field changes at these timescales.

`2.2 Introduction

In the last few years, a great improvement in the knowledge of the Earth magnetic field variability beyond the historical measurements (last ~ 400 years; e.g. Jackson et al., 2000) has been achieved. For instance, Laj et al. (2000) and Stoner et al. (2002) using high sediment accumulation-marine records from the North Atlantic and the South Atlantic respectively, have provided two high-resolution geomagnetic paleointensity stacks spanning the last ~ 80 kyr. However, if we focus on the Holocene period, much of the paleomagnetic secular variation (PSV) records were mainly derived from Northern Hemisphere continental lake sediments and full-vector reconstructions using stacked data from sedimentary sequences are still rare (e.g., Turner and Thompson, 1981; Stockhausen, 1998; King and Peck, 2001; Snowball et al., 2007). Combining paleomagnetic data from many PSV records has the advantage of reducing local lithological effects thus enhancing the true geomagnetic signal.

In addition, because the geomagnetic dipole moment affects the local cosmic ray rigidity cutoff (e.g., Elsasser et al., 1956) understanding the temporal variability of the geomagnetic field behaviour is the key factor to infer past solar activity (e.g., Solanki et al., 2004; Usoskin et al., 2006), as well as the long-term behaviour of the solar dynamo (Usoskin et al., 2007) derived from cosmogenic isotopes (^{14}C and ^{10}Be) in natural archives. On the other hand, using physic-based models, Kovaltsov and Usoskin (2007) and Usoskin et al. (2008) also highlighted the concomitant role of centennial geomagnetic and solar activity changes in affecting the regional tropospheric ionization, which provides new insights about the effect of cosmic rays on climate (e.g., Usoskin and Kovaltsov, 2008).

However, one of the major sources of incertitude in these physics-based models is an incomplete knowledge of how geomagnetic field varied in the past (e.g., Snowball and Muscheler, 2007).

In this paper, we provide the first radiocarbon-constrained Holocene paleomagnetic secular variation (PSV) and relative paleointensity (RPI) stack derived from six marine sedimentary sequences raised from the head to the mouth of the Laurentian Channel (eastern Canada). The quality and the accuracy of the stack are tested by comparing our record with other high-resolution Holocene Northern Hemisphere PSV and RPI records as well as the CALS7k.2 time-varying spherical harmonic model of the geomagnetic field (Korte and Constable, 2005). Lastly, we assess the North American geomagnetic field behaviour throughout the Holocene.

2.3 Geological setting

2.3.1 Stratigraphy and sedimentology

Piston cores MD99-2220, COR0602-36PC and COR0602-42PC (hereinafter 36PC and 42PC) were collected in the Lower St. Lawrence Estuary, whereas cores COR0503-CL03-35PC, COR0503-CL04-36 and COR0503-CL05-37 (hereinafter 35PC, CL04-36PC and 37PC) in the Gulf of St. Lawrence (Fig. 2.1; Table 2.1). Since the late 1970s, the Late Quaternary marine geology of the region was investigated by many authors using geophysical data principally derived from high-resolution seismic-reflection profiles (e.g., Syvitski and Praeg, 1989; Josenhans and Lehman, 1999; Duchesne et al., 2007; St-Onge et al., 2008; Duchesne et al., 2010), and by coring (e.g., Keigwin and Jones, 1995; Josenhans and Lehman, 1999; St-Onge et al., 2003, 2008; Cauchon-Voyer et al., 2008). Five major

stratigraphic units associated with the retreat of the Late Wisconsinan Ice Sheet and the establishment of postglacial conditions was recognized by Syvitsky and Praeg (1989) in the St. Lawrence Estuary. From the base to the top, these units were interpreted as: Unit 1, till or ice-contact sediments deposited by grounded glacial ice; Unit 2, ice-proximal, coarse-grained glaciomarine sediments deposited either during the rapid retreat of an ice terminus or in an ice-front stillstand setting; Unit 3, ice-distal, fine-grained glaciomarine sediments correlated to the Goldthwait Sea clays (Dredge, 1983) mapped onshore; Unit 4, paraglacial deltaic sediments; Unit 5, postglacial sediments deposited under modern oceanographic conditions. Based on detailed rock magnetic and sedimentological analyses performed on a long piston core (~ 51 m; core MD99-2220 utilized in this study) retrieved from the Lower St. Lawrence Estuary, St-Onge et al. (2003) confirmed the presence of units 3 and 5 reported by Syvisky and Praeg (1989), whereas St-Onge et al. (2008) cored and dated the ice-proximal glaciomarine unit (Unit 2 of Syvitski and Praeg 1989). Furthermore, during the last ~ 8500 cal BP, the mean sedimentation rate of core MD99-2220 was estimated to vary between ~ 1.2 and 4.2 m/kyr, whereas older glaciomarine sediments were deposited at rates higher than ~ 30 m/kyr (St-Onge et al., 2003). Similarly, using high-resolution seismo-stratigraphy and piston coring within the Gulf of St. Lawrence, Josenhans and Lehman (1999) identified, from the Late Pleistocene to the Holocene, till, glaciomarine sediments and postglacial muds. Moreover, Keigwin and Jones (1995) based on earlier studies on sedimentary sequences raised from the Gulf of St. Lawrence/Scotian margin region, observed distinctive changes in lithology from red terrigenous clays, silts and sand during the glaciation to brown and gray hemipelagic sediments on deglaciation.

Table 2.1. Coordinates of the selected cores.

Cores	Latitude (°N)	Longitude (°W)	Water depth (m)	Length (m)
MD99-2220	48°38.32'	68°37.93'	320	51.60
COR0602-42	49°07.193'	67°16.753'	320	7.53
COR0602-36	48°24.031'	69°14.328'	315	6.97
COR0503-CL03-35	46°24.5510'	58°53.6800'	380	7.59
COR0503-CL04-36	47°40.2860'	59°59.9850'	544	7.71
COR0503-CL05-37	48°20.0110'	61°29.9950'	408	7.90

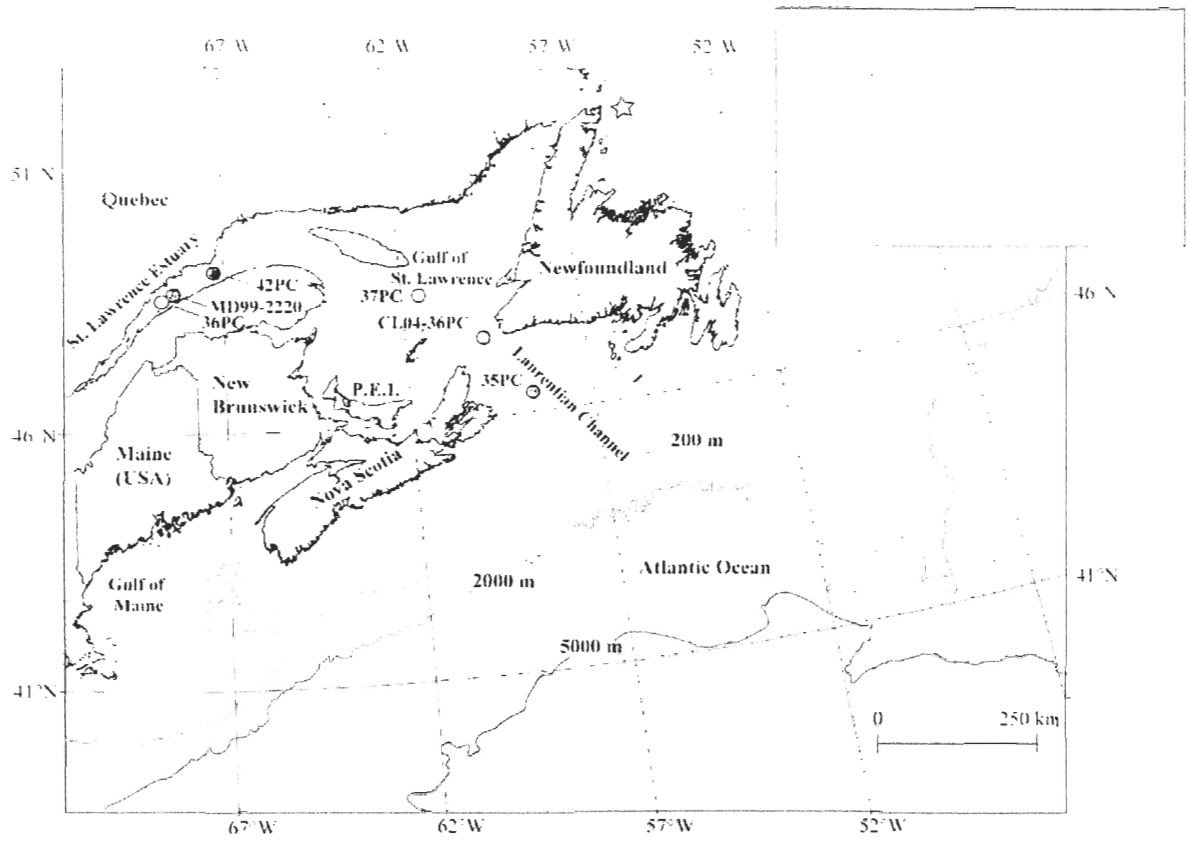

Fig. 2.1. Map of eastern Canada and location of the piston cores. The box in the inset shows the location of the study area whereas the open star indicates the first historical reading of magnetic declination made before 1590 AD according to Jonkers et al. (2003). Bathymetric contours at 200, 2000 and 5000 m, are also indicated. Modified from Shaw et al. (2002). P.E.I. = Prince Edward Island.

2.3.2 Holocene paleomagnetism in Eastern Canada: previous studies

According to Jonkers et al. (2003), only one direct measurement of magnetic declination was made offshore before 1590 AD northeast of Newfoundland (Fig. 2.1). Subsequently direct readings of the geomagnetic components (mainly magnetic declination) were made by European mariners in the Nova Scotia and Newfoundland margin area since 1590 AD. Apart from these historical measurements, a detailed paleomagnetic study (spanning the last ~ 8500 cal BP) from the St. Lawrence Estuary was conducted by St-Onge et al. (2003). This study revealed that the postglacial sediments from the St. Lawrence Estuary (core MD99-2220) preserved a millennial and even centennial time-scale reliable PSV and relative paleointensity (RPI) record. Other previous Holocene PSV studies come mainly from northern American continental lakes, notably: Fish Lake (Oregon, USA; Verosub et al., 1986), Lake St. Croix (Minnesota, USA; Lund and Banerjee, 1985), Lake Pepin (Minnesota, USA; Brachfeld and Banerjee, 2000) and the eastern US stack (obtained by combining PSV from three eastern North American lakes: Seneca Lake (New York), Lake LeBoeuf (Pennsylvania) and Sandy Lake (Pennsylvania); King and Peck, 2001). In addition, Hagstrum and Champion (2002) provided a Late Pleistocene to Holocene PSV record using ^{14}C-dated volcanic rocks from western North America.

2.4 Sampling and methods

Core MD99-2220 was collected during the IMAGES-V (International Marine Past Global Change Study) oceanographic campaign, in July 1999, on board the *Marion Dufresne II*, whereas all the other piston cores (PC) were collected on board the R/V

Coriolis II during two different cruises in June 2005 (COR0503) and 2006 (COR0602) respectively. The details of the methodology, as well as the results of core MD99-2220 utilized in this study are exhaustively described in St-Onge et al. (2003) and will not be further discussed.

On board the R/V *Coriolis II*, cores CL04-36PC, 35PC, 36PC, 37PC and 42PC were recovered using a modified version of a Benthos^{TM} piston corer, allowing the sampling of cores up to 7.90 m. All coring sites were targeted using high-resolution seismic profiles indicating high sediment accumulation areas not influenced by turbidites or other mass wasting events.

2.4.1 Multisensor Core Logger

On board, the cores were run into a GEOTEK Multisensor Core Logger (MSCL; e.g., St-Onge et al., 2007) for the determination of wet bulk density by gamma ray (γ) attenuation and volumetric magnetic susceptibility (k_{LF}). Both measurements were performed at 1 cm intervals. The values of k_{LF} primarily reflect changes in the ferrimagnetic concentration (e.g., magnetite or titanomagnetite), but are also sensitive to grain size variations (e.g., Dunlop and Özdemir, 1997). The γ–ray attenuation values, after proper calibration procedure, provide the wet bulk density of the sediment (St-Onge et al., 2007).

2.4.2 Diffuse spectral reflectance

Diffuse spectral reflectance (sediment color) data were acquired using an X-Rite DTP22 hand-held spectrophotometer immediately after splitting the cores at 5 cm intervals. Subsequently, the data were converted into the CIE (*Commission Internationale de l'Éclairage*/International Commission on Illumination) L* a* b* (L*, lightness; a*, from green to red; b*, from blue to yellow) colour space. In paleomagnetism, a* can be a useful parameter to detect variations in high-coercivity red minerals such as hematite (e.g., St-Onge et al., 2007).

2.4.3 Grain size

All grain size analyses were performed using a Beckman-Coulter LS-13320 (0.04 to 2000 μm) laser diffraction analyzer at 10 cm intervals. About 2 g of wet sediment were mixed in a solution of 20 gL^{-1} of Calgon electrolytic solution (sodium hexametaphosphate) and water. The samples were rotated for at least 3 hours using an in-house rotator and then sieved over the instrument (2 mm) prior to analysis. All the particle size distributions output were then processed using the Gradistat software (Blott and Pye, 2001). An average of at least two measurements was used for the calculations.

2.4.4 Magnetic remanence analyses

The natural remanent magnetization (NRM) was measured on u-channel samples using a high-resolution cryogenic magnetometer (2G Enterprises Model SRM-755) at 1 cm intervals. In order to isolate the characteristic remanent magnetization (ChRM), the NRM

was measured and progressively demagnetized using stepwise peak alternating fields (AF) up to 70 mT in 5 mT steps. Magnetic declination (Dec) and inclination (Inc) of the ChRM (labelled as ChRM Dec and ChRM Inc, respectively) were calculated at 1 cm intervals using the standard principal component analysis (PCA) of Kirschvink (1980). Since the cores were not azimuthally oriented, the ChRM Dec profiles are relative. The precision of the best-fit procedure was estimated by the maximum angular deviation (MAD; Kirschvink, 1980). In the context of PSV and RPI studies of Quaternary marine sediments, MAD values below 5^{o} are often considered as high quality data (Stoner and St-Onge, 2007).

An anhysteretic remanent magnetization (ARM) was imparted using a 100 mT AF field with a 50 μT direct current (DC) biasing field. The ARM was measured following progressive AF demagnetization up to 50 mT with steps every 5 mT. The ARM was also expressed as anhysteretic susceptibility (k_{ARM}) by normalizing the ARM with the biasing field. The k_{ARM} versus k_{LF} diagram was used to assess the extent and uniformity of the magnetic grain size distribution (King et al., 1983). An isothermal remanent magnetization (IRM) was imparted to the z axis of the u-channels with a DC pulse field of 0.3 T using a 2G Enterprises pulse magnetizer. The IRM was then demagnetized as the same AF steps of the ARM. Lastly, the median destructive fields of the NRM, ARM and IRM (labelled as MDF_{NRM}, MDF_{ARM} and MDF_{IRM}, respectively; i.e., the value of the peak AF necessary to reduce the magnetic remanence to half of its initial value) were calculated using the software developed by Mazaud (2005). In the case of single NRM component, the MDF_{NRM} reflects the mean coercivity state of the magnetic grain assemblage which in turn depends on both the grain-size and the mineralogy (e.g., Dunlop and Özdemir, 1997).

Furthermore, if the magnetic mineralogy is mainly controlled by single-domain (SD)/pseudo single domain (PSD) magnetite, the MDF_{IRM} are lower than MDF_{ARM} values (Dunlop and Özdemir, 1997). Accordingly, the use of these three parameters provides some indications concerning magnetic mineralogy and grain size variations.

2.4.5 Hysteresis properties and IRM acquisition curves

Hysteresis properties were measured using an alternating gradient magnetometer (AGM) MicroMag 2900 from Princeton Measurement Corporation on some pilot samples at intervals with important changes in the diffuse spectral reflectance measurements (a* profiles). Hysteresis loops along with backfield remanence curves were used to determine saturation magnetization (Ms), coercive force (Hc), saturation remanence (Mrs) and coercivity of remanence (Hcr). The ratios Mrs/Ms and Hcr/Hc can be used as grain size proxies (the so-called Day plot) as well as to identify the magnetic domain state when the principal remanence-carrier mineral is magnetite (Day et al., 1977). Lastly, a stepwise IRM acquisition was conducted on the AGM applying a magnetic induction field up to ~ 1 T. This type of experiment is useful to determine the range of coercivities over which significant acquisition occurs (e.g., Jackson, 2007).

2.4.6 Radiocarbon dating

The chronology of each core was determined using AMS-^{14}C measurements on marine shell fragments for a total of 28 dates (Supplemental materials, Table A). All radiocarbon ages were calculated using Libby's half-life and corrected for natural and

sputtering fractionation ($\delta^{13}C$= -25 ‰ versus Vienna Pee-Dee Belemnite (VPDB)) following the convention of Stuiver and Polach (1977). The conventional ^{14}C ages were then calibrated using the on-line CALIB 5.0.2 software (Stuiver et al., 2005) and the Hughen et al. (2004) marine dataset. A standard marine reservoir correction of ~ 400 years (ΔR=0) to account for the apparent age of dissolved inorganic carbon in high-latitude North Atlantic waters was applied to all dates (Bard, 1998). The chronology of each core is presented only between the uppermost and lowermost radiocarbon dates.

2.5 Results

2.5.1 Stratigraphy

As revealed from grain size measurements, the overall trend in the mean grain size of all cores appears quite similar (Fig. 2.2). As a whole, the sediments of all cores consist of two distinct sedimentary units. The upper unit is composed of dark gray, bioturbated silty clays to sandy mud, whereas the lower unit is composed of lighter gray and relatively homogenous, slightly bioturbated to massive clayey silts to silty clays (Fig. 2.2). According to the previous studies of Josenhans and Lehman (1999) and St-Onge et al. (2003), the lowermost and the uppermost units were interpreted as glaciomarine and postglacial sediments, respectively. As depicted from Fig. 2.2, the transition from the two units is sharp (see also St-Onge and Long 2009), seems synchronous and clearly evident along the West-East coring transect, suggesting a possible common origin. As already pointed out by St-Onge et al. (2003), the best candidate to explain this transition could be the re-rerouting of the Laurentide Ice Sheet meltwaters through Hudson Bay and Strait

following the catastrophic drainage of the glacial Lake Agassiz-Ojibway at ~ 8470 cal BP (e.g., Barber et al., 1999; Lajeunesse and St-Onge, 2008).

2.5.2 Chronology

Five age models were constructed using the available calibrated ages on a composite depth-scale corrected for the missing sediment due to the piston coring process (Supplemental materials, Fig. A). Apart from 42PC, where a linear fit was used (R = 0.998), a third degree polynomial fit was utilized for cores 36PC (R = 0.994) and 35PC (R = 1) whereas an interpolation function was used for cores CL04-36PC and 37PC (Fig. 2.3). An abrupt change in the mean sedimentation rate of core 37PC from ~ 190 to ~ 40 cm/kyr is observed, at around 8500 cal BP. An important change in sedimentation rates is also observed in core MD99-2220 (St-Onge et al., 2003) and was previously associated with an important reduction in sediment inputs following the re-routing of the Laurentide Ice Sheet meltwaters from the St. Lawrence Estuary to the Hudson Bay and Strait after the outburst flood of Lake Agassiz-Ojibway. Unfortunately, the dating of core 36PC and 42PC does not go far back in time to see that transition, whereas in the two cores located at the most seaward locations and possibly due to the scarcity of dated material prior to ~ 8500 cal BP, no drastic changes in the sedimentation rates are apparent throughout the Holocene.

Fig. 2.2. Mean grain size against depth. Also illustrated are the calibrated ages (see text for details). Glaciomarine and postglacial sediments are indicated with the gray and olive area, respectively. The grain size data were computed using the Gradistat software (Blott and Pye, 2001). The sediment texture is indicated on the right of each diagram. St-c = Silty clays; C-st = Clayey silts; St = Silts; S-md = Sandy muds.

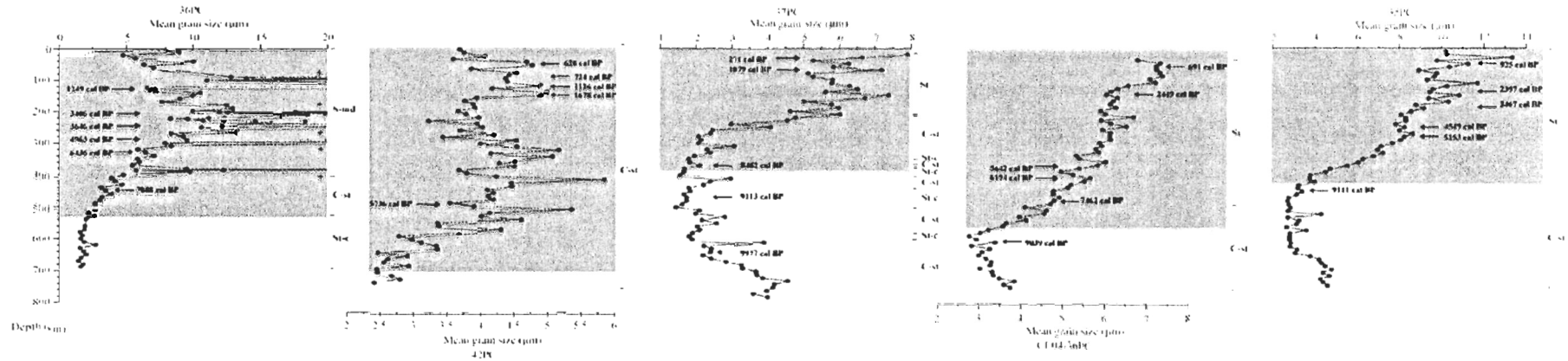
Postglacial sediments
Glaciomarine sediments

Fig. 2.3. Age models. The vertical dash line depicts the important change in the sedimentation rates observed in cores 37PC and MD99-2220 from the Lower St. Lawrence Estuary at ~ 8500 cal BP (see text for details).

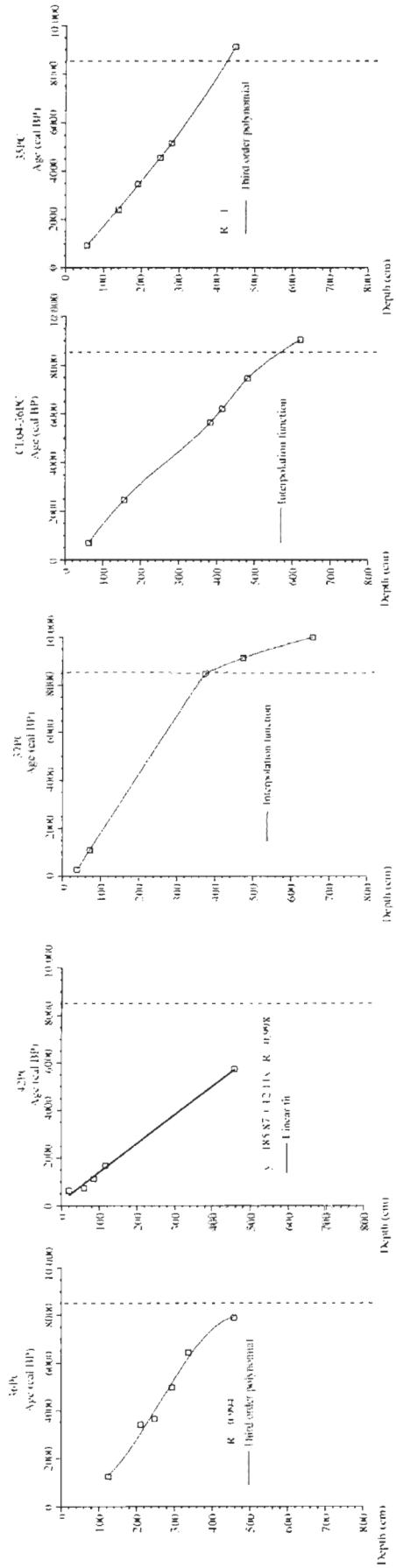
Age (cal BP)
Depth (cm)
Third order polynomial
Interpolation function
Linear fit

2.5.3 Magnetic mineralogy and grain size

As revealed by the k_{ARM} versus k_{LF} diagrams (Supplemental materials, Fig. B; King et al., 1983), magnetic granulometry of cores 36PC and 42PC are compatible with the presence of magnetite in the ~ 1-5 and ~ 0.1-15 μm grain-size range, respectively. In contrast, magnetite grain size of cores 35PC, CL04-36PC and 37PC is comprised between 1 and ~ 15 μm. Both hysteresis loops and IRM acquisition curves indicate saturation fields below ~ 150 mT and coercivities typical of magnetite (e.g., Dunlop and Özdemir, 1997; Supplemental materials, Fig. C). However, an applied field of ~ 600 mT was necessary to saturate the sample at 758 cm of core 37PC indicating also the presence of a high-coercivity magnetic mineral (Supplemental materials, Fig. C). On the other hand, the MDF_{NRM} and MDF_{ARM} values range between 25 and ~ 30 mT for all cores whereas the MDF_{IRM} values are lower (Supplemental materials, Fig. D). These values are compatible with the presence of magnetite as the dominant ferrimagnetic mineral. According to the Day plot, much of the pilot samples (selected in intervals of apparent lithological changes) fall in the coarse end of the PSD region (Supplemental material, Fig. E). However, some data points are not comprised in the usual SD/MD mixing line implying either a different magnetic state domain distribution or a more complex magnetic mineralogy (or both). Theoretical calculations show that a mixture of SD/MD and superparamagnetic (SP) particles (the maximum size for SP behaviour is generally taken to be ~ 30 nm; Dunlop, 1973) with increasing grain size tends to increase the Hcr/Hc ratio outside the usual PSD region for synthetic magnetite (e.g., Krása and Fabian 2007 and references therein).

2.5.4 Paleomagnetism

For all cores, a stable, well-defined paleomagnetic direction was isolated by PCA analysis (Kirschvink, 1980) using at least 5 consecutive AF steps at peak field between 15 and 70 mT. MAD values are almost always lower than 10° and in most of the cores lower than 5° (Fig. 2.4). Nevertheless, in some intervals of cores CL04-36PC and 35PC, the ChRM is not as well-defined as indicated by MAD values higher than 5°. These intervals are likely associated with a more complex magnetic mineralogy as reflected by changes in MDF and a* profiles (Supplemental materials, Figs. D and F) as well as a coarse sediments texture (Fig. 2.2). In addition, the upper ~ 150 cm of core 35PC are characterized by high-amplitude variations of the ChRM Inc. This is probably due to coring disturbance. However, apart from these intervals, all the ChRM Inc values fluctuate around the expected inclination (I_{GAD}) calculated with the geocentric axial dipole (GAD) model, (Fig. 2.4) thus supporting a coherent record of the PSV of the geomagnetic field.

2.5.5 Relative paleointensity determinations (RPI)

Estimation of relative paleointensity of the geomagnetic field in sedimentary sequences is obtained by dividing the measured NRM by an appropriate normalizer in order to compensate for the variable concentration of ferrimagnetic minerals (Tauxe, 1993). Concentration-dependent parameters such as ARM, IRM or k_{LF} are generally employed as normalizer. The use of IRM as a normalizer was successfully employed by St-Onge et al. (2003) for core MD99-2220 using the criteria proposed by Tauxe (1993) and King et al. (1983). Following the recommendations proposed by Stoner and St-Onge

(2007) for Quaternary RPI studies, the NRM should be characterized by a strong, well-defined single component magnetization with MAD values <5° carried by magnetite in the ~ 1-15 μm (SD/PSD) grain-size range (e.g., Dunlop and Özdemir, 1997). Moreover, due to the effect of magnetostatic interaction between ferrimagnetic particles on the ARM acquisition (Sugiura, 1979), concentration of magnetite should not vary downcore by more than a factor of 10 (Tauxe, 1993). As previously discussed, the magnetic mineralogy is compatible with the presence of magnetite in the PSD grain-size range (Supplemental materials, Fig. B). Furthermore, the ChRM is also well-defined (MAD < 10°; Fig. 2.4) whereas the low-field magnetic susceptibility varies within a factor of 10 (Supplemental materials, Fig. F).

The choice for the appropriate normalizer can be discussed in several ways (see review of Valet 2003). Levi and Banerjee (1976) suggested using the remanence whose demagnetization curve most closely resembles that of NRM. This can be assessed by comparing the AF coercivity spectra of the NRM, ARM and IRM. As depicted from Fig. G (Supplemental materials; left diagrams) coercivity spectra of the ARM and NRM are nearly identical in the selected coercivity windows (shaded regions) while that of the IRM is much softer. Furthermore, the ratio of NRM/IRM (and hence the assumed paleointensity) is more sensitive to the AF field used for demagnetization than the NRM/ARM ratio (Supplemental materials, Fig. G; right diagrams). Based on these results, the ARM activates the same magnetic assemblages carried by the NRM and therefore is the preferred normalizer for all cores. Lastly, to construct the RPI proxies, we calculate the average of the NRM/ARM ratio over the 20-30 mT AF range and then divided each mean by the standard deviation.

Fig. 2.4. Characteristic remanent magnetization (ChRM) declination (Dec) and inclination (Inc) as well as the corresponding maximum angular deviation (MAD) values (the vertical solid line in the MAD diagrams is the 5°). The broken vertical lines in the ChRM Inc diagrams represent the expected magnetic inclination (I_{GAD}) according to a geocentric axial dipole (GAD) model. Note that the ChRM Dec values are relative.

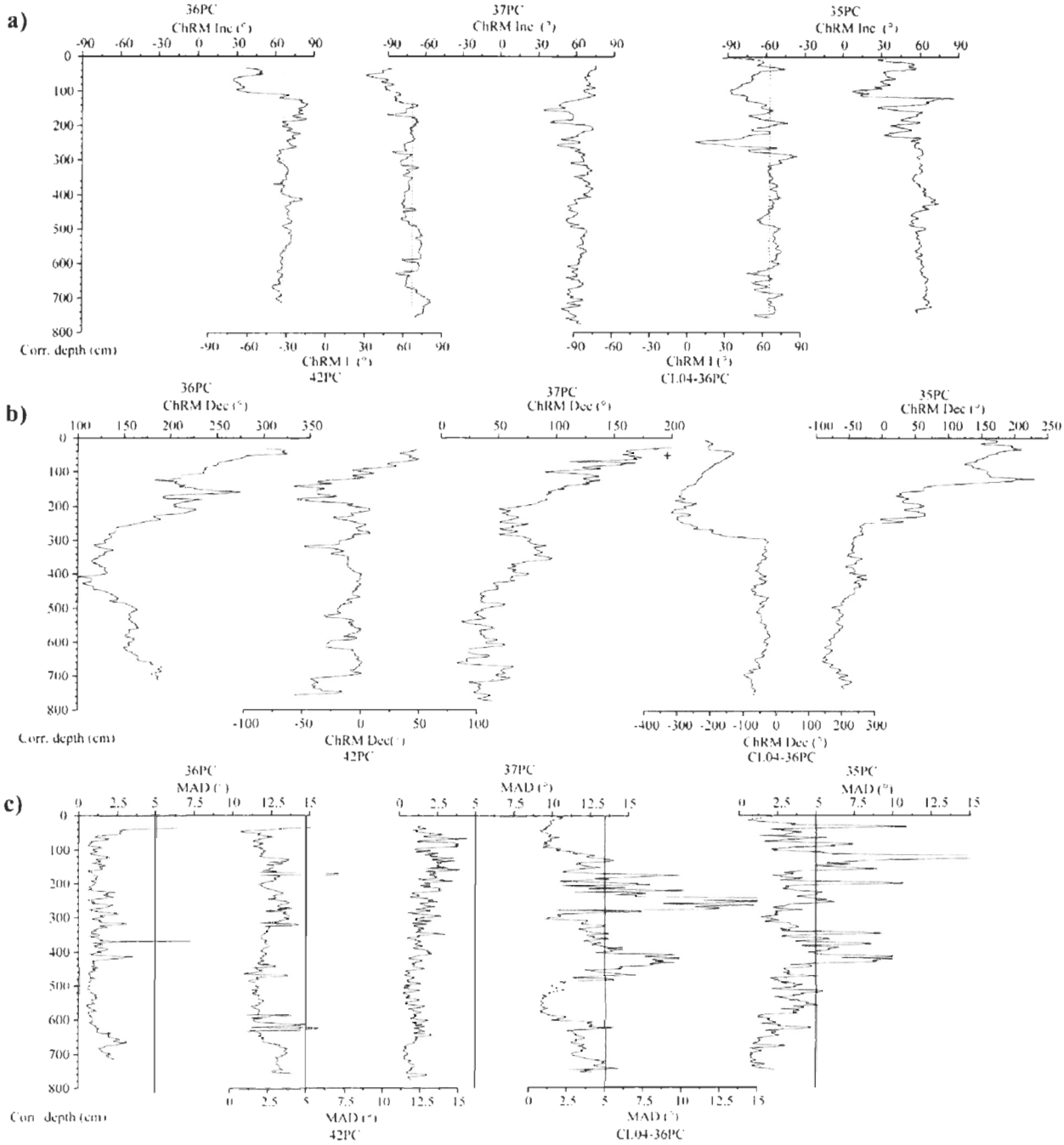
a)
36PC
ChRM Inc (°)
37PC
ChRM Inc (°)
35PC
ChRM Inc (°)
Corr. depth (cm)
ChRM I (°)
42PC
ChRM I (°)
CL04-36PC
b)
36PC
ChRM Dec (°)
37PC
ChRM Dec (°)
35PC
ChRM Dec (°)
Corr. depth (cm)
ChRM Dec (°)
42PC
ChRM Dec (°)
CL04-36PC
c)
36PC
MAD (°)
37PC
MAD (°)
35PC
MAD (°)
Corr. depth (cm)
MAD (°)
42PC
MAD (°)
CL04-36PC

2.5.6 Paleomagnetic data distribution

Two frequency histograms were constructed for the paleomagnetic direction and RPI stacks according to bins of 500 yr (Supplemental materials, Fig. H). The sample population for the directional and RPI data are 3441 and 3422, respectively. During the period between 8500 and 8000 cal BP, a maximum in the number of data points is observed (~ 260). As discussed in the previous section, this period corresponds to an important increase in sediment accumulation rate. In contrast, in the period earlier than 9000 cal BP and after 500 cal BP the number of data points does not exceed 100 due to coring disturbance in the uppermost part of the records and the limited ^{14}C ages in each individual record.

2.5.7 Construction of the stack

Because changes in the ChRM Dec profile of each core and the ones from previously published papers are relative, the ChRM Dec of each sedimentary sequence was initially standardized by subtracting from each ChRM Dec value the arithmetic mean and then dividing by the standard deviation. All these new variables are thus characterized by an arithmetic mean of zero and a standard deviation of 1. The same procedure was performed for the RPI records. In contrast, no treatment was necessary for the ChRM Inc as the values are absolute and vary between 0° and 90°. Subsequently, all the records were combined according to their own chronology. As revealed from Figs. 2.5 and 2.6, similar magnetic directional and relative paleointensity features can be easily detected among the records suggesting the geomagnetic field as the principal source of these variations.

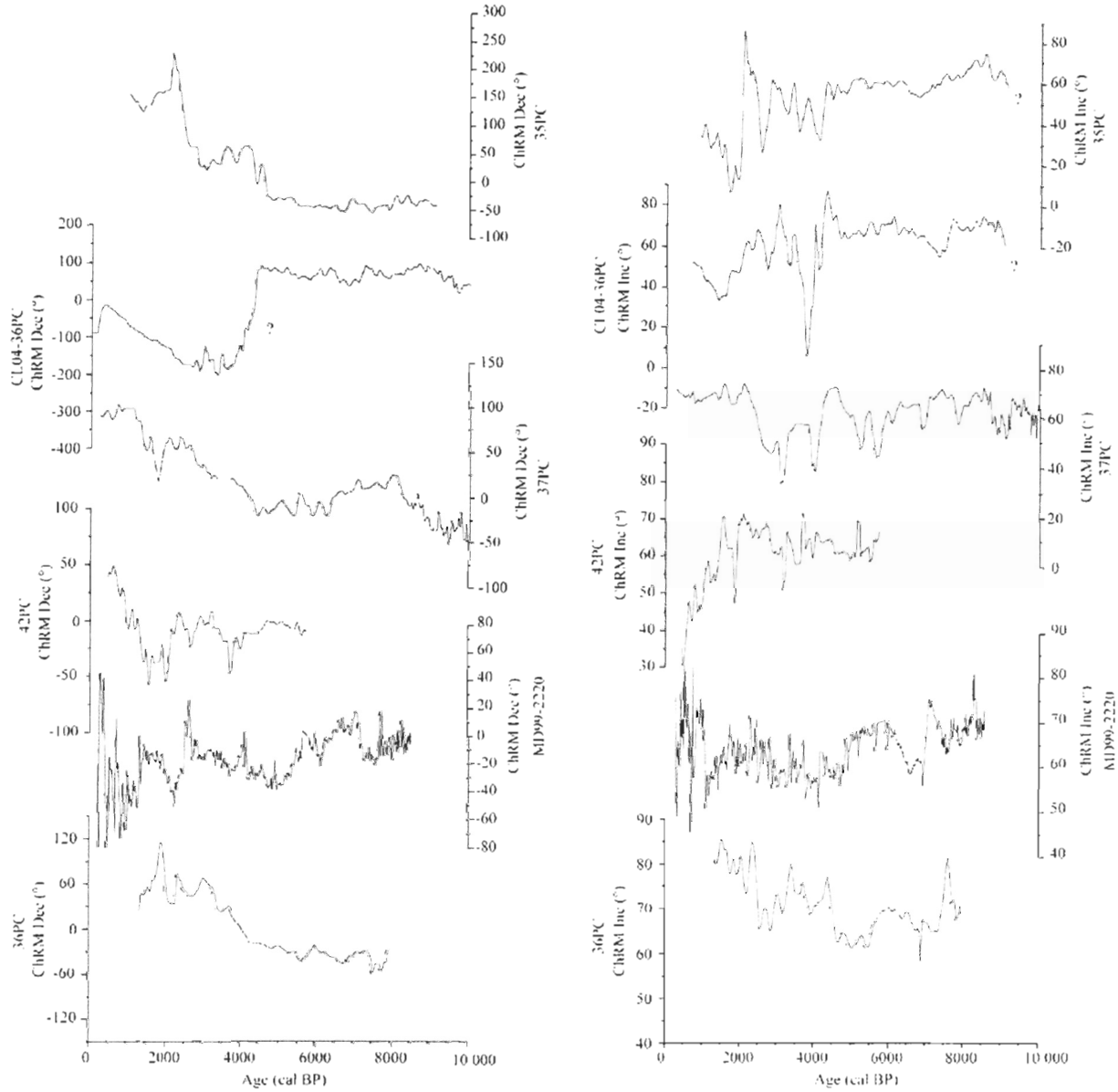

Fig. 2.5. Declination (left diagrams) and inclination (right diagrams) profiles for the six sedimentary sequences on their own chronologies. Some correlative magnetic features are indicated.

Fig. 2.6. Relative paleointensity (RPI) records for all cores displayed on their own chronology. Correlative paleointensity features are indicated (p-1 to p-6).

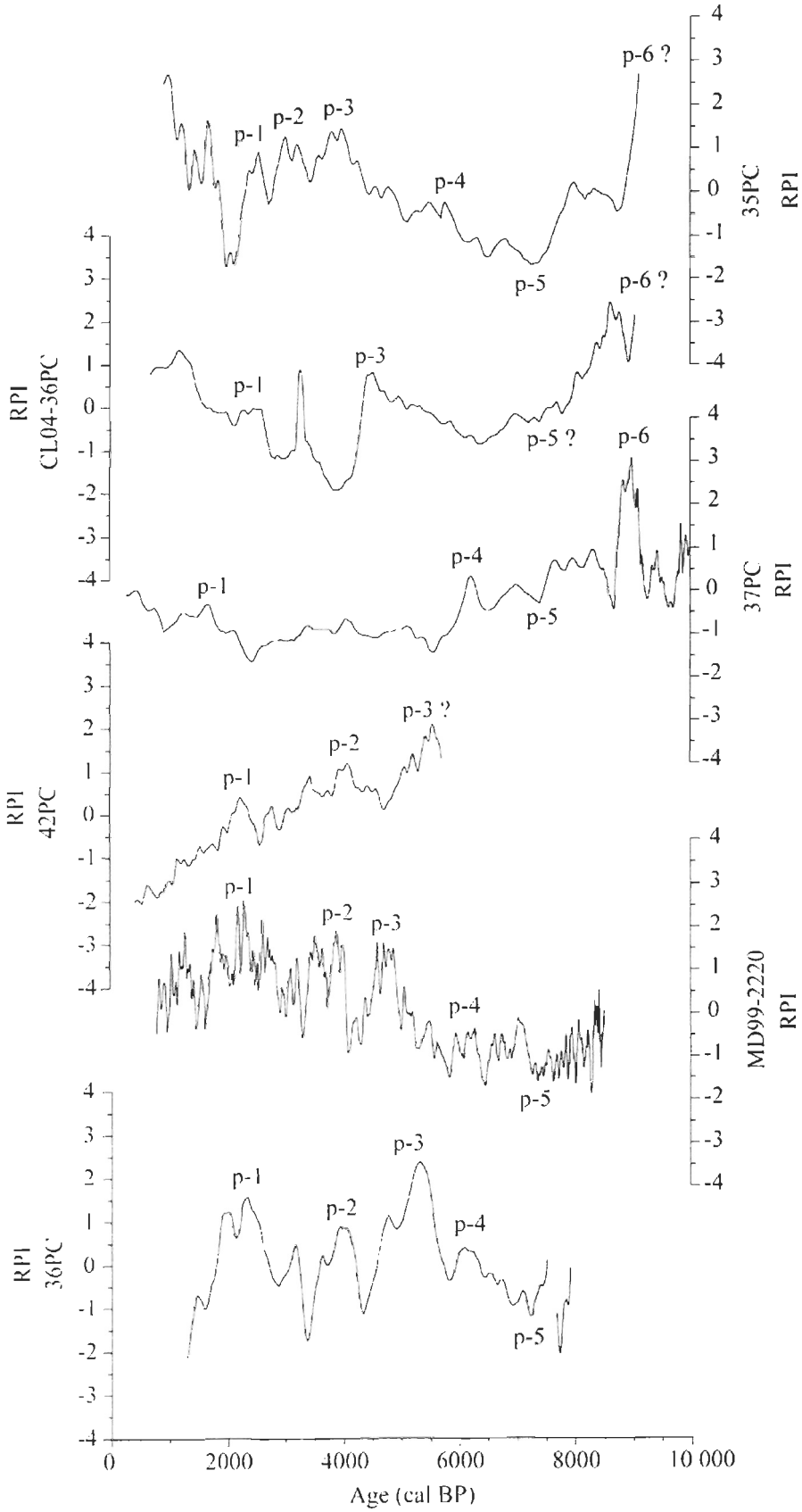
RPI
CL04-36PC
p-1
p-2
p-3
p-4
p-5
p-6 ?
35PC
RPI
p-1
p-3
p-5 ?
p-6 ?
37PC
RPI
p-1
p-4
p-5
p-6
RPI
42PC
p-1
p-2
p-3 ?
MD99-2220
RPI
p-1
p-2
p-3
p-4
p-5
RPI
36PC
p-1
p-2
p-3
p-4
p-5
0
2000
4000
6000
8000
10 000
Age (cal BP)

Nevertheless, some discrepancies are observed in the amplitude of the PSV and RPI individual records. Differences in the amplitude of these records can originate from true changes in geomagnetic field, different sedimentation rates (Fig. 2.3), lock-in processes as well as the nature of the sediment (Fig. 2.2). Other possible non-magnetic causes of variation can be ascribed to sediment coring artefacts, sediment deformation and analytical errors. Furthermore, another source of incertitude reflected in the offset between the peaks and the troughs is associated with the chronology of each individual record. Accordingly, some smoothing of the data is needed to enhance the signal/noise ratio (i.e. geomagnetic signal versus local environmental effects). A 20-point smoothing was applied to all data in order to reduce the high-frequency scatter. Subsequently, upper and lower 95% confidence limits associated to each smoothed value (X) were calculated using the formula

$$\text{Upper (lower) limit } 95\% = X \pm (\text{SEM} \cdot 1.96),$$

where SEM is the standard error of the mean and 1.96 is the approximate value of the 0.975 quantile of the normal distribution (e.g.,Taylor, 1997).

2.6 Discussion

2.6.1 Holocene Northern Hemisphere paleomagnetic secular variation comparison

Fig. 2.7 shows the magnetic declination and inclination profiles of the eastern Canadian stack along with North American PSV records from Fish Lake (Oregon, USA; Verosub et al., 1986), Lake St. Croix (Minnesota, USA; Lund and Banerjee, 1985), Lake Pepin (Minnesota, USA; Brachfeld and Banerjee, 2000), the eastern US stack (King and

Peck, 2001) and the PSV record from lava flows (western North America; Hagstrum and Champion, 2002). In order to assess the spatial extent of the PSV features, the Icelandic (Stoner et al., 2007) and the Fennoscandian stack records (Snowball et al., 2007) are also displayed. As observed from Fig. 2.7, a large number of magnetic declination and inclination features can be easily correlated within the North American and even in the European regions suggesting that such directional patterns are likely hemispheric in scale. Notably, a large magnetic declination swing is observed at ~ 2500 cal BP in all records. This magnetic feature ("f-event") was previously noted in Northern lacustrine European PSV records by Turner and Thompson (1981) and more recently it has also been observed in two other PSV records from Icelandic lakes (Olafsdottir et al., 2009). The different nature of these records (marine, lacustrine and volcanic) further corroborates the geomagnetic origin of these records. However, as already discussed by St-Onge et al. (2003), much of the temporal offset observed among the North American PSV records could be ascribed to the dating technique, lock-in processes as well as incertitude in the age models used. Furthermore, the main problem with radiocarbon dating of bulk carbon from lacustrine sediment is the contamination by "old" carbon. For instance, for the Lake St. Croix (Lund and Banerjee, 1985) and in the construction of the eastern US stack (King and Peck, 2001) records, the authors systematically corrected each radiocarbon date for "old" carbon contamination assuming that the same correction was valid throughout the Holocene. The same potential chronological offset could be found in the Lake Pepin record, where the chronology was partially obtained after paleomagnetic correlation with the Lake St. Croix record. In addition, "old" carbon contamination was also evocated by Hagstrum and Champion (2002) to explain the ~ 280 year offset observed between the Fish

Lake and lava flows records for the last ~ 3500 yr BP. Similarly, even if marine carbonates dated with the AMS-^{14}C dating method are not affected by this problem, an unknown (and variable) reservoir age effect could lead to an error in the age determination. Based on these considerations, all the proposed correlations are most likely within dating uncertainties and not different in their timing.

Fig. 2.7. Comparison of Holocene PSV records from the Northern Hemisphere. Declination (left diagrams) and inclination (right diagrams) profiles of the eastern Canadian stack compared with the Fish Lake (Oregon, USA; Verosub et al., 1986), Lake St. Croix (Minnesota, USA; Lund and Banerjee, 1985), Lake Pepin (Minnesota, USA; Brachfeld and Banerjee, 2000), eastern US stack (King and Peck, 2001) and the PSV from lava flows records (orange squares in the web version; Hagstrum and Champion, 2002). The PSV Icelandic and Fennoscandian stacks are from Stoner et al. (2007) and Snowball et al. (2007), respectively. The black curve in the Icelandic record is a weighted function applied to the raw data (gray curve in the web version) whereas the dotted curves in the relative inclination record from Fennoscandia are 95% confidence limits. The Fish Lake data were calibrated using the Stuiver et al. (1998) radiocarbon calibration curve (K. Verosub, personal communication, 2008). Lakes St. Croix, Pepin and the eastern US stack records were calibrated using the atmospheric data from Reimer et al. (2004). Proposed correlative declination and inclination features are indicated. The magnetic declination swing at ~ 2500 cal BP is labelled as the "f-event" (see text for details). The black curve in the eastern Canadian stack represents a 20-point smoothing of the data whereas the light gray shaded area represents upper and lower 95% confidence limits. All the declination data were standardized to allow direct comparison. Note that the inclination scales are not identical.

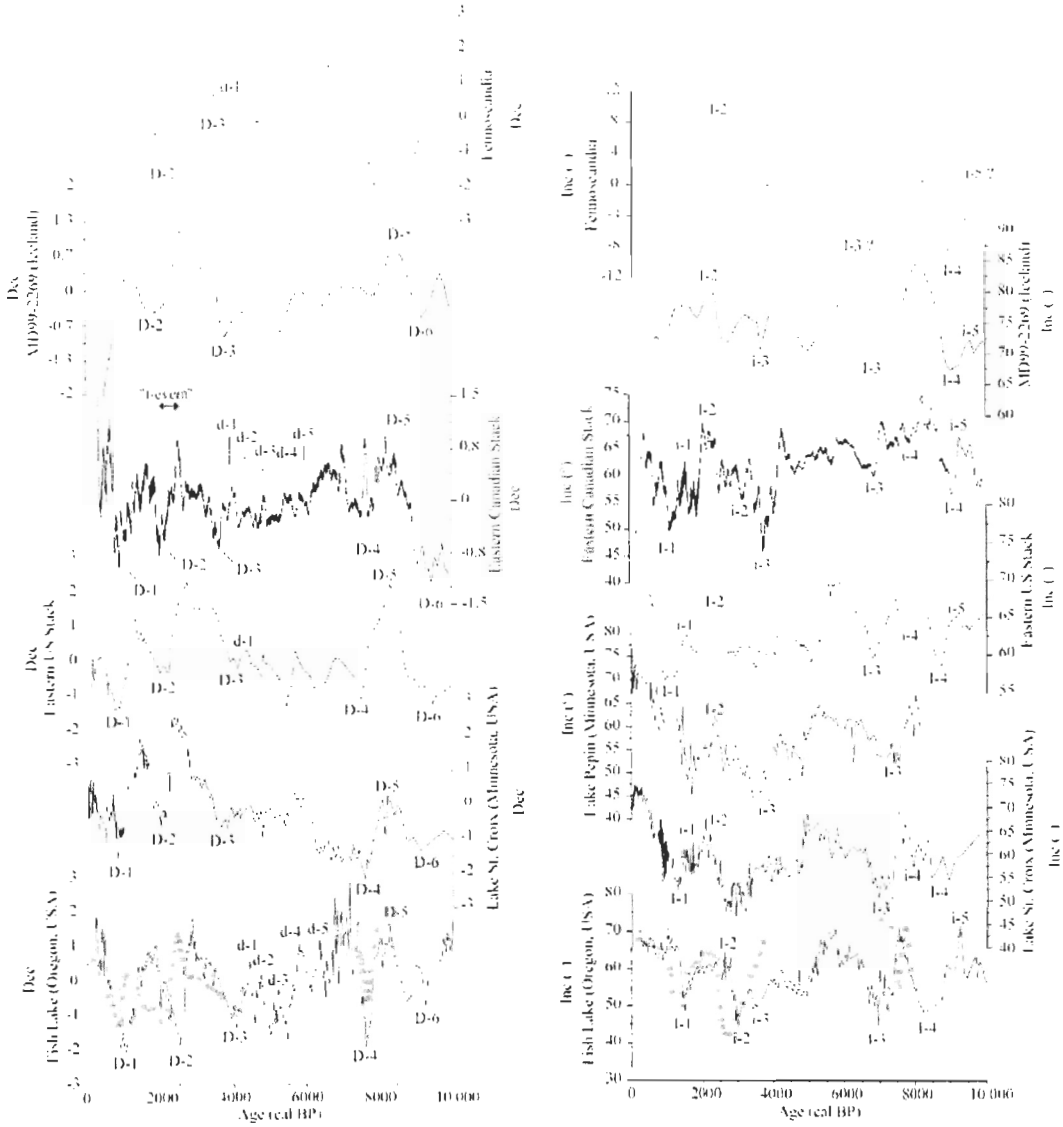
Dec
MD99-2269 (Iceland)
Fennoscandia
Eastern Canadian Stack
Eastern U.S. Stack
Lake St. Croix (Minnesota, USA)
Fish Lake (Oregon, USA)
Lake Pepin (Minnesota, USA)
Inc ( )
"reversal"
Age (cal BP)
0
2000
4000
6000
8000
10 000

2.6.2 Eastern Canada PSV stack versus the CALS7k.2 model

As observed from Fig. 2.8, a general agreement is found between the eastern Canadian PSV stack and the time-varying spherical harmonic model of the geomagnetic field CALS7k.2 (Korte and Constable, 2005). Much of the directional features detected in Fig. 2.8 are well reproduced in the CALS7k.2 model, notably for the last ~ 4000 cal BP. The "f-event" is also well reproduced. Despite the limitation due to both the time resolution (~ 100 years) and the heterogeneous coverage of the northern American PSV database used to constrain the model, much of the northern American directional features are thus quite well reproduced by CALS7k.2.

2.6.3 Eastern Canadian RPI stack versus global dipole moment compilations and North American RPI records

The smoothed relative paleointensity stack from eastern Canada was compared to several global Holocene dipole moment (DM) reconstructions (Fig. 2.9). Apart from the synthetic record Ohno and Hamano (1993) based on a compilation of selected paleomagnetic directional data, both the recent paleointensity reconstructions of Knudsen et al. (2008) and Kovacheva et al. (2009) are based on absolute archeointensity data. The virtual axial dipole moment (VADM) spanning the last 7000 cal BP as expected from the CALS7k.2 model is also considered and illustrated in Fig. 2.9. As depicted from Fig. 2.9, the RPI record of the eastern Canadian stack reveals similar millennial-scale variations with both the record of Ohno and Hamano (1993) and Knudsen et al. (2008) between ~ 4000 and 10 000 cal BP. Interestingly, a common broad peak in the paleointensity is

observed between these two DM reconstructions and the RPI stack at ~ 9000 cal BP. Barletta et al. (2008) already recognised this magnetic feature in a long Holocene piston core retrieved from the Chukchi Sea (Arctic Alaskan margin) and recently Snowball et al. (2010) observed an analogous paleointensity peak between 8200 and 9000 cal BP in a Holocene marine sedimentary sequence collected from the Disko Bay (Western Greenland) thus supporting a geomagnetic origin of this feature. In addition, if we focus on the period between 1000 and 4000 cal BP, a good agreement is observed between the eastern Canadian RPI stack and the other North American RPI records as well as with the VADM reconstruction of Knudsen et al. (2008) (Fig. 2.10). Many sub-millennial RPI features can be clearly correlated, within the dating uncertainties, among the records suggesting a common geomagnetic origin. On the other hand, the VADM values computed with the CALS7k.2 model reveal more discrepancies compared to the RPI stack both in term of fluctuation and amplitude (Fig. 2.10) as well as they systematically underestimate the reconstructed VADMs of Knudsen et al. (2008) and Kovacheva et al. (2009) (Fig. 2.10). Korte and Constable (2005b) attributed this overestimation in the reconstructed VADMs due to the presence of persistent non-dipole magnetic fields aggravated by strong regional bias in data distribution. Conversely, Knudsen et al. (2008) and Valet et al. (2008) invoked an unequal repartition of energy to higher harmonics to minimize the misfit between the inversion procedure and the data as the cause of the reduction of the global dipole moment derived from the CALS7k.2 model. However, based on the results displayed in Figs. 2.9 and 2.10 the dipole field seems to significantly drive the observed variations in the reconstructed RPI stack throughout the Holocene.

Fig. 2.8. Comparison between the eastern Canadian PSV stack and the CALS7k.2 model (Korte and Constable, 2005). (A) and (B) diagrams show the inclination (Inc) and declination (Dec) with associated 95% confidence limits (light gray shaded area), respectively. The correlative magnetic directional features illustrated are the same as labelled in Fig. 7. Note that the inclination scales are not identical.

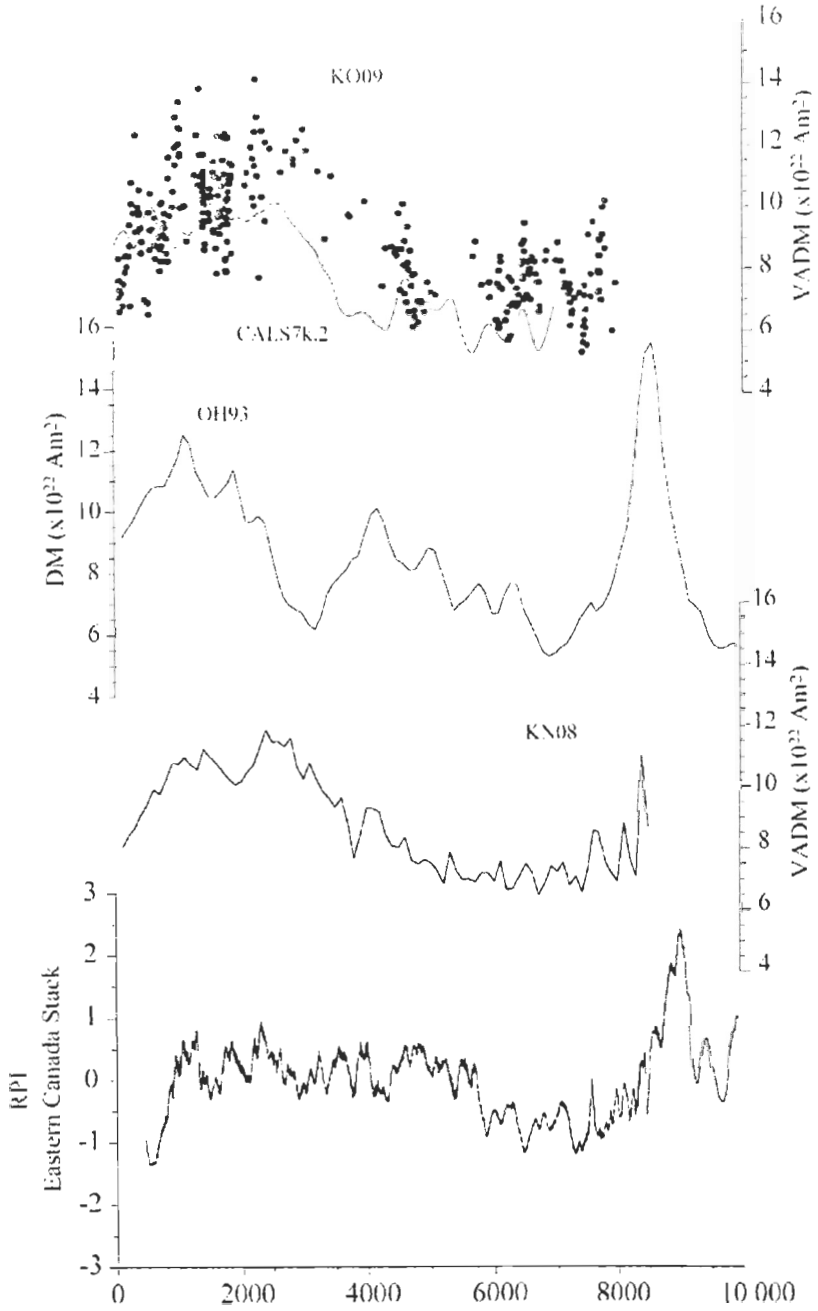
KO09
CALS7K.2
OH93
KN08
DM (x10²² Am²)
VADM (x10²² Am²)
RPI
Eastern Canada Stack
16
14
12
10
8
6
4
3
2
1
0
-1
-2
-3
0
2000
4000
6000
8000
10 000

Fig. 2.9. Comparison of the smoothed relative paleointensity record (RPI) of the eastern Canadian stack with several dipole moment (DM) reconstructions. The light gray shaded area in the RPI record represents 95% confidence limits. KN08 and KO09 are the virtual axial dipole moment (VADM) reconstructions of Knudsen et al. (2008) and Kovacheva et al. (2009) respectively. Here the KN08 record is considered with a 100 year time resolution. The dark gray shaded area in the KN08 record represents the 2σ uncertainties calculated using a bootstrap approach (Knudsen et al., 2008). OH93 illustrates the global DM reconstruction of Ohno and Hamano (1993). The local magnetic induction field (at the CL04-36PC core site) as expected from the CALS7k.2 model (blue curve in the web version) of Korte and Constable (2005) was converted in VADM values whereas the KO09 data were reduced to the CL04-36PC core location.

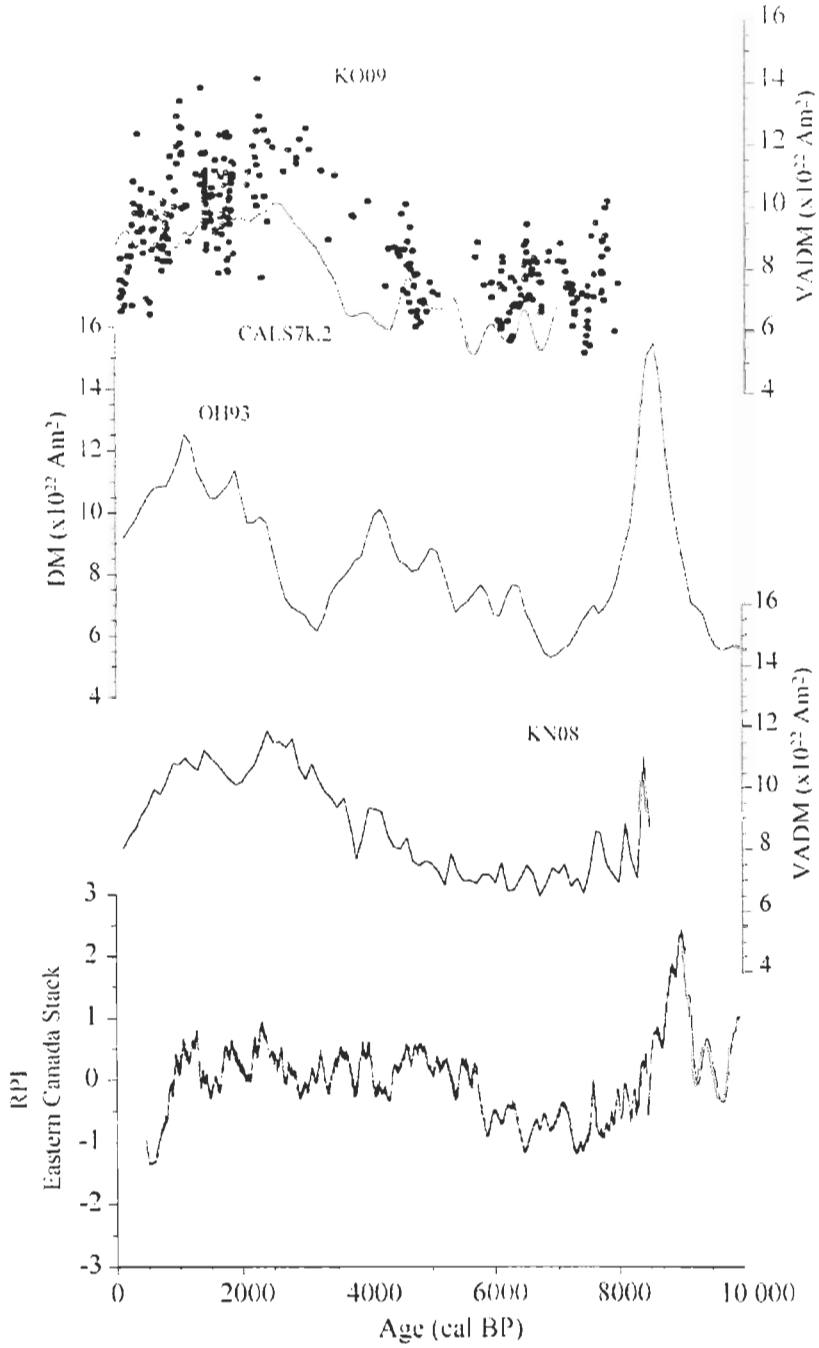
KO09
CALS7k.2
OH93
KN08
DM (x10²² Am²)
VADM (x10²² Am²)
RPI
Eastern Canada Stack
Age (cal BP)
0
2000
4000
6000
8000
10 000

2.7 Conclusion

Both magnetic declination and inclination profiles of the eastern Canadian stack can be correlated with other North American PSV lacustrine and volcanic records at the millennial and even centennial time scale during the Holocene (Fig. 2.7). Notably, between ~ 2000 and ~ 3500 cal BP, relative fluctuations in the declination appear coherent over ~ 140° of longitude in all the considered PSV records (Fig. 2.7). These results corroborate and extend the previous work of Lund (1996) concerning the analysis of the Holocene paleosecular variation within the North American continent. According to Lund (1996), North American PSV features appear spatially coherent over ~ 4000 km in the West-East direction. Moreover, based on the study of the historical secular variation, Thompson (1984) also noted a similar scale of spatial coherence. As suggested from Fig. 2.7, this PSV spatial scale can be further extended beyond the North American continent to Iceland and Europe. In addition, centennial- to millennial-scale fluctuations of the Holocene eastern Canadian RPI stack appear coherent with the VADM reconstruction of Knudsen et al. (2008) based on absolute paleointensity data (Fig. 2.9) as well as with other North American lacustrine RPI records (Fig. 2.10) suggesting the predominance of large-scale geomagnetic field fluctuations (dipolar) in controlling the observed Holocene paleomagnetic secular variation. These results thus reveal fundamental insights about the generation of the Holocene geomagnetic field and from a practical point of view, open the possibility of using the eastern Canadian PSV and RPI stacks as a chronostratigraphic tool for eastern North America and possibly for the rest of Canada and the United States.

Fig. 2.10. Comparison of northern American RPI records spanning the last 4000 cal BP. Correlative centennial-scale RPI features are indicated (P-1 to P-5). The light gray shaded area in the RPI stack indicates 95% confidence limits. The green broken and thick blue lines represent the VADM reconstructions of Knudsen et al. (2008) and Korte et al (2005) respectively. Note that all the RPI data are standardized for correlative purpose.

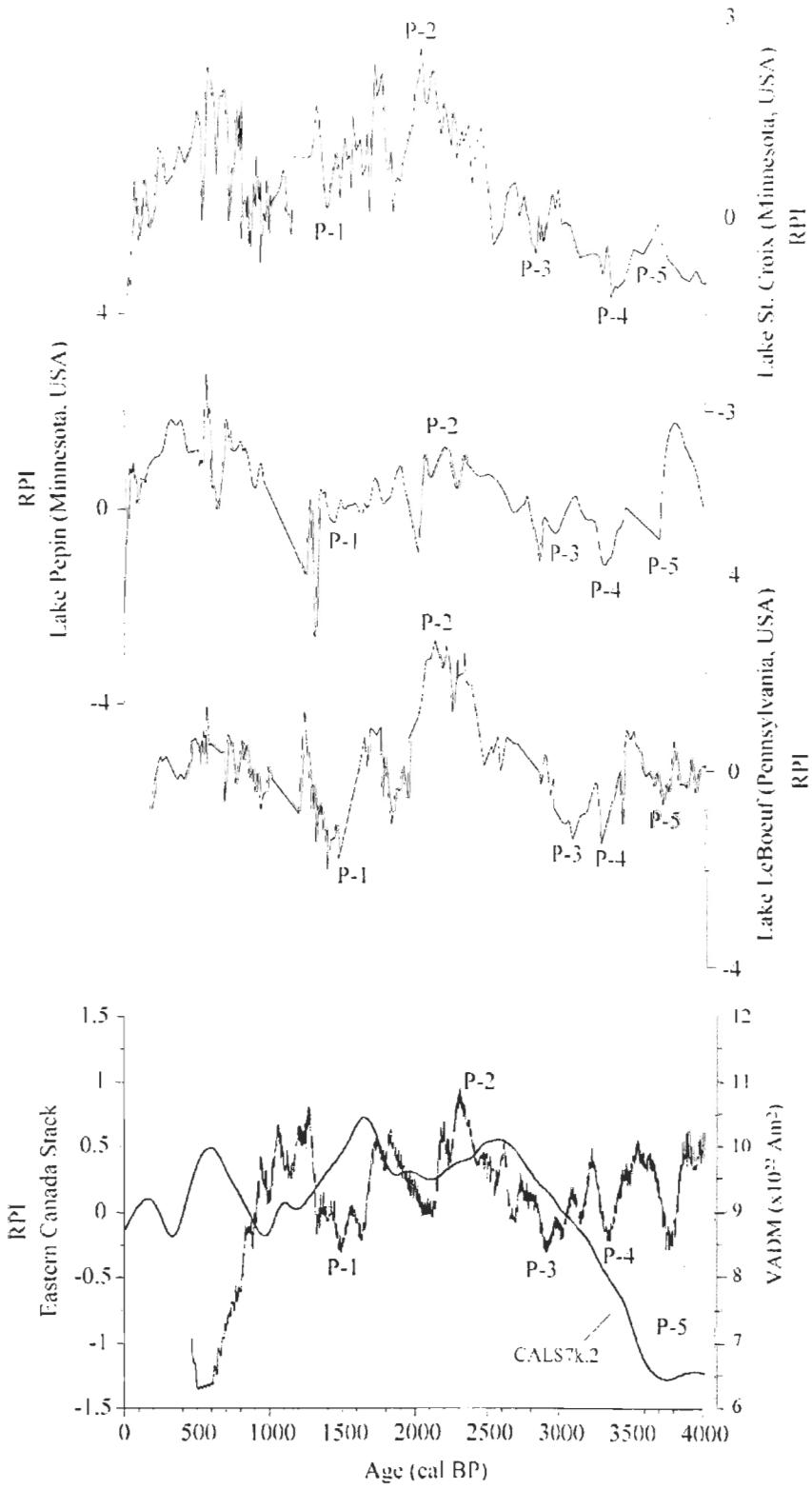
P-1
P-2
P-3
P-4
P-5
Lake St. Croix (Minnesota, USA)
RPI
Lake Pepin (Minnesota, USA)
RPI
Lake LeBoeuf (Pennsylvania, USA)
RPI
Eastern Canada Stack
RPI
VADM (x10²² Am²)
CALS7k.2
Age (cal BP)

2.8 Acknowledgements

We wish to thank the captain, officers, crew and scientists on board the R/V *Coriolis II* for the successful recovery of the cores from the COR0503 and COR0602 expeditions. We also thank two anonymous reviewers, Dr. Leonardo Sagnotti (INGV) and Dr. Vadim A. Kravchinsky for their thorough reviews and helpful comments. We also thank Dr. M. Korte for providing the CALS7k.2 model outputs. Finally, we wish to thank Sylvain Leblanc and Mélanie Simard for the grain size measurements as well as Jacques Labrie for Matlab computations. This study was supported by NSERC (Natural Science and Engineering Research Council of Canada) through Discovery and ship time grants to G.S., J.L. and P.L. and FQRNT (Fonds québécois de recherche sur la nature et les technologies) through a New researcher grant to P.L. This is a GEOTOP contribution no. 2010-0006.

2.9 References

Barber, D.C., Dyke, A., Hillaire-Marcel, C., Jennings, A.E., Andrews, J.T., Kerwin, M.W., Bilodeau, G., McNeely, R., Southon, J., Morehead, M.D., Gagnon, J.-M., 1999. Forcing of the cold event of 8,200 years ago by catastrophic drainage of Laurentide lakes. Nature vol. 400, 344–348.

Bard, E., 1998. Geochemical and geophysical implications of the radiocarbon calibration, Geochimica et Cosmochimica Acta vol. 62, 2025–2038.

Barletta, F., St-Onge, G., Channell, J.E.T., Rochon, A., Polyak., L., Darby, D.A., 2008. High-resolution paleomagnetic secular variation and relative paleointensity records

from the western Canadian Arctic: implication for Holocene stratigraphy and geomagnetic field behaviour. Canadian Journal of Earth Sciences 45, 1265–1281.

Blott, S.J., Pye, K., 2001. Gradistat: a grain size distribution and statistics package for the analysis of unconsolidated sediments. Earth Surface Processes and Landforms 26, 1237–1248.

Brachfeld, S., Banerjee, S.K., 2000. A new high-resolution geomagnetic relative paleointensity record for the North American Holocene: A comparison of sedimentary and absolute intensity data. Journal of Geophysical Research 105, 821–834.

Cauchon-Voyer, G., Locat, J., St-Onge, G., 2008. Late-Quaternary morpho-sedimentology and submarine mass movements of the Betsiamites area, Lower St. Lawrence Estuary, Quebec, Canada. Marine Geology 251, 233–252.

Day, R., Fuller, M., Schmidt, V.A., 1977. Hysteresis properties of titanomagnetites, grain size and compositional dependence. Physics of the Earth and Planetary Interiors vol. 13, 260–267.

Dredge, L., 1983. Surficial geology of the Sept-Îles area, Québec North Shore. Geological Survey of Canada, Memoir, 408. 40 pp.

Duchesne, M., Pinet, N., Bolduc, A., Bédard, K., Lavoie, D., 2007. Seismic Stratigraphy of the Lower St. Lawrence Estuary Quaternary Deposits and Seismic Signature of the Underlying Geological Domains. Current Research 2007-D2. Geological Survey of Canada, Ottawa.

Duchesne, M.J., Pinet, N., Bédard, K., St-Onge, G., Lajeunesse, P., Campbell, C. Bolduc, 2010. Role of the bedrock topography in the Quaternary filling of a giant semi-

enclosed basin: the Lower St. Lawrence Estuary, Eastern Canada. Basin Research doi: 10.1111/j.1365-2117.2009.00457.x

Dunlop, D.J., 1973. Superparamagnetic and single-domain threshold sizes in magnetite, Journal of Geophysical Research 78, pp. 1780–1793.

Dunlop, D.J., Özdemir, Ö., 1997. Rock Magnetism, Cambridge: Cambridge University Press.

Elsasser, W., Ney, E.P., Winckler, J.R., 1956. Cosmic-ray intensity and geomagnetism. Nature vol. 178, 1226–1227.

Hagstrum, J.T., Champion, D.E., 2002. A Holocene paleosecular variation record from 14C-dated volcanic rocks in western North America. Journal of Geophysical Research 107, 1–14.

Hughen, K.A., Baillie, M.G.L., Bard, E., Bayliss, A., Beck, J.W, Bertrand, C.J.H., et al. 2004. Marine04 Marine radiocarbon age calibration, 0-26 Cal Kyr BP. Radiocarbon 46, 1059–1086.

Jackson, A., Jonkers, A.R.T., Walker, M.R., 2000. Four centuries of geomagnetic secular variation from historical records, Philosophical Transactions of the Royal Society London A 358, 957–990.

Jackson, M., 2007. Magnetization, isothermal remanent. *In* Encyclopedia of geomagnetism and paleomagnetism. Edited by David Gubbins and Emilio Herrero-Bervera. Published by Springer, Dordrecht, The Netherlands.

Jonkers, A.R.T., Jackson, A., Murray, A., 2003. Four centuries of geomagnetic data from historical records. Reviews of Geophysics 41(2), 1006, doi: 10.1029/2002RG000115.

Josenhans, H., Lehman, S., 1999. Late glacial history of the Gulf of St. Lawrence, Canada. Canadian Journal of Earth Sciences vol. 36, 1327–1345.

Keigwin, L.D., Jones, G.A., 1995. The marine record of deglaciation from the continental margin off Nova Scotia, Paleoceanography vol. 10, no.6, 973–985.

King, J., Peck, J., 2001. Use of paleomagnetism in studies of lake sediments. *In* W.M. Last & J.P. Smol (eds.). Tracking Environmental Change Using Lake Sediments. Volume 1: Basin analysis, Coring, and Chronological Techniques. Kluwer Academic Publishers, Dordrecht, The Netherlands.

King, J.W., Banerjee, S.K., Marvin, J.A., 1983. A new rock magnetic approach to selecting sediments for geomagnetic paleointensity studies: application to paleointensity for the last 4000 years. Journal of Geophysical Research 88, 5911–5921.

Kirschvink, J.L., 1980. The least-squares line and plane and the analysis of paleomagnetic data. Geophysical Journal of the Royal Astronomical Society 62, 699–718.

Knudsen, M.F., Riisager, P., Donadini, F., Snowball, I., Muscheler, R., Korhonen, K., Pesonen, L.J., 2008. Variations in the geomagnetic dipole moment during the Holocene and the past 50 kyr. Earth and Planetary Science Letters 272, 319–329, doi: 10.1016/j.epsl.2008.04.048.

Korte, M., Constable, C.G., 2005. Continuous geomagnetic field models for the past 7 millennia: 2. CALS7K. Geochemistry Geophysics and Geosystems 6 Q02H16, doi:10.1029/2004GC000801.

Korte, M., Genevey, A., Constable, C.G., Frank, U., Schnepp, E., 2005a. Continuous geomagnetic field models for the past 7 millennia: 1. A new global data

compilation. Geochemistry Geophysics and Geosystems 6, Q02H15, doi:10.1029/2004GC000800.

Korte, M., Constable, C., 2005b. The geomagnetic dipole moment over the last 7000 years - new results from a global model. Earth and Planetary Science Letters 236, 348–358.

Kovacheva, M., Boyadziev, Y., Kostadinova-Avramova, M., Jordanova, N., Donadini, F., 2009. Updated archeomagnetic data set of the past 8 millennia from the Sofia laboratory, Bulgaria. Geochemistry Geophysics and Geosystems 10, Q05002, doi:10.1029/2008GC002347.

Kovaltsov, G.A., Usoskin, I.G., 2007. Regional cosmic ray induced ionization and geomagnetic field changes. Advanced in Geosciences 13, 31–35.

Krása, D., Fabian, K., 2007. Rock magnetism, hysteresis measurements. *In* Encyclopedia of geomagnetism and paleomagnetism. Edited by David Gubbins and Emilio Herrero-Bervera. Published by Springer, Dordrecht, The Netherlands.

Laj, C., Kissel, C., Mazaud, A., Channell, J.E.T., Beer, J., 2000. North Atlantic paleointensity stack since 75 ka (NAPIS-75) and the duration of the Laschamp event. Philosophical Transactions of the Royal Society, Series A 358, 1009–1025.

Lajeunesse, P., St-Onge, G., 2008. Subglacial origin of Lake Agassiz-Ojibway final outburst flood. Nature Geoscience 3, 184–188.

Levi, S., Banerjee, S.K., 1976. On the possibility of obtaining relative paleointensities from lake sediments. Earth and Planetary Science Letters vol. 29, 219–226.

Lund, S.P., Banerjee, S.K., 1985. Late Quaternary paleomagnetic field secular variation from two Minnesota Lakes. Journal of Geophysical Research 90, 803–825.

Lund, S.P., 1996. A comparison of paleomagnetic secular variation records from North America. Journal of Geophysical Research vol. 101, 8007–8024.

Mazaud, A., 2005. User-friendly software for vector analysis of the magnetization of long sediment cores. Geochemistry Geophysics and Geosystems 6, doi:10.1029/2005GC001036.

Ohno, M., Hamano, Y., 1993. Global analysis of the geomagnetic field; time variation of the dipole moment and the geomagnetic pole in the Holocene. Journal of Geomagnetism and Geoelectricity vol. 45, 1455–1466.

Olafsdoddir, S., Stoner, J., Geirstoddir, A., Miller, G., 2009. High-resolution Holocene paleomagnetic secular variation records from Iceland: marine–terrestrial synchronization. GSA Annual Meeting, Abstract volume.

Reimer, P.J., Baillie, M.G.L., Bard, E., Bayliss, A., Beck, J.W., Bertrand, C., Blackwell, P.G., Buck, C.E., Burr, G., Cutler, K.B., Damon, P.E., Edwards, R.L., Fairbanks, R.G., Friedrich, M., Guilderson, T.P., Hughen, K.A., Kromer, B., McCormac, F.G., Manning, S., Bronk, Ramsey, C., Reimer, R.W., Remmele, S., Southon, J.R., Stuiver, M.,. Talamo, S., Taylor, F.W., van der Plicht, J., Weyhenmeyer, C.E., 2004. IntCal04 Atmospheric radiocarbon age calibration, 26-0 ka BP. Radiocarbon 46, 1026–1058.

Sagnotti, L., Rochette, P., Jackson, M., Vadeboin, F., Dinarès-Turell, J., Winkler, A., "Mag-Net" Science Team, 2003. Inter-laboratory calibration of low-field magnetic and anhysteretic susceptibility measurements. Physics of the Earth and Planetary Interiors 138, 25–38.

Shaw, J., Gareau, P., Courtney, R.C., 2002. Palaeogeography of Atlantic Canada 13–0 kyr. Quaternary Science Reviews vol. 21, 1861–1878.

Snowball, I., Zillén, L., Ojala, A., Saarinen, T., Sandgren, P., 2007. FENNOSTACK and FENNORPIS: Varve dated Holocene palaeomagnetic secular variation and relative palaeointensity stacks for Fennoscandia. Earth and Planetary Science Letters 255, 106–116.

Snowball, I., Muscheler, R., 2007. Palaeomagnetic intensity data: an Achilles heel of solar activity reconstructions. The Holocene 17, 6, 851–859.

Snowball, I., Nilsson A., Sandgren, P., Lloyd, J., McCarthy, D., Moros, M., 2010. Holocene palaeomagnetic secular variation records and a relative palaeointensity estimate from Western Greenland (Disko Bugt). Geophysical Research Abstracts Vol. 12, EGU2010-3422-2, EGU General Assembly.

Solanki, S.K., Usoskin, I.G., Kromer, B., Schüssler, M., Beer, J., 2004. Unusual activity of the Sun during recent decades compared to the previous 11,000 years. Nature vol. 431, 1084–1087.

Stockhausen, H., 1998. Geomagnetic palaeosecular variation (0-13000 yr BP) as recorded in sediments from three maar lakes from the West Eifel (Germany). Geophysical Journal International vol. 135, issue 3, pp. 898–910.

Stoner, J.S., Laj, C., Channell, J.E.T., Kissel, C., 2002. South Atlantic and North Atlantic geomagnetic paleointensity stacks (0–80 ka): implications for inter-hemispheric correlation. Quaternary Science Reviews 21, 1141–1151.

Stoner, J.S., St-Onge G., 2007. Magnetic Stratigraphy: Reversals, Excursions, Paleointensity and Secular Variation, *In* Development in Marine Geology: Volume

1, Proxies in Late-Cenozoic Paleoceanography, C. Hillaire-Marcel and A. de Vernal editors, Elsevier, 99–138.

Stoner, J.S., Jennings, A., Kristjansdottir, G.B., Dunhill, G., Andrews, J.T., Hardardottir, J., 2007. A paleomagnetic approach toward refining Holocene radiocarbon based chronologies: Paleoceanographic records from North Iceland (MD99-2269) and East Greenland (MD99-2322) margins. Paleoceanography 22, 1–23.

St-Onge, G., Stoner, J.S., Hillaire-Marcel, C., 2003. Holocene paleomagnetic records from the St. Lawrence Estuary: centennial- to millennial-scale geomagnetic modulation of cosmogenic isotopes. Earth and Planetary Science Letters 209, 113–130.

St-Onge, G., Mulder, T., Francus, P., Long, B., 2007. Continuous physical properties of cored marine sediments. *In*: C. Hillaire-Marcel and A. de Vernal (Eds.), Proxies in Late Cenozoic Paleoceanography, Elsevier, pp. 63–98.

St-Onge, G., Lajeunesse, P., Duchesne, M.J., Gagné, H., 2008. Identification and dating of a key Late Pleistocene stratigraphic unit in the St. Lawrence Estuary and Gulf (Eastern Canada). Quaternary Science Reviews 27, 2390–2400.

St-Onge, G., Long, B. 2009. CAT-scan analysis of sedimentary sequences: an ultrahigh-resolution paleoclimatic tool. Engineering Geology 103, 127—133.

Stuiver, M., Polach, H.A., 1977. Discussion: Reporting of ^{14}C data. Radiocarbon vol. 19, no. 3, 355–363.

Stuiver, M., P.J., Reimer, E., Bard, J.W., Beck, G.S., Burr, K.A., Hughen, B., Kromer, G., McCormac, van der Plicht, J., and Spurk, M., 1998. INTCAL98 Radiocarbon Age Calibration, 24000-0 cal BP. Radiocarbon 40, 1041–1083.

Stuiver, M., Reimer, P.J., Reimer, R.W., 2005. CALIB 5.0. Available from http://radiocarbon.pa.qub.ac.uk/calib/.

Sugiura, N., 1979. ARM, TRM, and magnetic interactions: concentration dependence. Earth and Planetary Science Letters 42, 451–455.

Syvitski, J.P.M., Praeg, D.B., 1989. Quaternary sedimentation in the St. Lawrence Estuary and adjoining areas, eastern Canada: an overview based on high resolution seismo-stratigraphy. Géographie physique et Quaternaire vol. 43, 291–310.

Tauxe, L., 1993. Sedimentary records of relative paleointensity: theory and practice, Reviews of Geophysics vol. 31, 319–354.

Taylor, J.R., 1997. An introduction to error analysis: the study of uncertainties in physical measurements. University Science Books.

Thompson, R., 1984. Geomagnetic evolution: 400 years of change on planet. Physics of the Earth and Planetary Interiors vol. 36, 61–77.

Turner, G.M., Thompson, R. (1981). Lake sediment record of the geomagnetic secular variation in Britain during Holocene times. Geophysical Journal of the Royal Astronomical Society 65(3), 703–725.

Usoskin, I.G., Solanki, S.K., Korte, M., 2006. Solar activity reconstructed over the last 7000 years: The influence of geomagnetic field changes. Geophysical Research Letters vol. 33, L08103, doi:10.1029/2006GL025921.

Usoskin, I.G., Solanki, S.K., Kovaltsov, G.A., 2007. Grand minima and maxima of solar activity: new observational constraints. Astronomy and Astrophysics 471, 301–309, doi: 10.1051/0004-6361:20077704.

Usoskin, I.G., Korte, M., Kovaltsov, G.A., 2008. Role of centennial geomagnetic changes in local atmospheric ionization. Geophysical Research Letters vol. 35, L05811, doi:10.1029/2007GL033040.

Usoskin, I.G., Kovaltsov, G.A., 2008. Cosmic rays and climate of the Earth: Possible connection. C. R. Geoscience 340, 441–450.

Valet, J.-P., 2003. Time variations in geomagnetic intensity. Reviews of Geophysics 41, (1): 1004. doi:10.1029/2001RG000104.

Valet, J.-P., Herrero-Bervera, E., LeMouël, J.-L., Plenier, G., 2008. Secular variation of the geomagnetic dipole during the past 2000 years. Geochemistry Geophysics and Geosystems 9, Q01008, doi:10.1029/2007GC001728.

Verosub, K., Mehringer, P. Jr., Waterstraat, P., 1986. Holocene Secular Variation in Western North America: Paleomagnetic Record from Fish Lake, Harney County, Oregon. Journal of Geophysical Research 91, 3609–3623.

2.10 Supplementary materials

Figure A. Visual correlation between the piston (PC) and trigger weight (TWC) cores magnetic properties. A 30 and 20 cm depth corrections were applied in cores 36PC and 37PC respectively, based on MDF_{NRM} and NRM profiles. In contrast, based on similar comparisons, no missing sediments seem to be observed for the others cores.

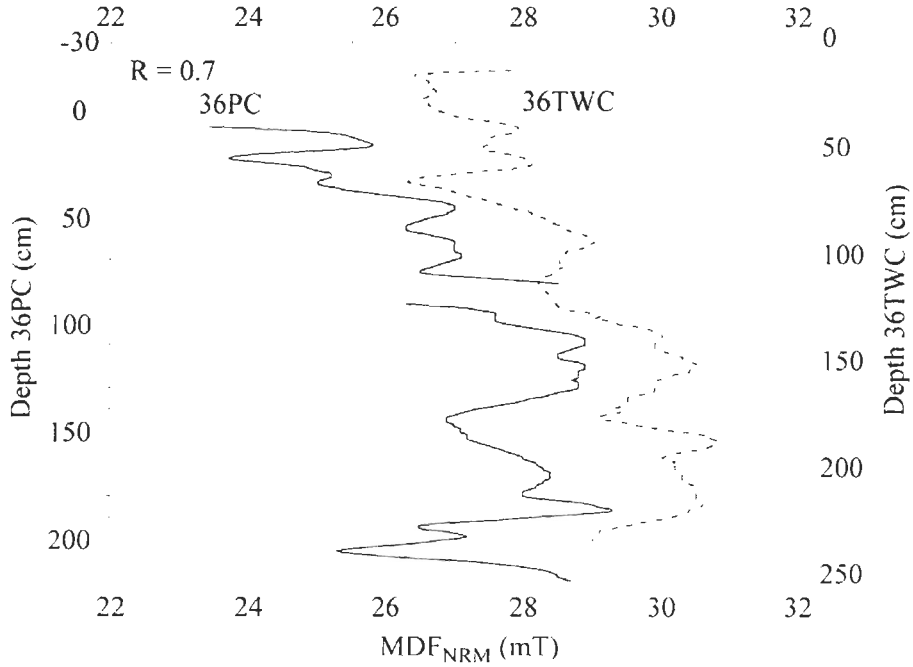
22
24
26
28
30
32
-30
0
50
100
150
200
250
R = 0.7
36PC
36TWC
Depth 36PC (cm)
Depth 36TWC (cm)
MDF$_{NRM}$ (mT)

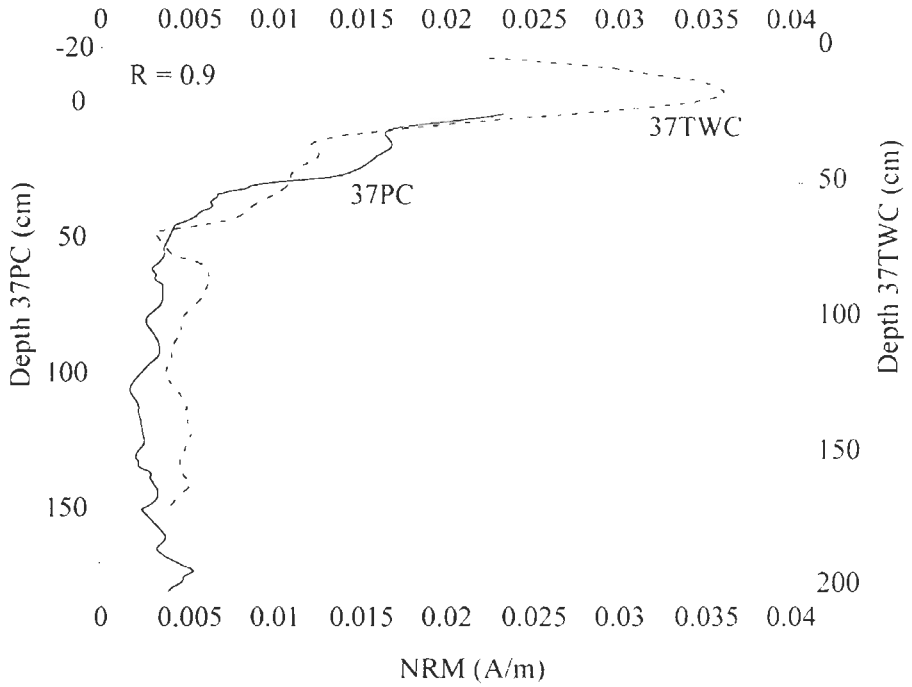
0
0.005
0.01
0.015
0.02
0.025
0.03
0.035
0.04
-20
0
50
100
150
200
R = 0.9
37TWC
37PC
Depth 37PC (cm)
Depth 37TWC (cm)
NRM (A/m)

Figure B. Magnetic grain size estimation for cores 42PC (a), 36PC (b), 35PC (c), CL04-36PC (d) and 37PC (e). Grain size contour lines are based on measurement performed on synthetic magnetite samples by King et al. (1983). Despite these estimates should be taken with caution as ARM intensities are strongly dependent on the employed experimental settings (Sagnotti et al., 2003) all cores are characterized by a relatively uniform magnetic grain size.

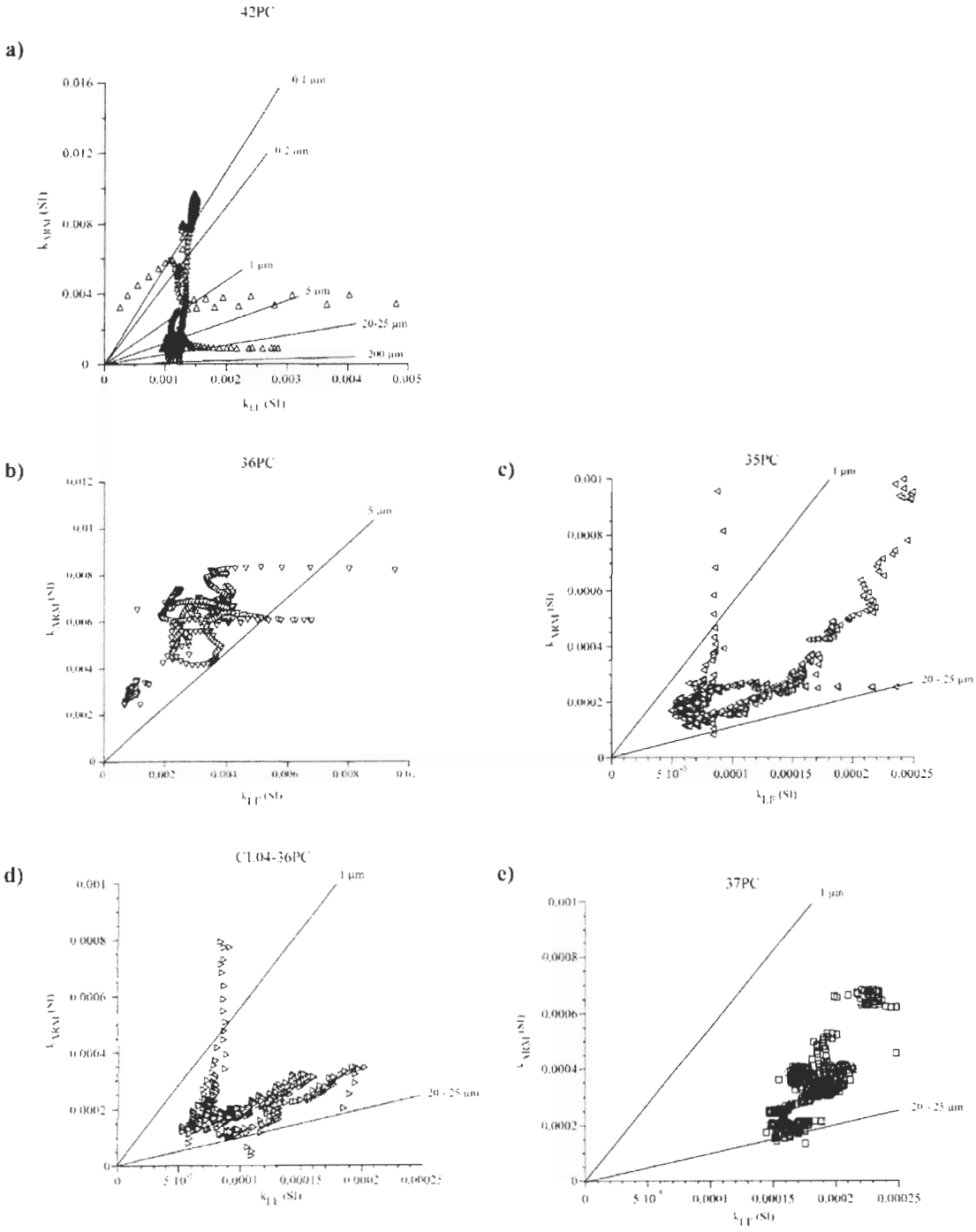
42PC
a)
0.016
0.012
0.008
0.004
0
0.001
0.002
0.003
0.004
0.005
0.1 µm
0.2 µm
1 µm
5 µm
20-25 µm
200 µm
b)
36PC
5 µm
c)
35PC
1 µm
0.0008
0.0006
0.0004
0.0002
20 - 25 µm
d)
CL04-36PC
e)
37PC

Figure C. Representative hysteresis loop diagrams (left diagrams) and IRM acquisition curves (right diagrams) at one selected depth for all cores. The vertical line in the IRM acquisition diagrams represents the 100 mT field. The hysteresis parameters (saturation magnetization (M_S), saturation remanence (M_R) and coercivity (H_C)) were determined from the paramagnetic-corrected data (broken curve in the left diagram). For all the selected samples, significant acquisition occurs at field of ~ 100 mT, suggesting the presence of magnetite as the dominant magnetic mineral. However, the selected sample from core 37PC reaches the saturation at field of ~ 600 mT indicating the presence of a high-coercivity mineral. The presence of a high-coercivity mineral is also suggested in the increase in the a* values at this depth (see Fig. F).

Core 36PC

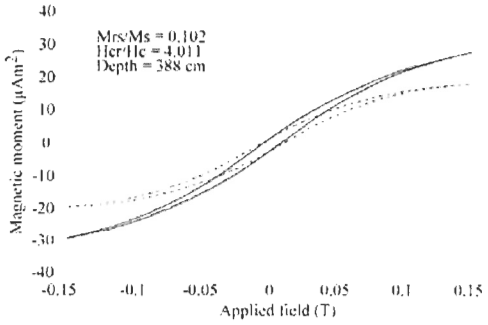

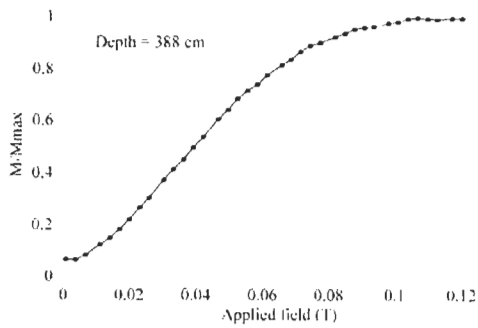

Core 42PC

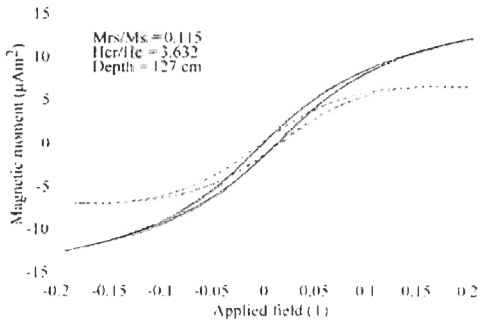

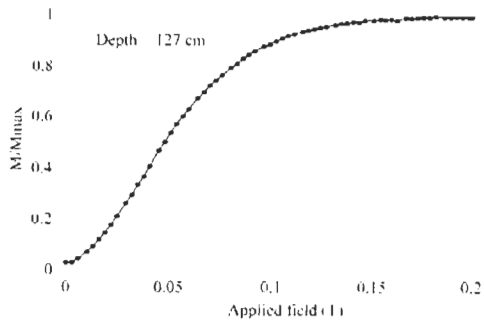

Core 37PC

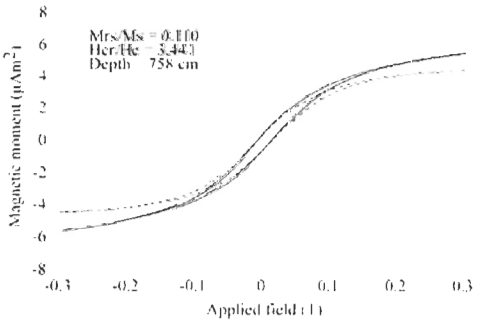

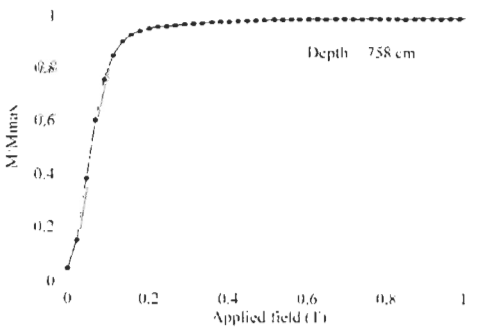

Core 35PC

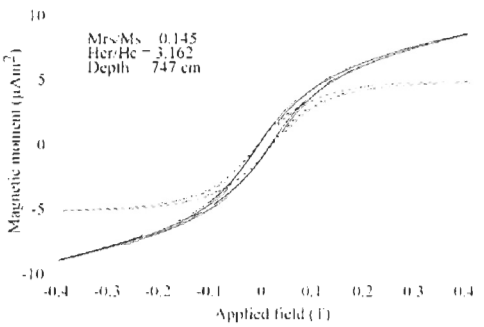

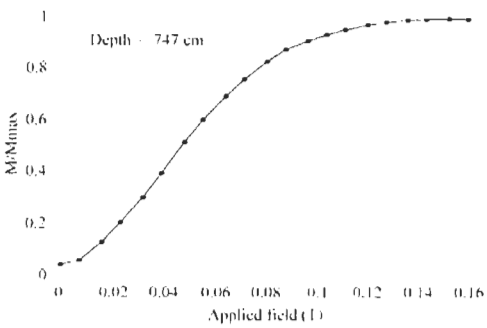

Figure D. (a) The natural remanent magnetization (NRM) profiles versus depth after an AF demagnetization step of 30 mT. (b) The median destructive fields of the NRM (MDF_{NRM}), anhysteretic remanent magnetization (MDF_{ARM}) and isothermal remanent magnetization (MDF_{IRM}) versus depth. The MDFs values are calculated using the software developed by Mazaud (2005).

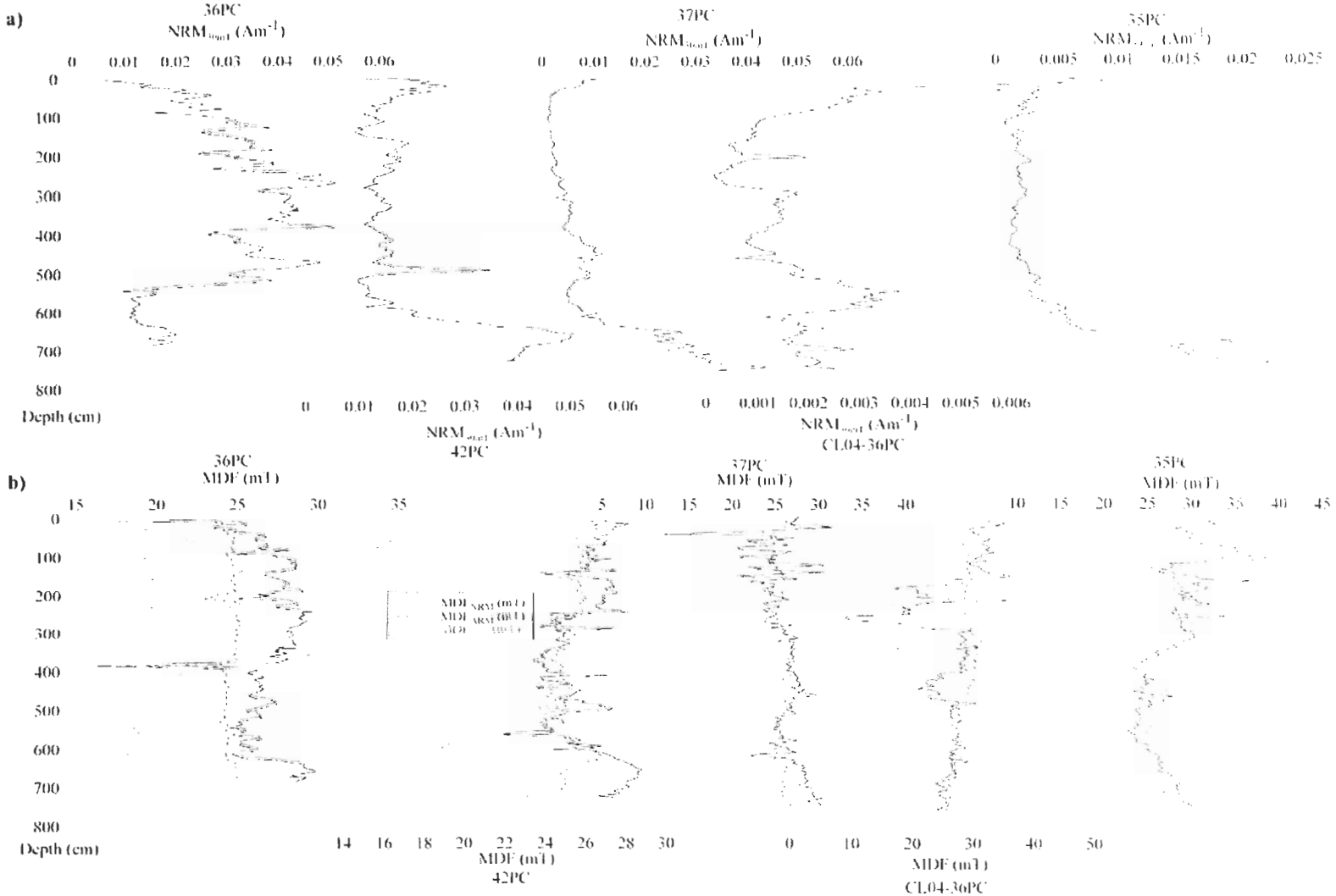
a)
36PC
37PC
35PC
Depth (cm)
42PC
CL04-36PC
b)
MDF (mT)

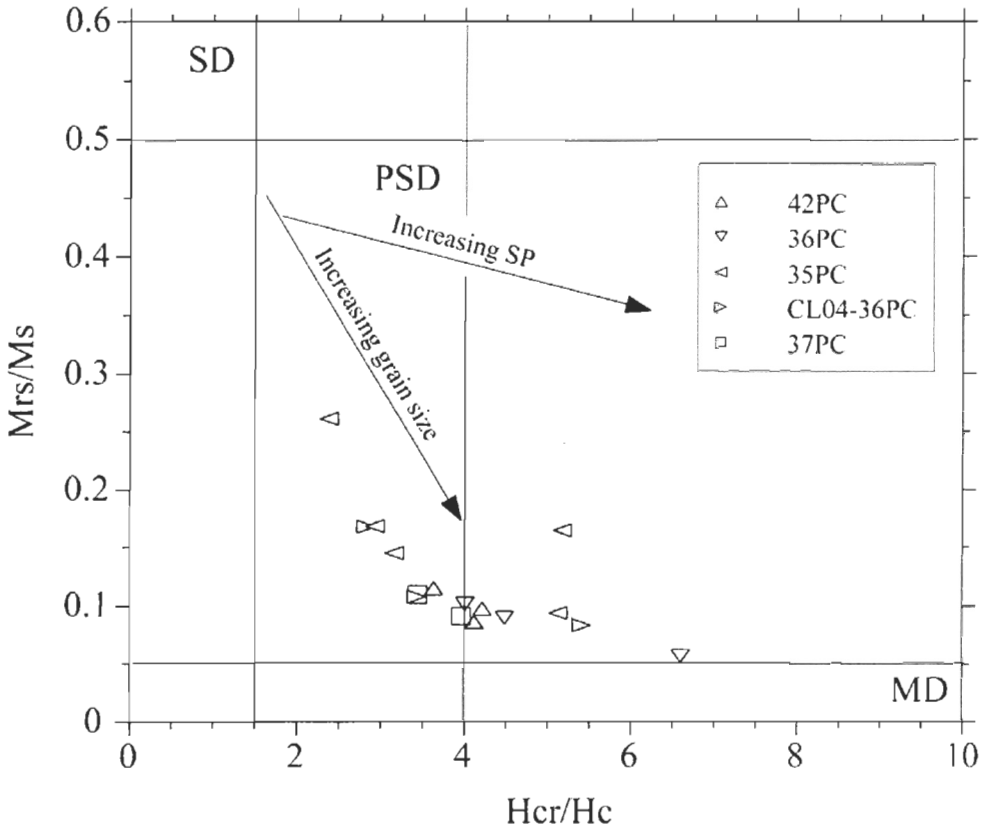

Figure. E. Day plot (Day et al., 1977). Most of the analyzed samples fall in the coarse end of the pseudo-single domain (PSD) region. The samples outside the PSD region are associated either with a more complex magnetic mineralogy or with the presence of superparamagnetic (SP) particles. The sample in the multi domain (MD) region of the Day plot comes from the glaciomarine unit of core 36PC.

Figure F. (a) The low-field volumetric magnetic susceptibility (k_{LF}) and (b) the wet bulk density profiles versus depth. These data were acquired on board the R/V *Coriolis II* using a GEOTEK Multisensor Core Logger (MSCL). (c) The a* (green-red) diffuse spectral reflectance profiles. The asterisk in the a* diagrams indicates the selected samples used to derive the magnetic domain state of the ferrimagnetic minerals based on the day Plot (Day et al., 1977). PSD = Pseudo-single domain magnetite; MD = Multi domain magnetite. The question mark indicates that the selected sample falls outside the usual region of SD/MD mixture for magnetite (see text for details) whereas the tilde indicates a sample in the coarse end of the PSD region for magnetite ($Hcr/Hc \geq 4$). Note that spikes in the k_{LF} profiles of cores 36PC and 42PC are associated to the coarse grain size fraction.

a)

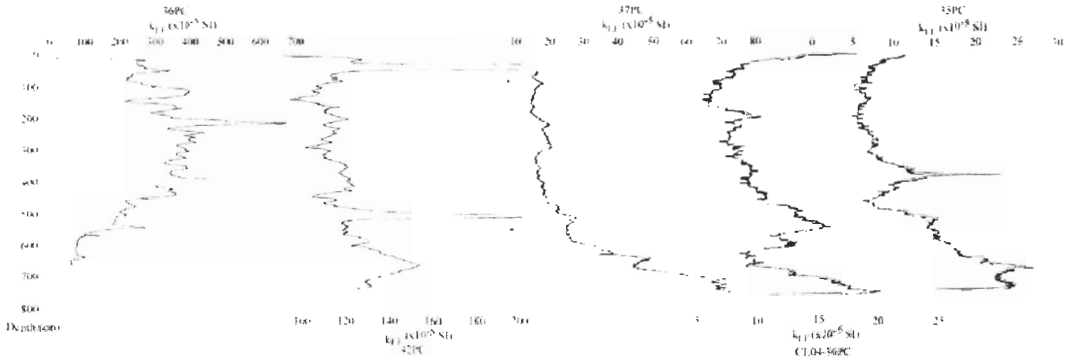

b)

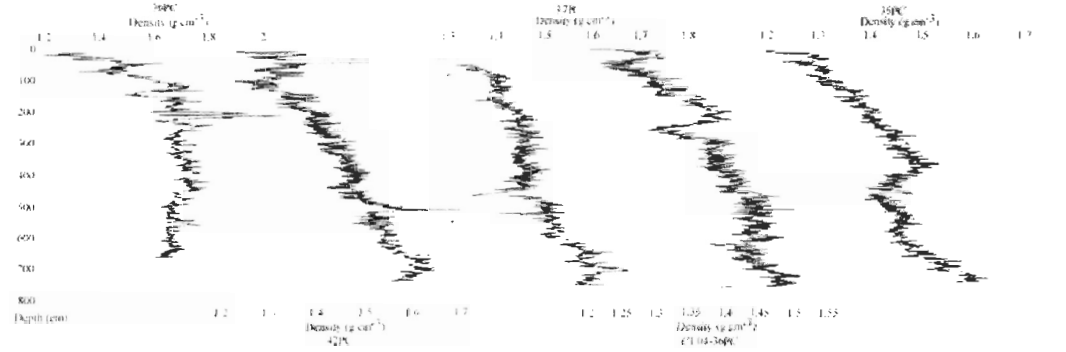

c)

Figure G. Representative normalized demagnetization curves for the NRM, ARM and IRM at one selected depth for all cores (left diagrams). The NRM/ARM (solid symbols) and NRM/IRM (open symbol) versus AF demagnetizing field for the same samples (right diagrams). The selected shaded gray area depicts the AF coercivity window which activates the same magnetic grain assemblages carrying the NRM (see text for detail).

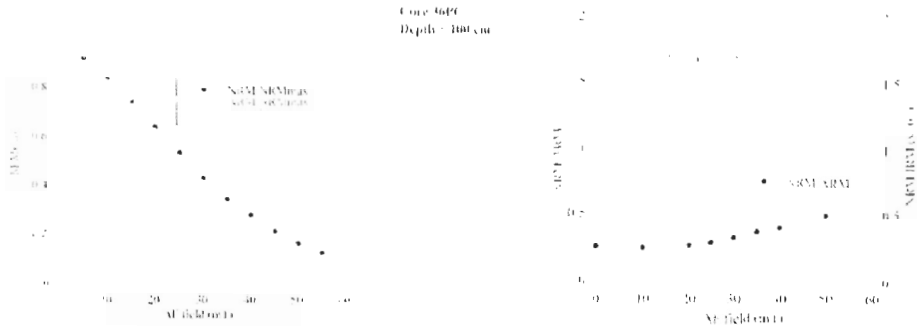

Core 66PC
Depth = 100 cm

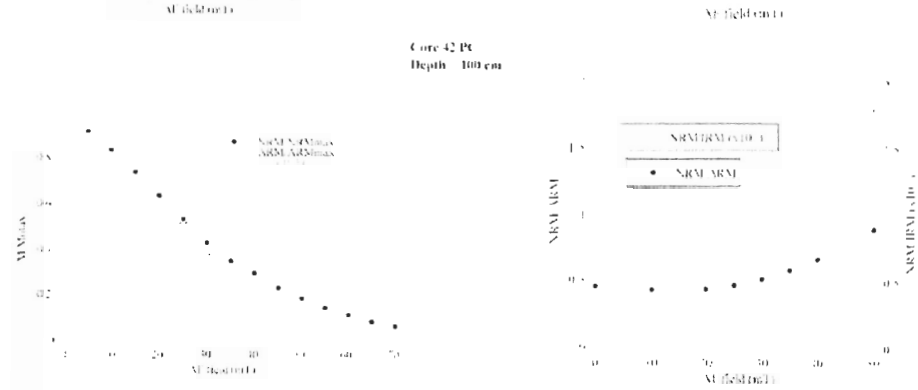

Core 42 PC
Depth = 100 cm

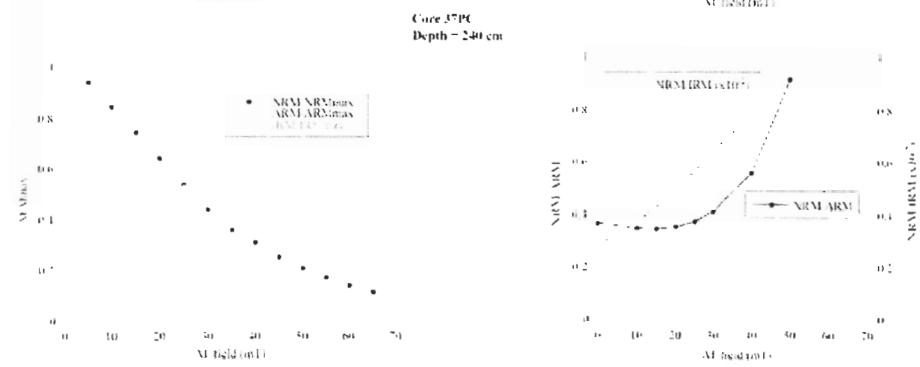

Core 57PC
Depth = 240 cm

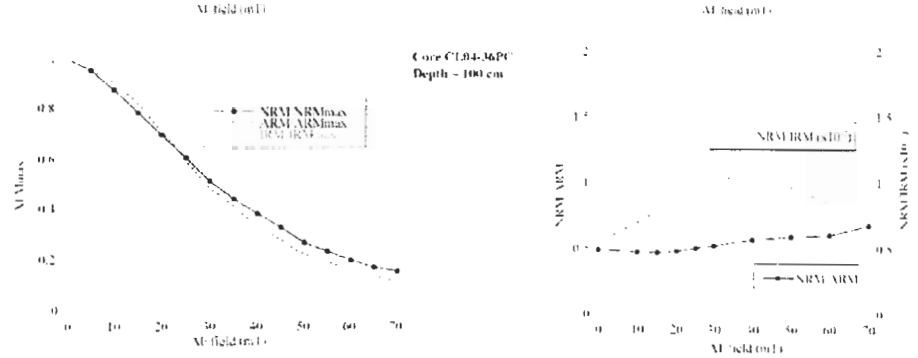

Core CL04-36PC
Depth = 100 cm

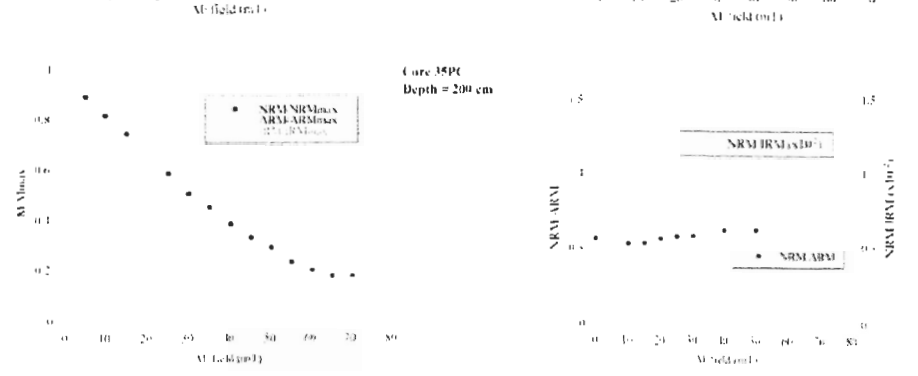

Core 35PC
Depth = 200 cm

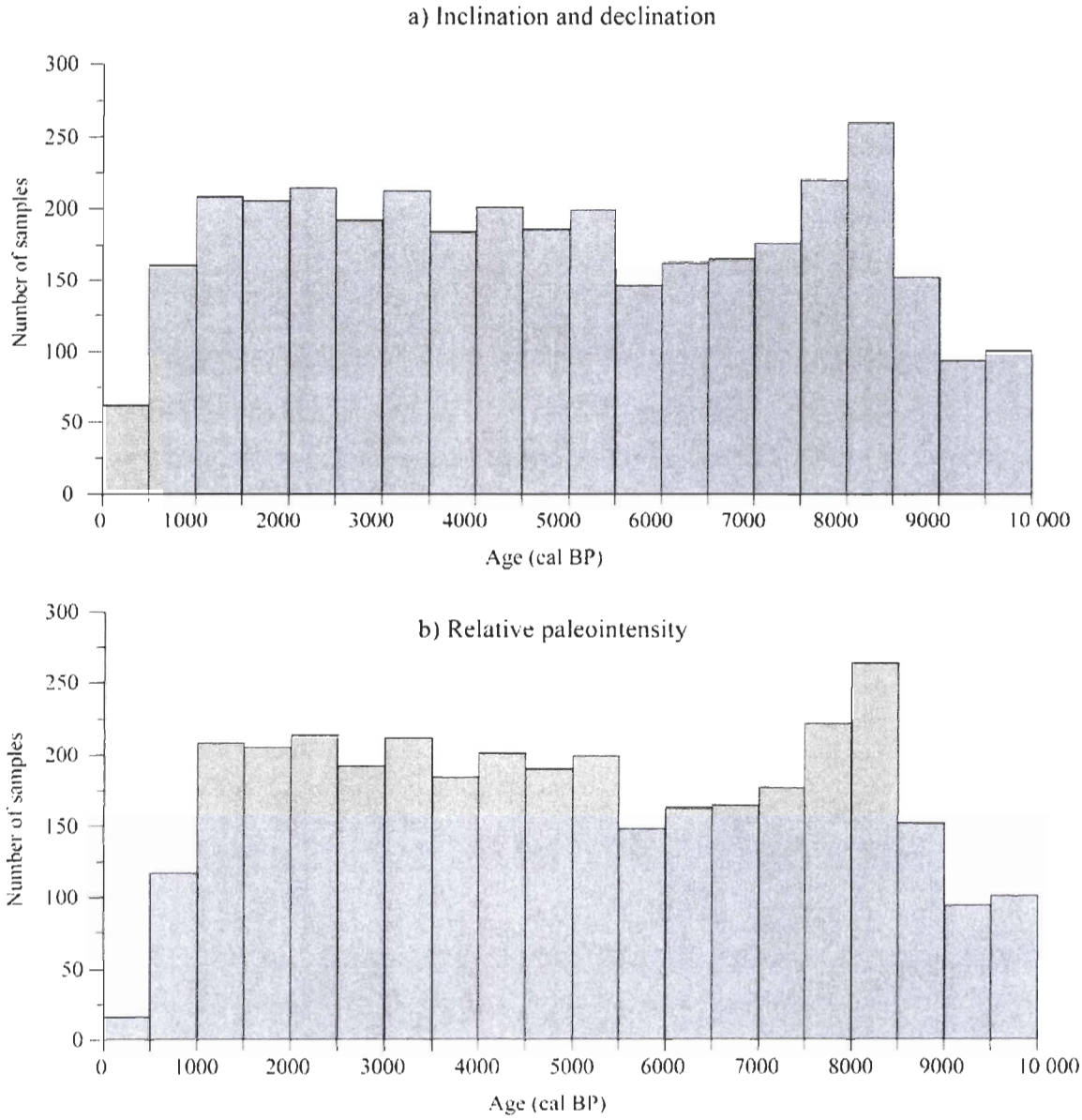

Figure H. Histograms for the directional (a) and relative paleointensity (b) data according to bins of 500 yr.

Table A. Radiocarbon dates.

[a]Depth corrected for the missing sediment (see text for details). [b]All ages were measured by the AMS method and corrected for natural and sputtering fractionation ($\delta^{13}C$ = -25‰ versus VPDB). The statistical uncertainty of the age determination is given as one standard deviation (Stuiver and Polach, 1977). [c]Calibrated using the on-line CALIB 5.0.2 software (Stuiver et al., 2005) using the Hughen et al. (2004) marine dataset. A standard marine reservoir correction (~ 400 years, ΔR=0) was applied to all dates. The first and last ages, in parentheses, represent the 2σ cal age range. [d]TO, IsoTrace Radiocarbon Laboratory, Toronto, Canada; UCIAMS, Keck Carbon Cycle AMS Facility, University of California, Irvine, USA. *Prior to its AMS analysis at UC Irvine, the CO_2 was extracted at the Université Laval.

Core	Depth (cm)	Corr. depth (cm)[a]	Age (yr BP)[b]	Calibrated age (cal BP)[c]	Dated material	Lab. number[d]
COR0602-42PC	20	20	1070 ± 50	628 (538-717)	Pelecypod fragment	TO-13207
COR0602-42PC	60	60	1160 ± 50	724 (625-823)	Pelecypod valves	TO-13208
COR0602-42PC	86	86	1570 ± 50	1126 (1002-1249)	Pelecypod fragments	TO-13209
COR0602-42PC	117	117	2100 ± 50	1678 (1544-1811)	Pelecypod fragment	TO-13210
COR0602-42PC	457	457	5360 ± 100	5736 (5527-5945)	Pelecypod fragments	TO-13211
COR0602-36PC	95	125	1695 ± 15	1249 (1695-1298)	Shell fragment	UCIAMS-28833*
COR0602-36PC	181	211	3525 ± 15	3406 (3349-3462)	Shell fragment	UCIAMS-31219*
COR0602-36PC	218	248	3720 ± 60	3646 (3477-3814)	Shell fragment	TO-13212
COR0602-36PC	264	294	4690 ± 60	4963 (4792-5133)	*Astarte* sp.	TO-13213
COR0602-36PC	307	337	6020 ± 15	6436 (6371-6500)	Shell fragment	UCIAMS-31220*
COR0602-36PC	427	457	7425 ± 20	7888 (7829-7947)	Shell fragment	UCIAMS-31216*
COR0503-CL03-35PC	56	56	1375 ± 15	925 (876-973)	Bivalve	UCIAMS-40622*
COR0503-CL03-35PC	140	140	2700 ± 20	2397 (2322-2471)	Bivalve	UCIAMS-40616*
COR0503-CL03-35PC	191	191	3575 ± 20	3467 (3388-3546)	Bivalve	UCIAMS-41214*
COR0503-CL03-35PC	250	250	4405 ± 20	4549 (4445-4652)	Bivalve	UCIAMS-40627*
COR0503-CL03-35PC	280	280	4850 ± 20	5153 (5046-5260)	Shell fragments	UCIAMS-40624*
COR0503-CL03-35PC	448	448	8485 ± 20	9111 (9008-9213)	Gastropod fragment	UCIAMS-40617*
COR0503-CL04-36PC	62	62	1145 ± 15	691 (650-732)	Shell fragment	UCIAMS-40613*
COR0503-CL04-36PC	156	156	2690 ± 70	2449 (2240-2658)	*Yoldia* sp.	TO-13493

COR0503-CL04-36PC	383	383	5285 ± 20	5642 (5583-5701)	Shell fragment	UCIAMS-40628*
COR0503-CL04-36PC	414	414	5765 ± 20	6194 (6125-6263)	Gastropod shell	UCIAMS-40614*
COR0503-CL04-36PC	481	481	6955 ± 20	7462 (7410-7513)	Shell fragment	UCIAMS-40620*
COR0503-CL04-36PC	620	620	8425 ± 20	9039 (8971-9107)	*Yoldia* sp.	UCIAMS-40625*
COR0503-CL05-37PC	18	38	620 ± 15	271 (234-308)	Shell fragments	UCIAMS-40619*
COR0503-CL05-37PC	51	71	1525 ± 15	1079 (1004-1153)	Shell fragments	UCIAMS-40623*
COR0503-CL05-37PC	355	375	8030 ± 25	8482 (8406-8557)	Shell fragments	UCIAMS-40621*
COR0503-CL05-37PC	454	474	8555 ± 25	9113 (9086-9300)	Shell fragment	UCIAMS-40618*
COR0503-CL05-37PC	637	657	9160 ± 20	9977 (9845-10108)	Shell fragment	UCIAMS-40615*

CHAPITRE 3

DATING OF HOLOCENE WESTERN CANADIAN ARCTIC SEDIMENTS BY MATCHING PALEOMAGNETIC SECULAR VARIATION TO A GEOMAGNETIC FIELD MODEL

3.1 Abstract

A recently recovered ~ 6 m-long Holocene sedimentary sequence (piston Core 2004-804-650) collected from the Beaufort Sea (western Canadian Arctic) was dated by combining the paleomagnetic secular variation (PSV) and a time-varying spherical harmonic model of the geomagnetic field (CALS7k.2). A u-channel-based paleomagnetic study reveals the presence of a stable, single component of magnetization (MAD < 5°) carried by low-coercivity ferrimagnetic minerals (most likely magnetite) in the pseudo-single domain grain size range. An age-depth model spanning the last ~ 6000 cal BP was established from nine paleomagnetic tie points obtained by comparing the magnetic declination profiles of Core 650 and the CALS7k.2 model output. In order to verify the robustness of the method, both the magnetic inclination and the relative paleointensity (RPI) records of Core 650 were then compared with western North American lacustrine and volcanic Holocene PSV records, as well as with previously published RPI records from the Beaufort and Chukchi Seas. Several common magnetic inclination features and similar millennial-scale fluctuations are detected among the records, supporting a common geomagnetic origin of the records, and implying consistency of the derived age model. These results show the potential of using both the CALS7k.2 model output and PSV of the geomagnetic field as a practical dating tool.

3.2 Introduction

In the last decades, an increasing number of globally distributed paleomagnetic data (archeomagnetic and lacustrine paleomagnetic data) have lead to the development of a time-varying spherical harmonic model of the geomagnetic field CALS7k.2 over the last 7000 years (Korte and Constable, 2005). In the recent years, several studies have revealed the potential use of the CALS7k.2 model to determine episodes of eastward and westward drift of the geomagnetic field (e.g., Dumberry and Finlay, 2007) as well as the evolution of the position of the geomagnetic poles during the Holocene (Korte and Mandea, 2008), thus giving new insights about the generation of the dipole field. On the other hand, little attention has been given to the practical use of paleomagnetic secular variation (PSV) computed by CALS7k.2 as a dating tool.

For instance, Holocene paleoceanographic reconstructions from the Canadian Arctic environments are difficult to obtain due to lack of robust chronologies (e.g., Hillaire-Marcel, 2008). Indeed, datable material is often rare and (or) not well preserved in the Arctic (e.g., Ledu et al., 2008; McKay et al., 2008). Moreover, the radiocarbon dating technique by acceleration mass spectrometry (AMS) is complicated due to an often poorly constrained radiocarbon reservoir effect (Darby et al., 2009), and diagenetic effects distort the paleomagnetic record over much of the central Arctic ocean (Channell and Xuan, 2009; Xuan and Channell, 2010). In this paper, we show how it is possible to overcome some of the problems associated with dating an Arctic marine sedimentary sequence collected from the Beaufort Sea (western Canadian Arctic) using PSV in conjunction with the CALS7k.2 model output and one radiocarbon date.

3.3 Regional setting

Piston core 2004-804-650PC (hereinafter referred as to Core 650) was raised from the Beaufort Sea on the Mackenzie Shelf area (Fig. 3.1; Table 3.1). Previous studies revealed that Holocene postglacial sedimentary sequences collected from both the Arctic Alaskan and Canadian margins are characterized by higher sedimentation rates than in the rest of the central Arctic basin (e.g., Darby et al., 2006; Rochon et al., 2006; Darby et al., 2009; Bringué, 2009). Holocene average sedimentation rates were estimated to vary between 10 to 300 cm/kyr (e.g., Andrew and Dunhill, 2004; Keigwin et al., 2006; Rochon et al., 2006; Barletta et al., 2008; Lisé-Pronovost et al., 2009) thus offering the opportunity to reconstruct centennial-to millennial-scale geomagnetic field variations in the Arctic (e.g., Barletta et al., 2008; Lisé-Pronovost et al., 2009). Moreover, due to the proximity of the North Magnetic Pole (NMP; Fig. 3.1), sedimentary sequences from western Canadian Arctic have the advantage of recording higher amplitude PSV directional changes than the rest of the Earth.

Figures 3.1B and 3.1C illustrate the location of the global compilation of directional paleomagnetic and archeomagnetic data, respectively, used to constrain the CALS7k.2 model (Korte et al., 2005). The directional dataset used in the CALS7k.2 model is mainly derived from lacustrine sedimentary sequences and archaeological artefacts or volcanic rocks from the Northern Hemisphere.

Table 3.1. Coordinates of the core.

Core	Latitude (°N)	Longitude (°W)	Water depth (m)	Length (m)
2004-804-650	71°.18.52'	131°36.98'	246	6.08

Table 3.2. Radiocarbon date.

Core	Depth (cm)	Age (yr BP)[a]	Calibrated age (cal BP)[b]	Dated material	Lab. Number[c]
2004-804-650	135	4080 ± 40	3580 (3463-3701)	*Littorina* sp.	Beta-204830

The age was determined by the AMS method and corrected for natural and sputtering fractionation ($\delta^{13}C$ = -25‰ versus Vienna Pee-Dee Belemnite (VPDB)). The statistical uncertainty of the age determination is given as one standard deviation (Stuiver and Polach, 1977). [b]Calibrated using the on-line CALIB 5.0.2 software (Stuiver et al., 2005) using the Hughen et al. (2004) marine dataset. A total marine reservoir correction of ~ 800 years, was applied (ΔR = 400 yr). The first and last ages, in parentheses, represent the 2σ cal age range. [c]Beta analytic Inc., Miami, FL, USA.

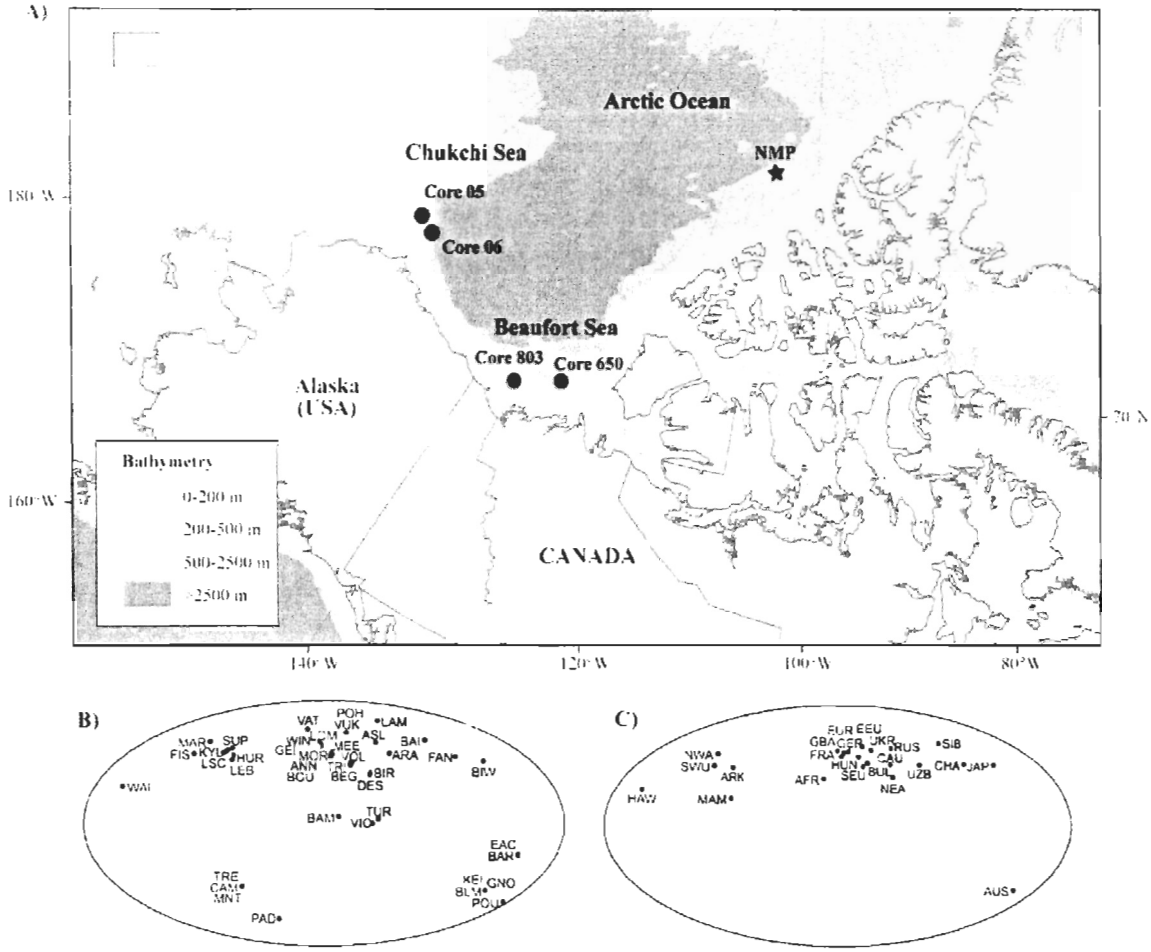

Fig. 3.1. (A) Location of Core 650 (this study) sampling site. Also illustrated is the location of Cores 05, 06 and 803 from the Chukchi and the Beaufort Seas (Barletta et al., 2008; Lisé-Pronovost et al., 2009). The position of the North Magnetic Pole (NMP) as determined by a joint Canada-France expedition in 2001 is indicated (Newitt et al., 2002). The box in the inset shows the location of the study area. (B) Location of the global directional paleomagnetic data compilation from sedimentary sequences and (C) from archeomagnetism used to constrain the CALS7k.2 model (modified from Korte et al., 2005). The details of the compilation are presented in Korte et al. (2005).

3.4 Materials and methods

Core 650 was collected on board the Canadian Coast Guard Icebreaker (CCGS) Amundsen during the 2004 Canadian Arctic Shelf Expedition Study (CASES). The core sections were split, described on board and then sampled with u-channel samples (u-shaped plastic liners of 2×2 cm cross-section and length up to 1.5 m) for paleomagnetic analyses. Apart from hysteresis properties and grain size analyses, all magnetic remanences as well as the low-field magnetic susceptibility (k_{LF}) measurements were carried out at the University of Florida (Gainesville, FL) using a 2G Enterprises Model 760R cryogenic magnetometer and a pulse magnetizer for the induction of isothermal remanent magnetizations. The continuous paleomagnetic measurements were performed at 1 cm intervals. Nonetheless, due to the response function of the magnetometer's pick-up coils each measurement integrates across a ~ 4.5 cm stratigraphic interval (Weeks et al., 1993). Therefore, the data from the upper and lower 4 cm of each u-channel were not used in order to eliminate edge effects (i.e., the integration of "no sediment" at the end and the beginning of each u-channel).

3.4.1 Magnetic measurements

U-channel samples were subjected to stepwise alternating field (AF) demagnetization of the natural remanent magnetization (NRM) at peak AF fields of 0, 10-60 mT in 5 mT steps, 70, and 80 mT. In order to determine the characteristic remanent magnetization (ChRM), the magnetic declination and inclination of the ChRM (labelled as ChRM D and ChRM I, respectively) were computed at 1 cm intervals using the standard

principal component analysis (PCA) of Kirschvink (1980) which also provide the maximum angular deviation (MAD) values. MAD values lower than 5° are indicative of high-quality directional data (e.g., Stoner and St-Onge, 2007). Subsequently, the stepwise acquisition and demagnetization of both the anhysteretic and isothermal remanent magnetizations (indicated as ARM and IRM, respectively) were acquired with the aim to characterize changes in magnetic mineral concentration. The ARM was imparted using a 100 mT AF field superposed to a direct current (DC) bias field of 50 μT whereas two IRMs were acquired applying a DC pulse field of 0.3 T and 0.95 T (corresponding to a saturated isothermal remanent magnetization, SIRM) respectively. These IRMs were used to construct a coercivity-dependent proxy by dividing the IRM at 0.3 T by the SIRM (St-Onge et al., 2003). This ratio is useful to estimate changes in magnetic mineralogy, with values close to 1 indicating a low-coercivity ferrimagnetic mineralogy (e.g., magnetite) and lower values indicating a higher coercivity, possibly antiferromagnetic (e.g., hematite) mineralogy.

Both the ARM and IRMs were then demagnetized at the same AF steps as the NRM. The ARM was also expressed as an anhysteretic susceptibility (k_{ARM}) by normalizing the ARM with the biasing field. AF demagnetization data were used to compute the median destructive fields of the NRM, ARM and IRM (labelled as MDF_{NRM}, MDF_{ARM}, MDF_{IRM}, respectively; i.e., the value of the peak AF necessary to reduce the magnetic remanence to half of its initial value) using the software developed by Mazaud (2005). These three parameters are useful to characterize the mean coercivity state of the ferrimagnetic minerals which in turn depends on both the magnetic mineralogy and grain size (e.g., Dunlop and Özdemir, 1997). Furthermore, the magnetic grain size was estimated

using k_{ARM} versus k_{LF} diagram (King et al., 1983). The objective here is not to determine the absolute size of the magnetic grains as it was previously shown that ARM measurements vary from one laboratory to the other (Sagnotti et al., 2003), but rather to assess the extent and uniformity of the magnetic grain size distribution. Finally, a small quantity of sediment was collected every 10 cm over the top 3 m and in some selected intervals in order to study both the hysteresis properties and the IRM acquisition curves using an alternating gradient force magnetometer (AGM) (Princeton Measurement Corporation model MicroMag 2900 AGM) at the Paleomagnetism laboratory of the *Institut des sciences de la mer de Rimouski* (ISMER).

3.4.2 Computerized axial tomography analysis (CAT-scan)

Digital X-ray images of all u-channel samples were obtained by computerized axial tomography (CAT-scan) analysis with a 1-mm downcore resolution. The resulting gray scale images allow us to extract a tomographic intensity profile (CT numbers; e.g., St-Onge et al., 2007). CT numbers primarily reflect changes in sediment bulk density, mineralogy as well as porosity and can be also useful to detect core deformation or coring artefacts (e.g., Guyard et al., 2007; St-Onge et al., 2007).

3.4.3 Grain size analyses

Grain size measurements on Core 650 were made using a Beckman-Coulter laser diffraction analyzer (Model LS-13320; 0.04-2000 μm) at ISMER at 10 cm intervals. About

0.5 g of wet sediment was mixed in Calgon electrolytic solution (sodium hexametaphosphate, 20 g/L). Subsequently, the samples were rotated for at least 3 hours using an in-house rotator and then sieved (<2 mm) over the instrument prior to analysis. The statistical grain size distribution was computed using the Gradistat software (Blott and Pye, 2001) using at least two measurements.

3.4.4 Radiocarbon dating

One radiocarbon age was derived from a marine shell (*Littorina* sp.) using the radiocarbon accelerator mass spectrometry (AMS) technique (Table 2). The AMS-^{14}C age was then calibrated using the on-line CALIB 5.0.2 software (Stuiver et al., 2005) using the Hughen et al. (2004) marine dataset. A regional reservoir correction (ΔR) of 400 yr was applied based on the average ΔR values derived from five dates realized on pelecypod shells from the Amundsen Gulf area collected prior to atmospheric nuclear testing (McNeely et al., 2006).

3.5 Results

3.5.1 Stratigraphy

According to the visual description, Core 650 consists of bioturbated olive dark-gray (5YR 4/1) mud (Fig. 3.2A). As a whole, the mean grain size profile appears quite uniform (Fig. 3.2A). A gradual transition in sediment texture from silty-clays to clayey-silts is observed at 210 cm (Fig. 3.2A). The homogeneous and bioturbated sedimentary

facies that characterizes the entire core and the available AMS-^{14}C date suggest that Core 650 is composed entirely of postglacial sediments. This conclusion is consistent with recent cores collected in the Beaufort and Chukchi Seas (e.g., Andrews and Dunhill, 2004; Keigwin et al., 2006; Rochon et al., 2006; Barletta et al., 2008; Lisé-Pronovost et al., 2009; Polyak et al., 2009).

3.5.2 Magnetic properties

Occasional black horizons and diffuse laminae are observed in the core probably due to presence of iron sulfides. However, the magnetic mineralogy-dependent ratio SIRM/k_{LF} varies between ~ 7 and 12 kA/m, whereas the IRM/SIRM values are close to 1 (Fig. 3.2B). These values are consistent with a mixed assemblage containing magnetite and titanomagnetite (Peters and Thompson, 1998; Stoner and St-Onge, 2007).

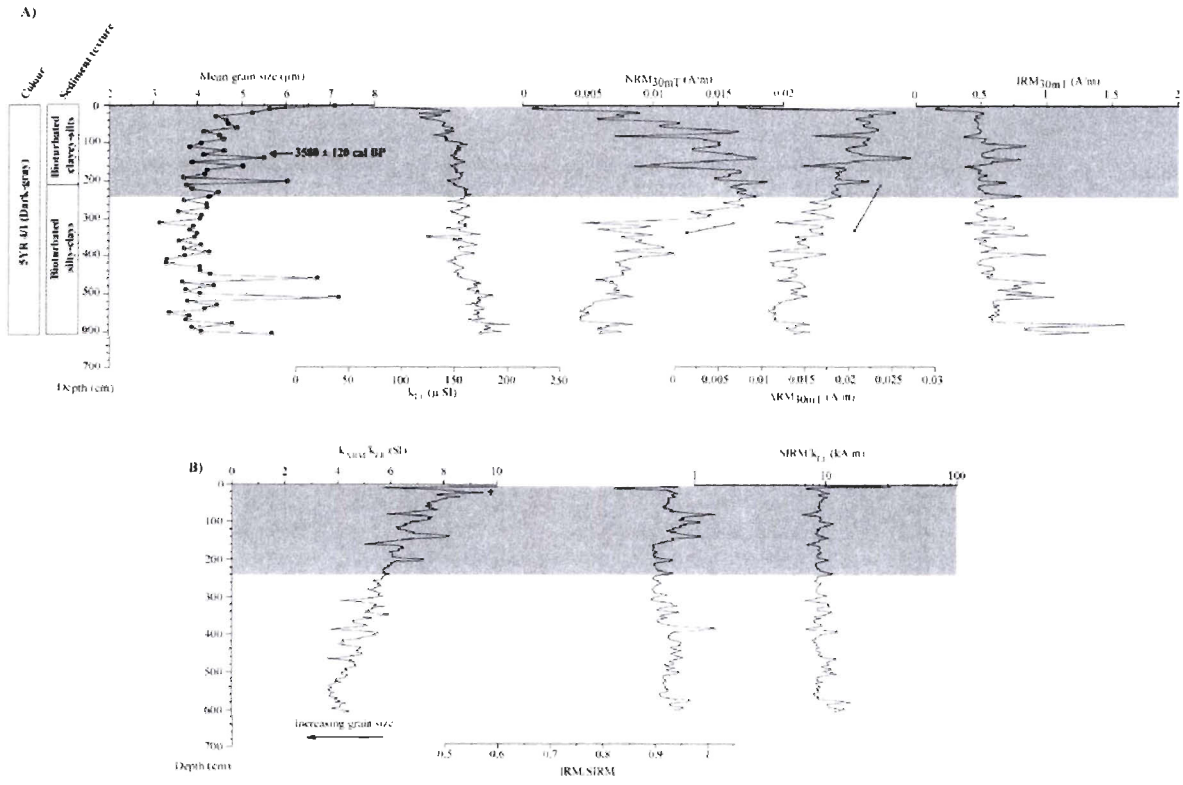

Fig. 3.2. Lithology and magnetic properties of Core 650. (A) Illustrated are mean grain size, low-field magnetic susceptibility (k_{LF}), natural remanent magnetization (NRM), anhysteretic remanent magnetization (ARM) and isothermal remanent magnetization (IRM) diagrams after an AF demagnetization at 30 mT. Arrows indicate decrease in remanence intensity with depth (see text for details). The only available AMS-^{14}C date is also indicated. (B) Magnetic parameters k_{ARM}/k_{LF}, IRM/SIRM and SIRM/k_{LF} against depth. The ratio IRM/SIRM is calculated after an AF demagnetization level of 30 mT in order to emphasize the relative importance of the high-coercivity component. The gray shaded area indicates the interval used for PSV and RPI reconstructions.

The magnetic concentration-dependent parameter ARM indicates that there is a slight decrease in remanence intensity with depth, suggesting possible downcore particle dissolution (Fig. 3.2A). The magnetic grain size sensitive ratio k_{ARM}/k_{LF} also displays a gradual downcore decrease suggesting a coarsening of the magnetic grain size, due to dissolution of fine grained magnetite (Fig. 3.2B). On the other hand, the low-field magnetic susceptibility (k_{LF}) and IRM records are less affected by the possible dissolution process as they are dominated by the coarser magnetic grain size fraction (Fig. 3.2A). Both hysteresis loop and IRM acquisition diagrams indicate saturation fields at ~ 100 mT with coercivities typical for magnetite (Fig. 3.3; e.g., Dunlop and Özdemir, 1997). According to the k_{ARM} versus k_{LF} diagram (King et al., 1983) magnetic grain size are compatible with the presence of magnetite in the ~ 0.1-5 μm size range (Fig. 3.4A), with a finer assemblage above 3 m: the interval used for PSV and RPI reconstructions. Similarly, the Mrs/Ms and Hcr/Hc ratios (where: Ms =saturation magnetization; Hc = coercive force; Mrs = saturation remanence; Hcr = coercivity of remanence) are typical for pseudo-single domain (PSD) magnetite according to the Day plot (Fig. 3.4B; Day et al., 1977).

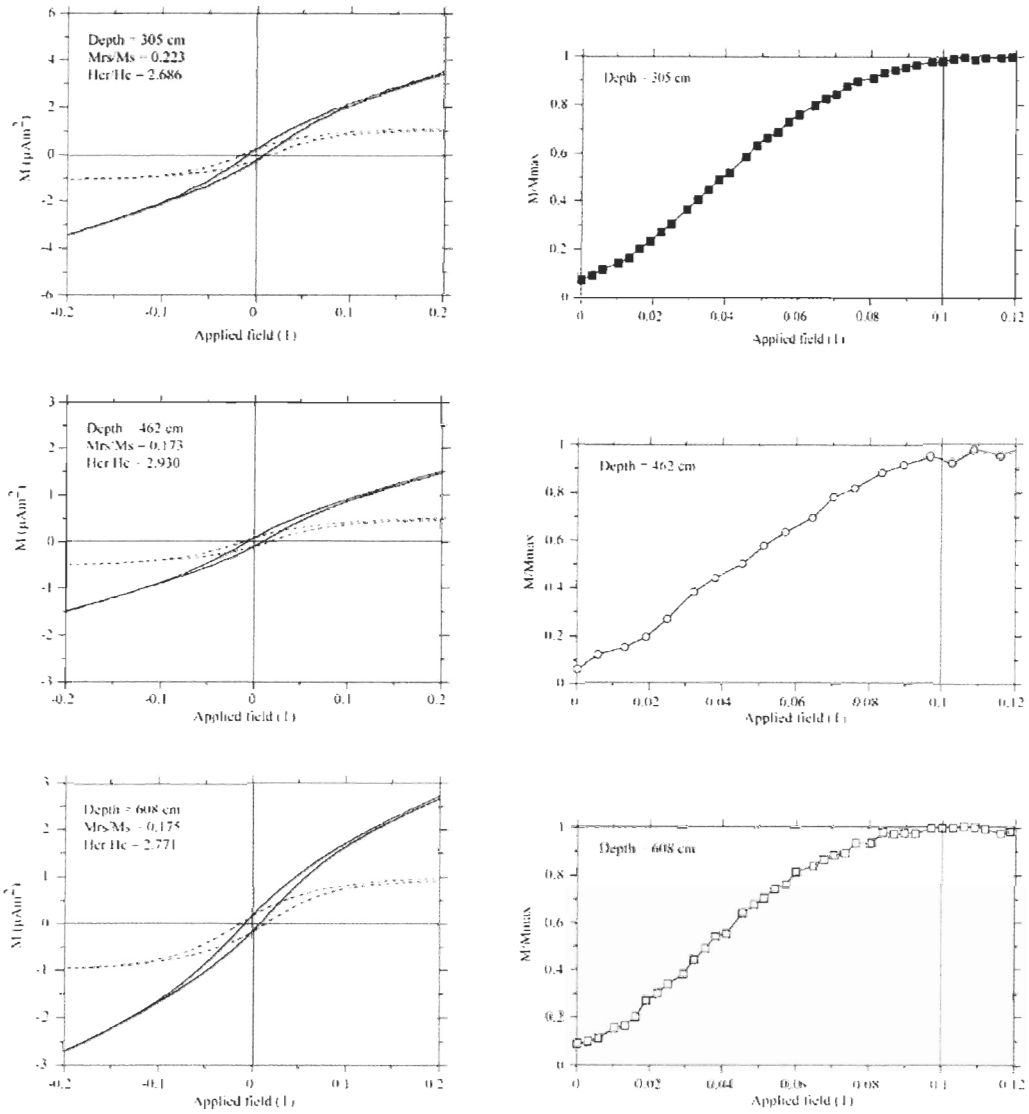

Fig. 3.3. (A) Representative hysteresis loops (left diagrams) with the corresponding IRM acquisition curves (right diagrams). The hysteresis parameters (saturation magnetization (M_S), saturation remanence (M_R) and coercivity (H_C)) were determined from the paramagnetic-corrected hysteresis data (broken curve in the left diagrams). Vertical line at 100 mT is for reference.

Fig. 3.4. (A) Magnetic grain size estimates. Blue triangles and green full circles symbols represent inferred grain size above and below 300 cm, respectively. Grain size contours are based on the measurement of synthetic magnetite samples by King et al. (1983). (B) Diagram of hysteresis ratios (Day plot) with single domain (SD), pseudo-single domain (PSD) and multi-domain (MD) regions for magnetite according to Day et al. (1977). The square and open symbols are associated to Fig. 3.3.

A)

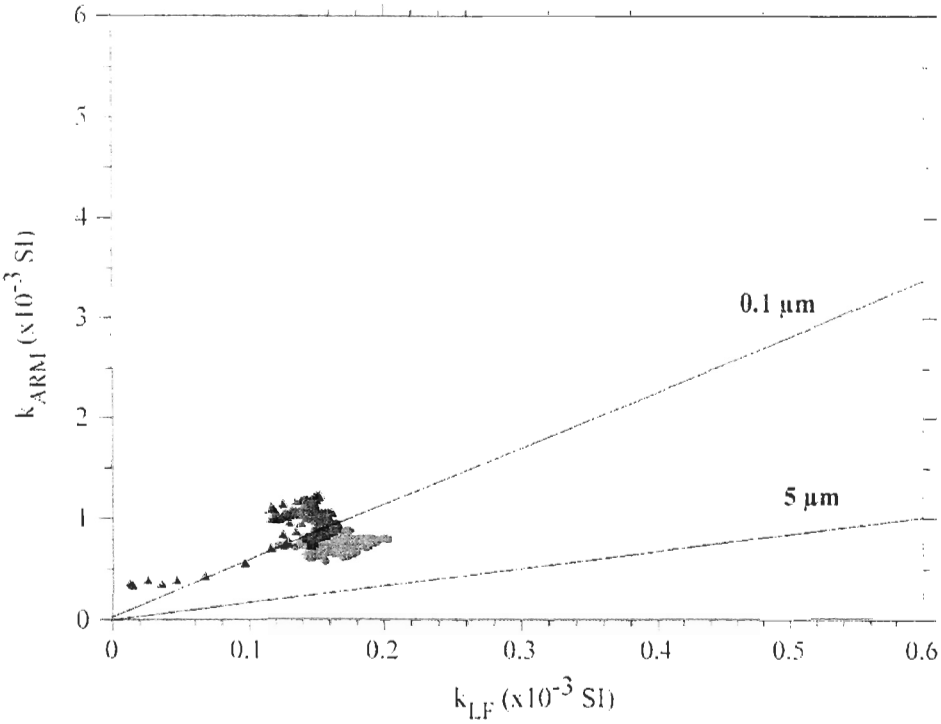
6
5
4
3
2
1
0
k_{ARM} (x10^{-3} SI)
0.1 µm
5 µm
0
0.1
0.2
0.3
0.4
0.5
0.6
k_{LF} (x10^{-3} SI)

B)

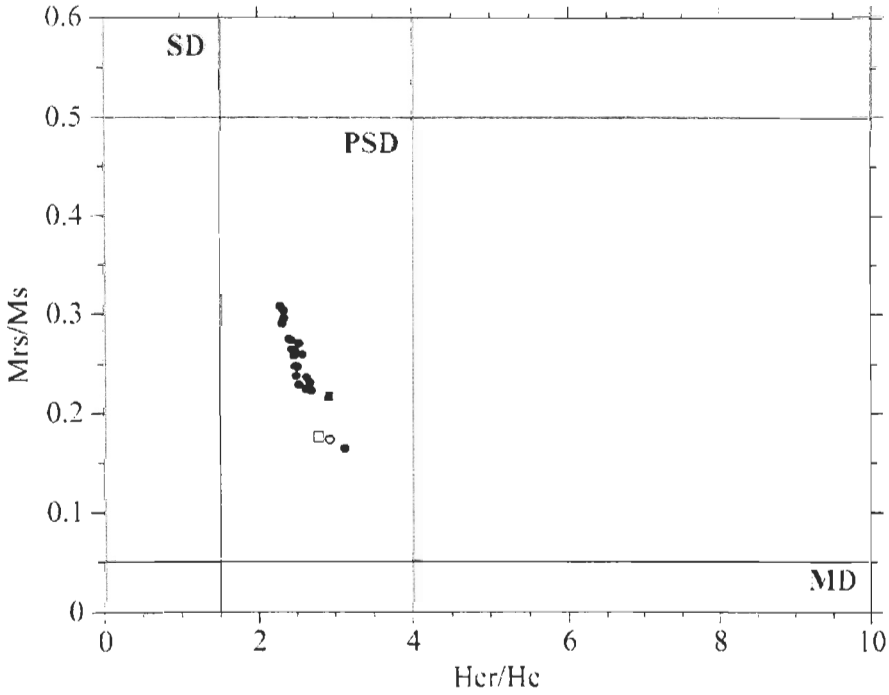
0.6
0.5
0.4
0.3
0.2
0.1
0
Mrs/Ms
SD
PSD
MD
0
2
4
6
8
10
Hcr/Hc

3.5.3 Natural remanent magnetization

The analysis of the vector end-point diagrams (Zijderveld, 1967) reveals the presence of two magnetic components (Fig. 3.5B): a low-coercivity component (viscous magnetization) in the 0-15 mT coercivity interval and a stable well-defined, characteristic magnetization. The latter was isolated by PCA analysis (Kirchivink, 1980) using 10 demagnetization steps between 20 and 80 mT. MAD values are well below 5° and the ChRM inclinations fluctuate around the expected inclination calculated according to the geocentric axial dipole (I_{GAD}) model at the coring site (80°) (Fig. 3.5A), indicating a well-preserved paleomagnetic signal. Moreover, the MDF_{NRM} and MDF_{ARM} vary around 35 mT and 30 mT respectively, whereas the MDF_{IRM} values are lower than the MDF_{ARM} values (Fig. 3.5A). These results indicate that the magnetic properties of Core 650 are mainly controlled by low-coercivity ferrimagnetic minerals such as magnetite (e.g., Dunlop and Özdemir, 1997).

If we focus on the top 240 cm (the interval used for the PSV and RPI reconstruction), only a single case of slight sediment disturbance is detected at the base of a u-channel at one of the section breaks (from 74 to 77 cm; Fig. 3.6). No deformation is observed at the top of the following u-channel (77-81 cm), nor at the other section break (from 153 to 160 cm; Fig. 3.6). In addition, no high MAD values were observed at the base or top of the u-channels (Figs. 3.5 and 3.6) in these two core breaks. In summary, even if possible dissolution may have occurred downcore, the sediments are characterized by well-defined, strong characteristic magnetization carried by PSD grains with a uniform grain size. In addition, all the magnetic parameters and hysteresis properties point to low-coercivity minerals, such as magnetite, as the main carriers of the magnetic remanence.

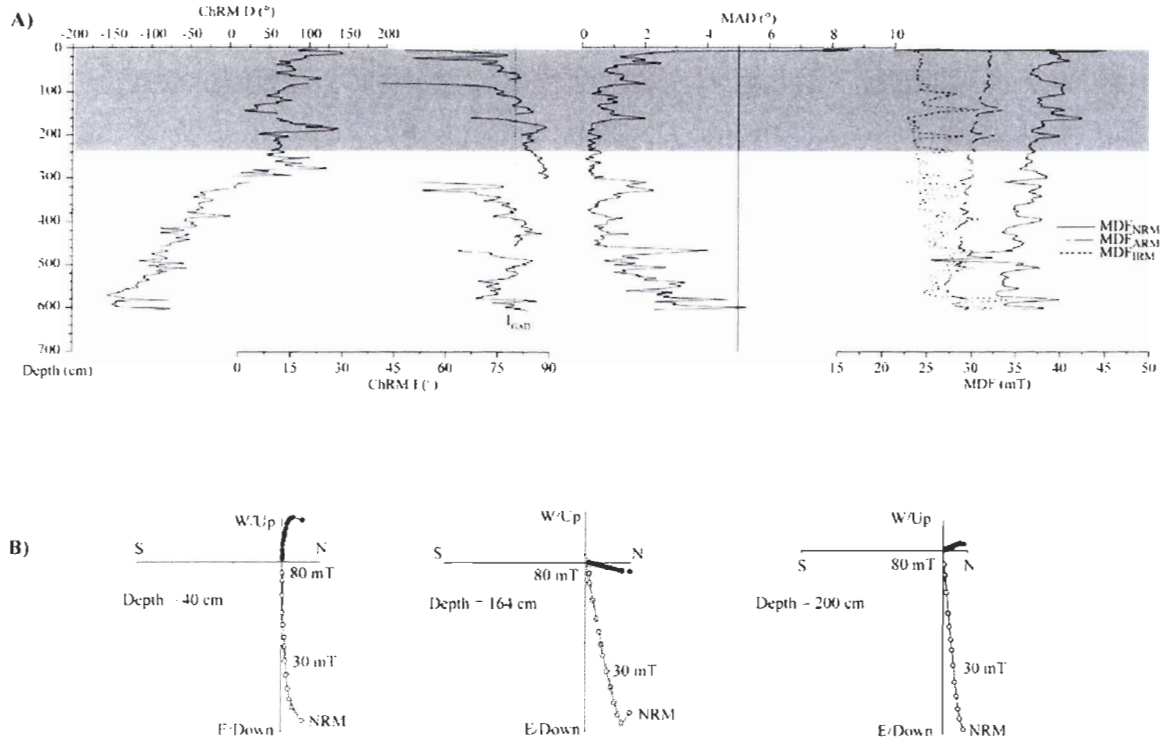

Fig. 3.5. The characteristic remanent magnetization (ChRM) of Core 650. (A) From left to right are displayed: the magnetic declination (D), inclination (I) of the ChRM as well as the corresponding MAD values and median destructive fields (MDF). Note that the ChRM D profiles are relative since the core was not azimuthally oriented. The broken vertical line in the ChRM inclination diagram represents the expected inclination (I_{GAD}) for a geocentric axial dipole model, whereas the solid vertical line indicates a MAD value of 5°. The gray shaded area indicates the interval used for PSV and RPI reconstructions. (B) Representative vector end-point orthogonal projection diagrams (Zijderveld, 1967) at three selected depths. AF demagnetization data reveal a stable single component magnetization that is directed toward the origin of the vector component diagram. Open (closed) symbols represent vector end points projected on the vertical (horizontal) plane, respectively. Peak alternating fields are indicated in mT.

Fig. 3.6. Magnetic inclination record of Core 650 (first 240 cm; lower diagram) and the computerized tomography (CT) numbers derived from the CAT-scan (Computerized Axial Tomography) analysis at the three core breaks (middle diagrams). Shaded dark gray areas indicate the three intervals affected by an edge effect at core breaks due the response function of the cryogenic magnetometer (see text for details), whereas the vertical line represent the precise location of the section breaks. The paleomagnetic data in these three intervals (0-4 cm, 74-81 cm and 153-160 cm) were excluded, but note the homogenous nature of the CT number profiles from 77 cm and below, as well as from 153 cm and below, indicative of undisturbed sediments. On the contrary, major changes in the CT number profile of the first ~ 12 cm are indicative of a coring artefact. The vector end-point orthogonal projection diagrams (upper diagrams) below and above each section break associated with the magnetic features I-1 and I-5 (see Fig. 3.9) reveal high quality component directions (MAD < 5°). Closed (open) symbols represent projection on the horizontal (vertical) planes of the orthogonal projections.

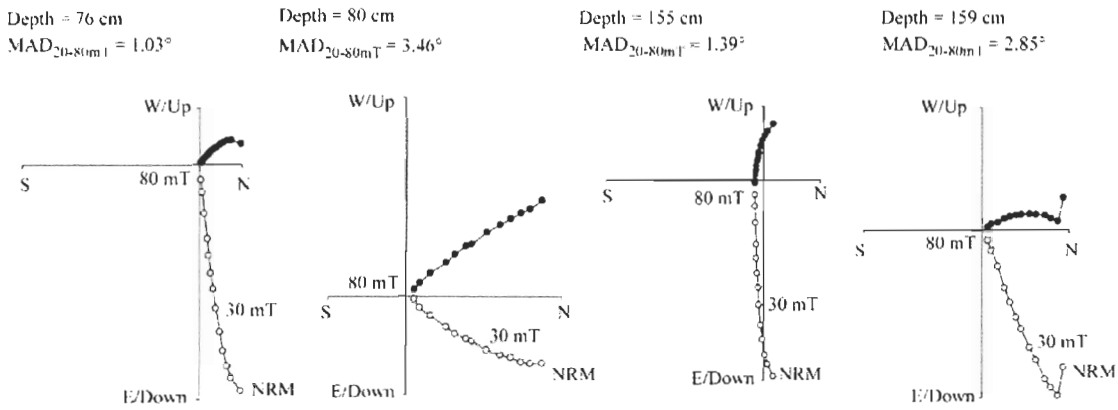
Depth = 76 cm
MAD20-80mT = 1.03°
Depth = 80 cm
MAD20-80mT = 3.46°
Depth = 155 cm
MAD20-80mT = 1.39°
Depth = 159 cm
MAD20-80mT = 2.85°
W/Up
S
N
80 mT
30 mT
NRM
E/Down

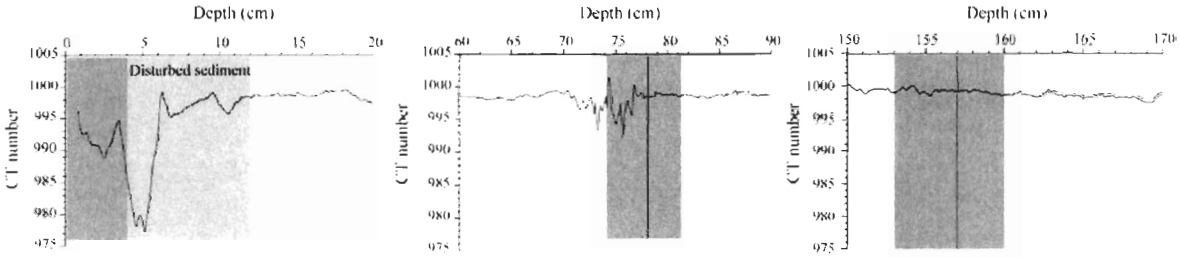
Depth (cm)
CT number
Disturbed sediment

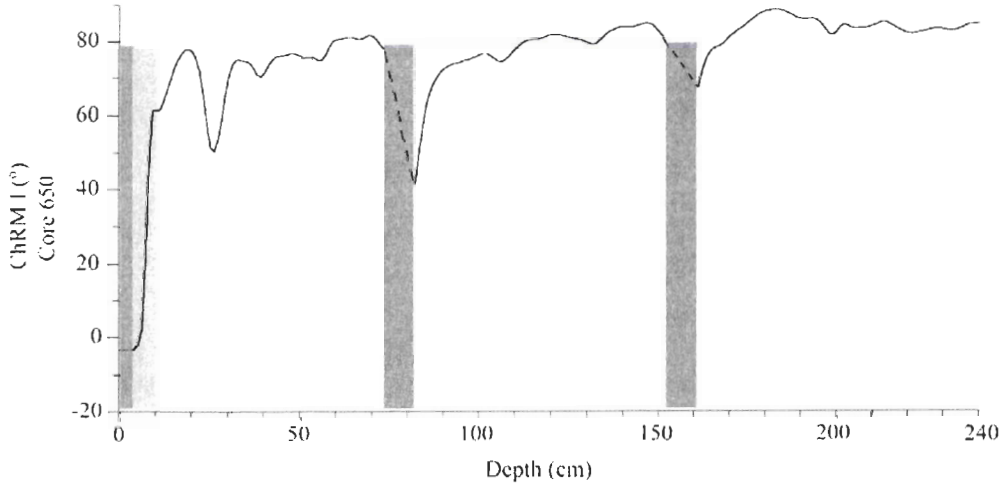
ChRM I (°)
Core 650
Depth (cm)

3.5.4 Relative paleointensity (RPI) determination

Estimation of relative paleointensity (RPI) from sediments can be obtained by normalizing the measured NRM by an appropriate magnetic parameter in order to compensate for the variable concentration of ferrimagnetic minerals (e.g., Tauxe, 1993). Concentration-dependent parameters such as ARM, IRM or k_{LF} are generally employed as normalizer. To assess the reliability of a RPI proxy some pre-established criteria must be satisfied. According to Tauxe (1993), the NRM must be characterized by a strong, stable, single component magnetization carried by (titano)magnetite in the 1-15 μm (SD/PSD) grain size range. Moreover, due to the effect of magnetostatic interaction between ferrimagnetic particles on the ARM acquisition (Sugiura, 1979) concentration of magnetite should not vary downcore by more than a factor of 10 (Tauxe, 1993). Finally, the normalized paleointensity records from the same geographical area should display similar pattern.

As shown in the previous sections, the ChRM of Core 650 is characterized by MAD values < 5° carried by relatively uniform fine-grained magnetite (Figs. 3.4A and 3.4B). The ARM varies by less than a factor of 3 (Fig. 3.2A). However, as stated in the previous sections, the ARM profile likely reflects a slight downcore coarsening (Fig. 3.2A). In addition, below ~ 1 μm the ARM is strongly grain size dependent (e.g., Dunlop and Özdemir, 1997). Therefore, due to the small magnetic grains observed in Core 650 (Fig. 3.4A), the use of the ARM as a normalizer may not be appropriate. In contrast, both k_{LF} and IRM are not affected in the same way as the ARM (Fig. 3.2A) and are therefore likely more suitable for these sediments. This is well illustrated in Fig. 3.10 where NRM/IRM and NRM/k_{LF} yield similar results both in terms of fluctuation and amplitude,

whereas NRM/ARM seems to capture a more pronounced long-term trend and lower amplitude fluctuations, especially from 2500 to 5000 cal BP. NRM/IRM and NRM/k_{LF} are also consistent with a previously published record from the Beaufort Sea (Core 803; Barletta et al., 2008; Fig. 3.10) and further support the use of k_{LF} or IRM as a normalizer.

3.5.5 Paleomagnetic dating of Core 650

A direct comparison (R = 0.71) of the relative ChRM declination of Core 650 and the computed declination from the CALS7k.2 model is possible for the first 240 cm and allows the detection of nine common paleomagnetic declination features during the last 6000 cal BP (Fig. 3.7). An age model was then constructed transferring these chronostratigraphic markers and the available AMS-^{14}C date on the first 240 cm of Core 650. A fifth-order polynomial fit (R = 0.999) was used between the uppermost and the lowermost dates (Fig. 3.8). With these assumptions, a mean sedimentation rate of ~ 33.4 cm/kyr was estimated.

In order to verify the robustness of this approach, the derived ChRM inclination profile of Core 650 is compared with other high-resolution western North American Holocene PSV records. As revealed from Fig. 3.9, two distinctive magnetic inclination features at ~ 1800 and ~ 2500 cal BP (magnetic features I-1 and I-2, respectively) are present in all the considered records as well as in the CALS7k.2 model. The different nature of the PSV records (marine: Cores 05 and 803 (Barletta et al., 2008); lacustrine: Mara Lake (Turner, 1987); volcanic rocks: paleomagnetic secular variation from lava flows (PSVL) compilation (Hagstrum and Champion, 2002) further corroborates the geomagnetic origin of these signals. Moreover, three magnetic inclination minima (I-3 ~ 3000 cal BP; I-4 ~ 3700 cal BP; I-5 ~ 4600 cal BP; Fig. 3.9) are observed in all the marine sedimentary

sequences from the Chukchi and Beaufort seas. However, as depicted from Fig. 3.9, the inclination values of the magnetic features I-2 and I-5 overlap two core breaks. Even though the deleted data represent a cumulative 8 cm at core break, the inclination minima I-2 and I-5 still reveal a clear trend reflected by several data points. Regardless of these two inclination minima and in addition to the inclination maxima, the overall correspondence between the inclination curves of the different records (Fig. 3.9) can be ascribed to variations in Earth's magnetic field.

The derived relative paleointensity record of Core 650 using both k_{LF} and IRM as normalizers (Fig. 3.10) depicts similar millennial-scale fluctuations when compared to other previously published RPI records from the same geographical area (Cores 05 and 803: Barletta et al., 2008; Core 06: Lisé-Pronovost et al., 2009; see Fig. 3.1 for location) further supporting the derived age model. Two RPI highs at ~2000 and 4000 cal BP are notably observed (P-1 and P-3; Fig. 3.10) and were previously recognised by Barletta et al. (2008) as two distinctive western Canadian Arctic chronostratigraphic markers.

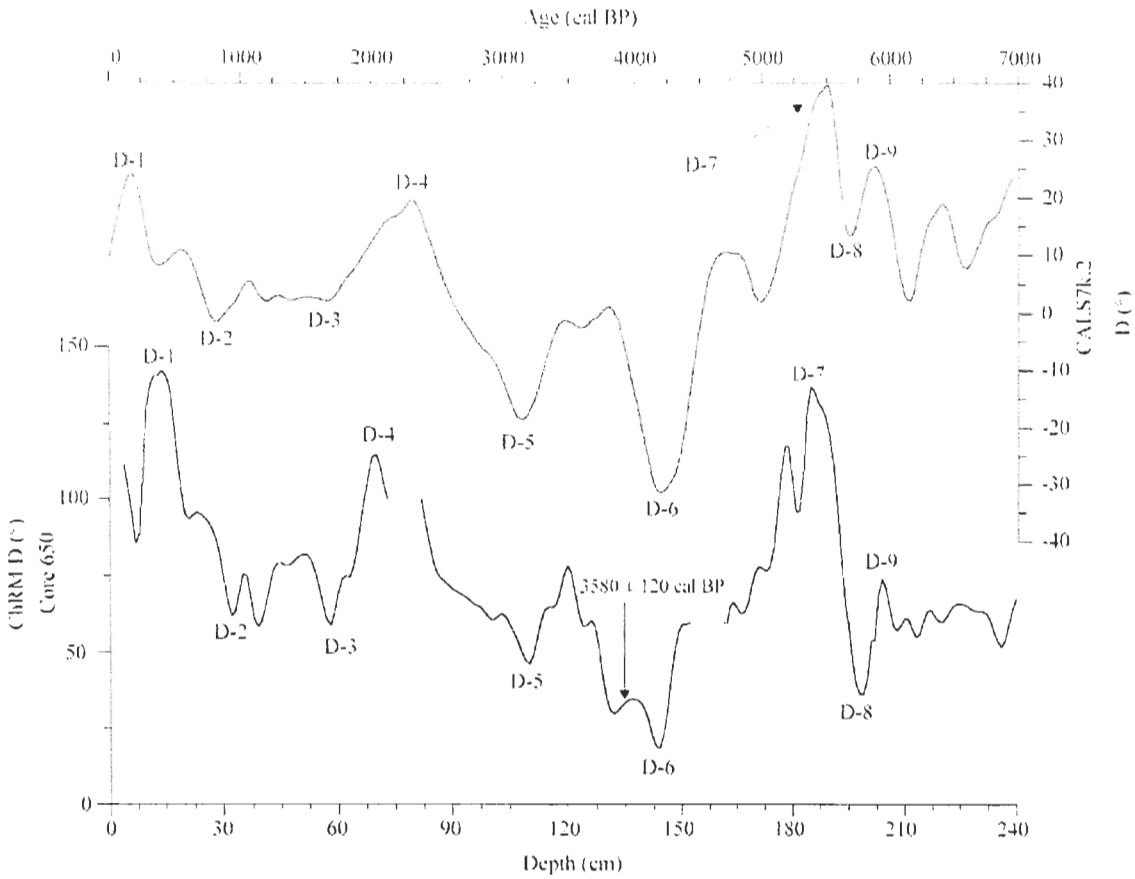

Fig. 3.7. The calculated magnetic declination (upper blue curve) from the CALS7k.2 model for the past 7000 cal BP (as expected for the Beaufort Sea region) and the relative ChRM declination curve of Core 650 versus depth (lower black curve). The proposed nine magnetic declination features (D-1 to D9) as well as the available AMS-^{14}C date used to construct the age model are indicated. Note that the declination scales are not identical.

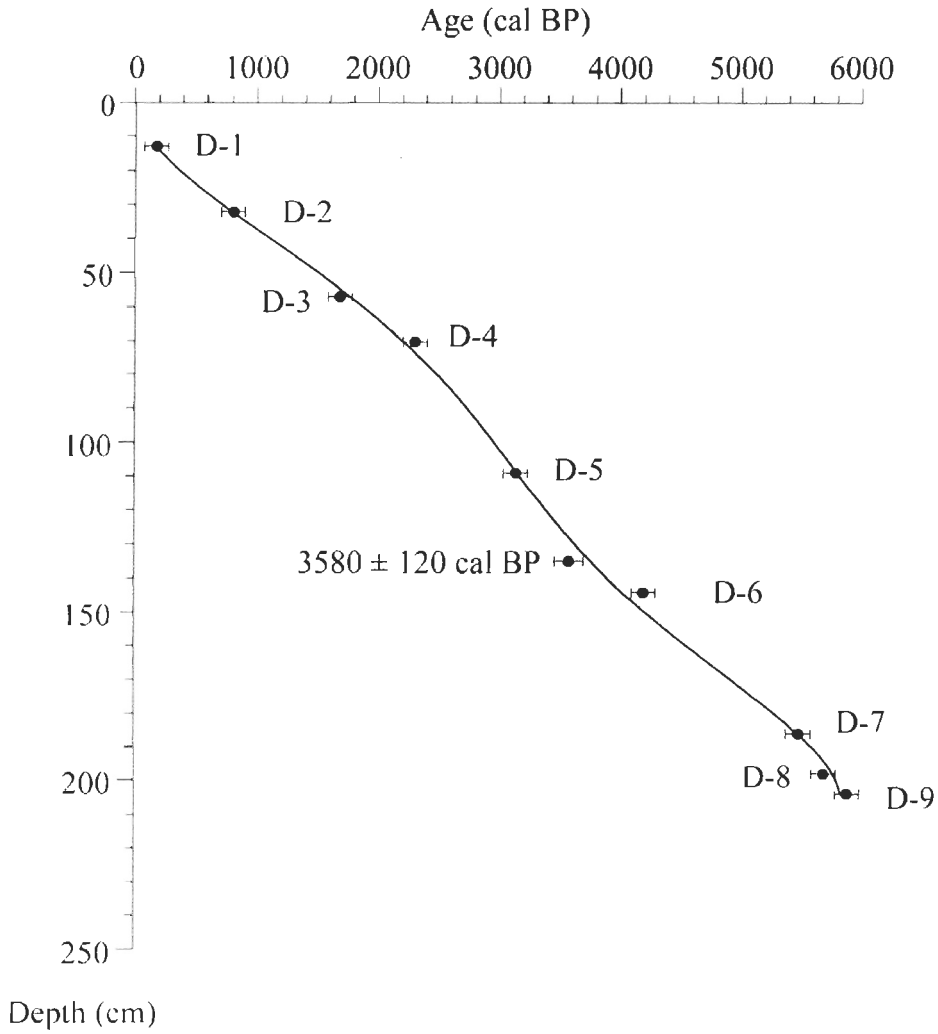

Fig. 3.8. Age model of Core 650. The age model was constructed using a fifth-order polynomial fit (R = 0.999) between the chronostratigraphic markers of Fig. 3.7 and the available AMS-^{14}C date of Core 650. Uncertainties associated with the magnetic declination features are assumed to be ~ 100 years according to the temporal resolution of the CALS7k.2 model (Korte and Constable, 2005).

Fig. 3.9. Comparison of western North American magnetic inclination records for the past 6000 cal BP. Common magnetic inclination features are indicated. PSV records are from: Mara Lake, British Columbia, Canada (Turner, 1987); PSVL = paleomagnetic secular variation record from lava flows, Western North America, USA (Hagstrum and Champion, 2002); Cores 05 and 803 from the Chukchi and the Beaufort seas, respectively (Barletta et al., 2008); Core 650, this study (note that the data along the u-channels section breaks are excluded because they are affected by an "edge effect" due to the response function of the cryogenic magnetometer). The magnetic inclination expected for the Beaufort Sea from the CALS7k.2 model is also displayed (blue upper curve). The original PSV record from Mara Lake was calibrated using the IntCal04 radiocarbon calibration curve (Reimer et al., 2004). Note that the magnetic inclination scales are not identical.

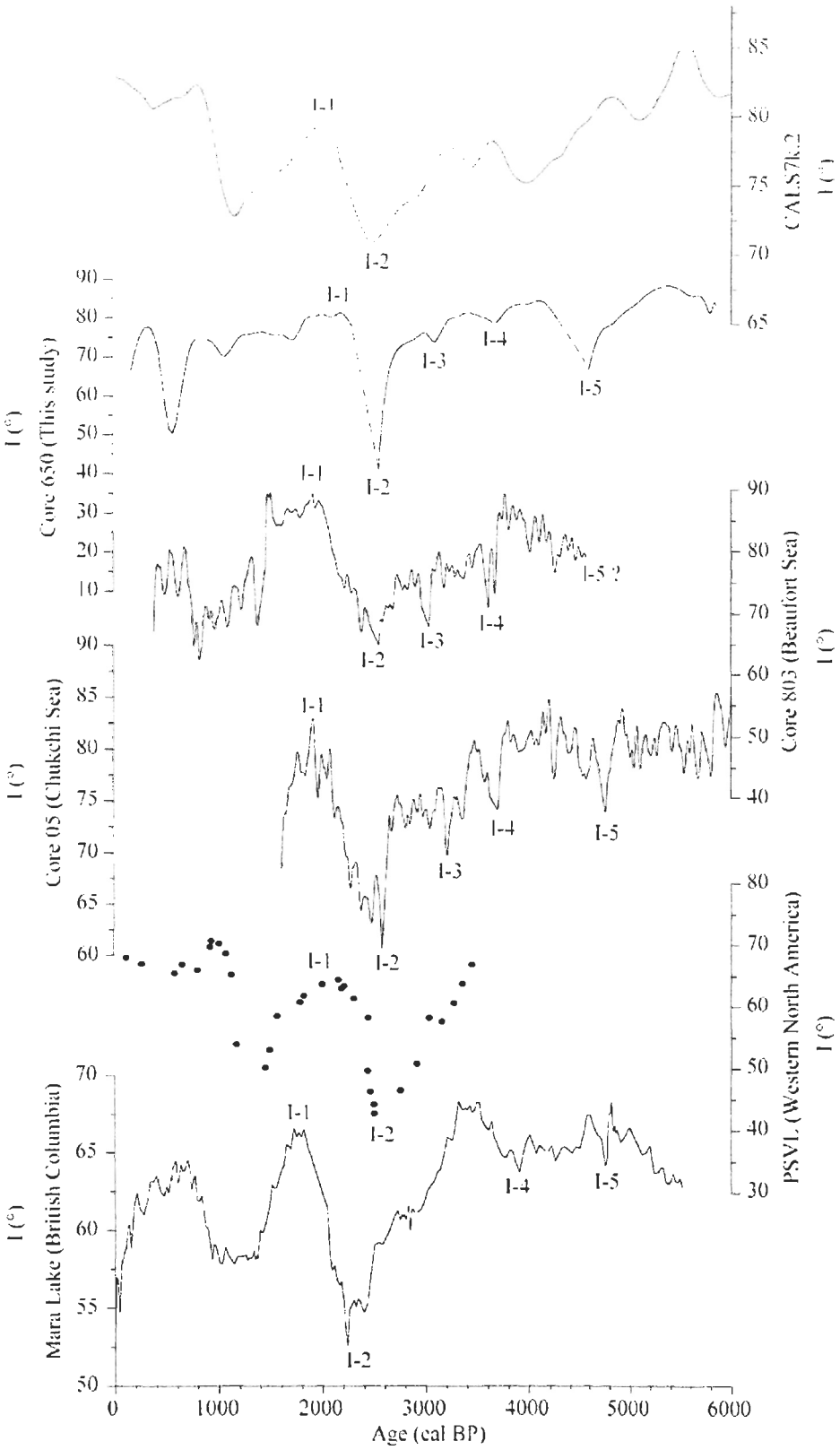
I-1
I-2
I-3
I-4
I-5
I-5 ?
I (°)
CALS7k.2
Core 650 (This study)
Core 803 (Beaufort Sea)
Core 05 (Chukchi Sea)
PSVL (Western North America)
Mara Lake (British Columbia)
Age (cal BP)
0
1000
2000
3000
4000
5000
6000

Fig. 3.10. Relative paleointensity (RPI) records of Cores 05 (Barletta et al., 2008), 06 (Lisé-Pronovost et al., 2009), 650 (this study) and 803 (Barletta et al., 2008) on their own chronologies. The RPI data of Core 650 were obtained by dividing the NRM after an AF demagnetization of 30 mT by the k_{LF} (thick black curve), ARM (light gray curve) and IRM (dark gray curve), respectively. Note the similarities in both shape and amplitude of the derived RPI proxies of Core 650 using both k_{LF} and IRM as normalizer as well as the general agreement between the RPI record of Core 650 and the other RPI records. All the data are standardized according to their mean and standard deviation. The curve fit in the RPI record of Core 803 (red curve in the web version) was calculated by using the locally weighted least squares method with a 9 % weighting function. Correlative paleointensity features are indicated (P-1 to P-3).

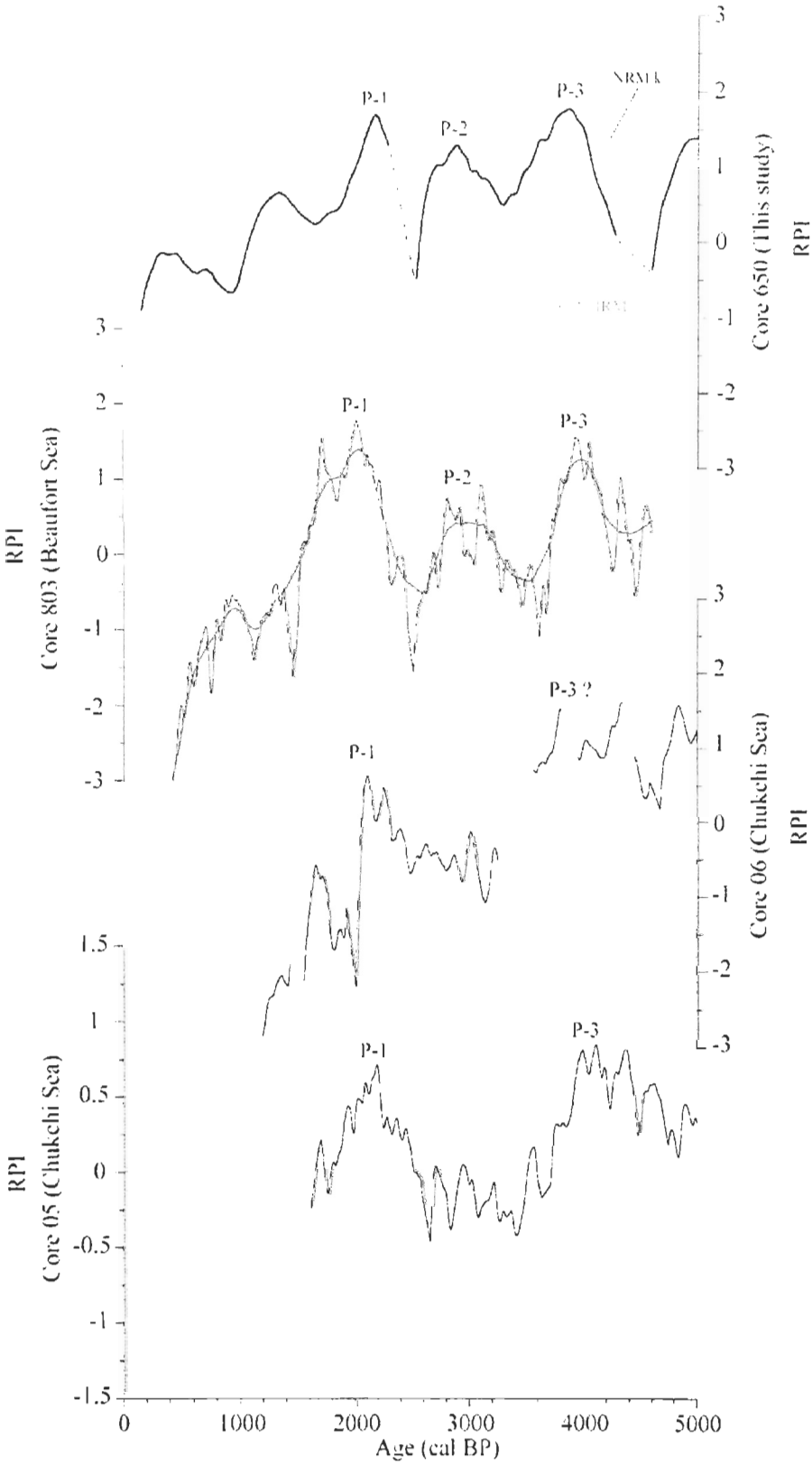
P-1
P-2
P-3
NRM1k
Core 650 (This study)
RPI
Core 803 (Beaufort Sea)
P-3 ?
Core 06 (Chukchi Sea)
Core 05 (Chukchi Sea)
Age (cal BP)
0
1000
2000
3000
4000
5000

3.6 Conclusion

In conclusion, our study reveals the potential of using the CALS7k.2 model as a relative dating tool in the Canadian Arctic. The actual North American database used to constrain the CALS7k.2 model seems sufficient to describe most of the millennial-scale Holocene PSV features observed in the western Canadian Arctic as previously highlighted by Barletta et al. (2008) and Lisé-Pronovost et al. (2009). Recently, Ledu et al. (accepted) used similarities in the magnetic inclination record and the CALS7k.2 output to improve the age model of a Holocene marine sedimentary sequence collected from the Lancaster Sound (eastern Canadian Arctic). Accordingly, these results open the possibility of using this chronostratigraphic approach in both the western and eastern Canadian Arctic.

3.7 Acknowledgements

We are in debt to the captain, officers, crew and scientists on board the CCGS Amundsen for the recovery of Core 2004-804-650. We wish to thank the two anonymous reviewers for their constructive reviews as well as Dr. M. Korte for providing the CALS7k.2 model output for the Beaufort Sea. We thank Jacques Labrie for his technical support. This study was supported by the Canadian Arctic Shelf Exchange Study (CASES), NSERC Discovery and Northern supplement as well as Special Research Opportunity (IPY) grants to G.S. and A.R. This is GEOTOP contribution number 2010-0004.

3.8 References

Andrews, J.T., Dunhill, G., 2004. Early to mid-Holocene Atlantic water influx and deglacial meltwater events, Beaufort Sea slope, Arctic Ocean. Quaternary Research 61, 14-21.

Barletta, F., St-Onge, G., Channell, J.E.T., Rochon, A., Polyak. L., Darby, D.A., 2008. High-resolution paleomagnetic secular variation and relative paleointensity records from the western Canadian Arctic: implication for Holocene stratigraphy and geomagnetic field behaviour. Canadian Journal of Earth Sciences 45, 265-1281.

Blott, S.J., Pye, K., 2001. Gradistat: a grain size distribution and statistics package for the analysis of unconsolidated sediments. Earth Surface Processes and Landforms 26, 1237-1248.

Bringué, M., 2009. Paléocéanographie et variabilité climatique sur le talus du Mackenzie (Mer de Beaufort, Arctique canadien) au cours de l'Holocène. M.Sc. thesis, Université du Québec à Rimouski, Rimouski, Canada, 104 pp.

Channell, J.E.T., Xuan, C., 2009. Self-reversal and apparent magnetic excursions in Arctic sediments. Earth and Planetary Science Letters 284, 124-131.

Darby, D.A., Polyak, L., Bauch, H.A., 2006. Past glacial and interglacial conditions in the Arctic Ocean and marginal seas – a review. Progress in Oceanography 71, 129-144.

Darby, D.A, Polyak, L., Jakobsson, M., 2009. The 2005 HOTRAX Expedition to the Arctic Ocean. Global and Planetary Change 68, 1-4.

Day, R., Fuller, M., Schmidt, V.A., 1977. Hysteresis properties of titano-magnetite: grain size and compositional dependence. Physics of the Earth and Planetary Interiors 13, 260-267.

Dumberry, M., Finlay, C.C., 2007. Eastward and westward drift of the Earth's magnetic field for the last three millennia. Earth and Planetary Science Letters 254, 146-157.

Dunlop, D.J., Özdemir, Ö., 1997. Rock Magnetism: Fundamentals and Frontiers. Cambridge University Press, Cambridge and New York.

Guyard, H., Chapron, E., St-Onge, G., Anselmetti, F., Arnaud, F., Magand, O., Francus, P., Mélières, M.-.A., 2007. High-altitude varve records of abrupt environmental changes and mining activity over the last 4000 years in the Western French Alps (Lake Bramant, Grandes Rousses Massif). Quaternary Science Reviews 26, 2644-2660.

Hagstrum, J.T., Champion, D.E., 2002. A Holocene paleosecular variation record from 14C-dated volcanic rocks in western North America. Journal of Geophysical Research 107, 1-14.

Hillaire-Marcel, C., 2008. Decadal- to millennial-scale variability of Arctic-Subarctic oceans and adjacent lands: a contribution of the Polar Climate Stability Network of Canada to the International Polar Year. Canadian Journal of Earth Sciences 45, 1199-1201.

Hughen, K.A., Baillie, M.G.L., Bard, E., Bayliss, A., Beck, J.W, Bertrand, C.J.H., et al., 2004. Marine04 Marine radiocarbon age calibration, 0-26 Cal Kyr BP. Radiocarbon 46, 1059-1086.

Keigwin, L.D., Donnelly, J.P., Cook, M.S., Driscoll, N.W., Brigham-Grette, J., 2006. Rapid sea-level rise and Holocene climate in the Chukchi Sea. Geology 34, 861-864.

King, J.W., Banerjee, S.K., Marvin, J., 1983. A new rock-magnetic approach to selecting sediments for geomagnetic paleointensity studies: application to paleointensity for the last 4000 years. Journal of Geophysical Research 88, 5911-5921.

Kirschvink, J.L., 1980. The least-squares line and plane and the analysis of paleomagnetic data. Geophysical Journal of the Royal Astronomical Society 62, 699-718.

Korte, M., Constable, C.G., 2005. Continuous geomagnetic field models for the past 7 millennia: 2. CALS7K. Geochem. Geophys. Geosyst. 6, Q02H16, doi:10.1029/2004GC000801.

Korte, M., Genevey A., Constable, C.-G., Frank, U., Schnepp, E., 2005. Continuous geomagnetic field models for the past 7 millennia: 1. A new global data compilation, Geochem. Geophys. Geosyst. 6, Q02H15, doi:10.1029/ 2004GC000800.

Korte, M., Mandea, M., 2008. Magnetic poles and dipole tilt variation over the past decades to millennia. Earth Planets Space 60, 937-948.

Ledu, D., Rochon, A., de Vernal, A., St-Onge, G., 2008. Palynological evidence of Holocene climate oscillations in the Eastern Arctic: a possible shift in the Arctic Oscillation at the millennial time scale. Canadian Journal of Earth Sciences 45, 1363-1375.

Ledu, D., Rochon, A., de Vernal, A., St-Onge, G., accepted. Holocene paleoceanography of the Northwest Passage, Canadian Arctic Archipelago: the possible onset of an Arctic Oscillation climate mode. Quaternary Science Reviews.

Lisé-Pronovost, A., St-Onge, G., Brachfeld, S., Barletta, F., Darby, D., 2009. Paleomagnetic constraints on the Holocene stratigraphy of the Arctic Alaskan margin. Global and Planetary Change 68, (1-2), 85-99.

Mazaud, A., 2005. User-friendly software for vector analysis of the magnetization of long sediment cores. Geochem. Geophys. Geosyst. 6, doi:10.1029/2005GC001036.

McKay, J.L., de Vernal, A., Hillaire-Marcel, C., Not, C., Polyak, L., Darby, D., 2008. Holocene fluctuations in Arctic sea-ice cover: Dinocyst-based reconstructions for the eastern Chukchi Sea. Canadian Journal of Earth Sciences 45, 1377-1397.

McNeely, R., Dyke, A.S., Southon, J.R., 2006. Canadian marine reservoir ages, preliminary data assessment. Open File 5049. Geological Survey Canada, Ottawa.

Newitt, L.R., Mandea, M., McKee, L.A., Orgeval, J.-J., 2002. Recent acceleration of the north magnetic pole linked to magnetic jerks. Eos Trans. AGU, 83(35), 381-389.

Peters, C., Thompson, R., 1998. Magnetic identification of selected natural iron oxides and sulfides. Journal of Magnetism and Magnetic Materials 183, 365-374.

Polyak, L., Bischof., J., Ortiz, J.D., Darby, D.A., Channell, J.E.T., Xuan, C., Kaufman, D.S., Løvlie, R., Schneider, D., Adler, R., Council, E., 2009. Late Quaternary stratigraphy and sedimentation patterns in the western Arctic Ocean. Global and Planetary Change 68, 5-17.

Reimer, P.J., Baillie, M.G.L., Bard, E., Bayliss, A., Beck, J.W., Bertrand, C., Blackwell, P.G., Buck, C.E., Burr, G., Cutler, K.B., Damon, P.E., Edwards, R.L., Fairbanks, R.G., Friedrich, M., Guilderson, T.P., Hughen, K.A., Kromer, B., McCormac, F.G., Manning, S., Bronk, Ramsey, C., Reimer, R.W., Remmele, S., Southon, J.R.,

Stuiver, M., Talamo, S., Taylor, F.W., van der Plicht, J., Weyhenmeyer, C.E., 2004. IntCal04 Atmospheric radiocarbon age calibration, 26-0 ka BP. Radiocarbon 46, 1026-1058.

Rochon, A., Scott, D.B., Schell, T.M., Blasco, S., Bennett, R., Mudie, P.J., 2006. Evolution of sea surface conditions during the Holocene: Comparison between Eastern (Baffin Bay and Hudson Strait) and Western (Beaufort Sea) Canadian Arctic. EOS Trans. AGU, 87(52), Fall Meet. Suppl. Abstract U43B-0867.

Sagnotti, L., Rochette P., Jackson, M., Vadeboin, F., Dinarès-Turell, J., Winkler, A., "Mag-Net" Science Team, 2003. Inter-laboratory calibration of low-field magnetic and anhysteretic susceptibility measurements. Physics of the Earth and Planetary Interiors 138, 25-38.

Stoner, J.S., St-Onge, G., 2007. Magnetic stratigraphy in paleoceanography: reversals, excursions, paleointensity and secular variation. In: Proxies in Late Cenozoic Paleoceanography. C. Hillaire-Marcel and A. de Vernal (Eds.), Elsevier, pp. 99-137.

St-Onge, G., Mulder, T., Francus, P., Long, B., 2007. Continuous physical properties of cored marine sediments. Developments in Marine Geology, Volume 1, doi: 10.1016/S1572-5480(07)01007-X.

St-Onge, G., Stoner, J.S., Hillaire-Marcel, C., 2003. Holocene paleomagnetic records from the St. Lawrence Estuary: centennial- to millennial-scale geomagnetic modulation of cosmogenic isotopes. Earth and Planetary Science Letters 209, 113-130.

Stuiver, M., Polach, H.A., 1977. Discussion: Reporting of 14C data. Radiocarbon 19, 355-363.

Stuiver, M., Reimer, P.J., Reimer, R.W., 2005. CALIB 5.0. Available from http://radiocarbon.pa.qub.ac.uk/calib/.

Sugiura, N., 1979. ARM, TRM, and magnetic interactions: concentration dependence. Earth and Planetary Science Letters 42, 451-455.

Tauxe, L., 1993. Sedimentary records of relative paleointensity: theory and practice. Reviews of Geophysics 31, 319-354.

Turner, G.M., 1987. A 5000 year geomagnetic paleosecular variation record from western Canada. Geophysical Journal International 91 (1), 103-121.

Weeks, R., Laj, C., Endignoux, L., Fuller, M., Roberts, A., Manganne, R., Blanchard, E., Goree, W., 1993. Improvements in long-core measurement techniques: applications in palaeomagnetism and palaeoceanography. Geophysical Journal International 114, 651-662.

Xuan, C., Channell, J.E.T., 2010. Origin of apparent magnetic excursions in deep-sea sediments from Mendeleev-Alpha Ridge, Arctic Ocean. Geochem. Geophys. Geosyst. 11, Q02003, doi:10.1029/2009GC002879.

Zijderveld, J.D.A., 1967. AC demagnetization of rock: analysis of results. In: Methods in Paleomagnetism. Collinson, D.W., Creer, K.M., Runcorn, S.K. Elsevier (Eds), Amsterdam, pp. 254-286.

DISCUSSION GÉNÉRALE

Pendant les derniers ~9000 ans, des variations séculaires de l'inclinaison et de déclinaison magnétique ont été observées dans les séquences sédimentaires 803 et 05 (Mer de Beaufort et Chukchi, respectivement; Fig. 1A, annexe) ainsi que dans d'autres enregistrements de haute résolution provenant de milieux différents (lacs et laves volcaniques; Fig. 1B, annexe) de l'ouest de l'Amérique du Nord (Barletta *et al.*, 2008) confirmant ainsi la possibilité d'utiliser ces enregistrements comme un outil de chronostratigraphie arctique à une échelle spatiale d'au moins 3000 km. Notamment, un minimum marqué de l'inclinaison magnétique, présent dans tous les enregistrements de l'ouest de l'Amérique du Nord à environ 2500 ans a aussi été détecté dans une autre séquence sédimentaire (carotte 650; Fig. 1A, annexe) prélevée au nord-ouest du Plateau du Mackenzie (Mer de Beaufort) grâce à la technique de datation paléomagnétique (Barletta et *al.*, 2009a). Par ailleurs, les séquences sédimentaires de l'ouest de l'Arctique canadien ont fourni le premier enregistrement holocène de la paléointensité relative du CMT dans l'Arctique, mettant en évidence la prépondérance du champ magnétique dipolaire à des échelles temporelles millénaires, voire séculaires (Barletta *et al.*, 2008). Les variations d'orientation et d'intensité du CMT reconstruites à partir de la séquence sédimentaire 05 se sont également révélées utiles pour corroborer la chronologie de deux autres séquences sédimentaires (carottes 06 et 08; Fig.1A, annexe) de la mission HOTRAX recueillies dans la mer de Chukchi (Lisé-Pronovost *et al.*, 2009) tandis que les résultats de l'analyse de la minéralogie magnétique de la séquence sédimentaire 05 (Mer de Chukchi) ont permis

l'identification de greigite (Fe_3S_4) dont les variations reflèteraient les variations de stratification de la colonne d'eau dans la région au cours de l'Holocène (Brachfeld *et al.*, 2009).

En ce qui concerne l'Est canadien (estuaire et golfe du St-Laurent), nous avons fourni une première compilation paléomagnétique (*paleomagnetic stack*) à l'Holocène en utilisant les données paléomagnétiques provenant de six séquences sédimentaires marines (Fig. 2A, annexe; Barletta *et al.*, 2009b) précédemment datées à l'aide de la méthode de datation au radiocarbone (^{14}C). Au cours de l'Holocène, l'inclinaison et la déclinaison magnétique peuvent être corrélées, à des échelles au moins séculaires, à des enregistrements lacustres ou volcaniques de l'Amérique du Nord ainsi que de l'Islande et l'Europe du Nord (Fig. 2B, annexe) suggérant une origine géomagnétique à l'échelle hémisphérique. Par ailleurs, au cours des derniers 10 000 ans, les variations séculaires de paléointensité relative sont également cohérentes avec d'autres enregistrements lacustres de paléointensité en Amérique du Nord ainsi qu'avec les variations dipolaires du CMT dérivées à partir d'enregistrements de paléointensité absolue et indiquent ainsi la prédominance des variations dipolaires au cours des derniers 10 000 ans en Amérique du Nord.

Un point important de cette thèse de doctorat a été l'évaluation des forces et des faiblesses des nouveaux modèles numériques des variations du CMT à l'Holocène. Les estimations fournies grâce au modèle en harmonique sphérique CALS7k.2 (Korte et Constable, 2005) se sont révélées assez satisfaisantes en ce qui concerne la reproduction des courbes de déclinaison et d'inclinaison magnétique dans les deux régions d'étude au cours des dernières 7000 ans. En particulier, la déclinaison magnétique fournie par le

modèle CALS7k.2 s'est révélée utile pour dater de façon relative une séquence sédimentaire (carotte 650; Fig. 1A, annexe) holocène recueillie dans la mer de Beaufort (Barletta *et al.*, 2009a). Ainsi, même si aucun des enregistrements de paléodirection contenus dans la banque de données utilisé par le modèle en Amérique du Nord ne dépasse la latitude de 51°N (Korte *et al.*, 2005a), cette étude a montré que le modèle CALS7k.2 est en mesure de décrire la plupart des variations millénaires d'orientation observées dans l'ouest de l'Arctique Canadien. Cependant, l'estimation de la paléointensité locale produite par le modèle CALS7k.2 semble être moins précise par rapport à l'estimation de paléodirection. En effet, la banque de données de paléointensité utilisée pour construire le modèle est fortement concentrée dans les régions de l'Europe où le nombre d'artéfacts (*e.g.*, céramiques, poterie etc.) est plus élevé (Korte *et al.*, 2005a). Par conséquent, les estimations de paléointensité en Amérique du Nord seraient fortement affectées par la distribution spatiale hétérogène des enregistrements de la banque de données utilisée pour construire le modèle (Barletta *et al.*, 2009b) et par les hypothèses à la base de la procédure d'inversion utilisée pour construire le modèle (Knudsen *et al.*, 2008).

CONCLUSIONS

Ce projet de doctorat a permis d'obtenir des informations sans précédent sur la variabilité séculaire à millénaire du CMT au cours de l'Holocène dans des régions difficilement accessibles. Grâce à notre travail, nous avons comblé un manque important d'informations concernant le CMT aux hautes latitudes. Les enregistrements séculaires de la paléodirection du CMT qui se situent environ à la même latitude géographique sont cohérents à l'échelle régionale voire hémisphérique tandis que les fluctuations millénaires de la paléointensité reflèteraient les variations dipolaires du CMT à ces échelles temporelles. Ces résultats corroborent et étendent les précédentes études sur la variation séculaire paléomagnétique en Amérique du Nord (*e.g.*, Lund, 1996) et dans l'Est canadien (*e.g.*, St-Onge *et al.*, 2003).

La quantité de données que nous avons générée pourra être potentiellement utilisée pour des études de magnétisme environnementale (*e.g.*, Brachfeld *et al.*, 2009), pour améliorer le modèle mathématique CALS7k.2 du CMT (*e.g.*, Korte et Constable, 2006) ainsi qu'à des fins de chronostratigraphie (*e.g.*, Barletta *et al.*, 2008; Lisé-Pronovost *et al.*, 2009; Barletta *et al.*, 2009a; Barletta *et al.*, 2009b), spécialement dans l'Arctique où les reconstitutions paléocéanographiques sont plus compliquées à cause de la rareté du matériel pour la datation. Par exemple, l'ensemble des données produit dans le cadre de cette thèse sur le comportement du champ magnétique terrestre est actuellement en cours d'utilisation pour la création d'une nouvelle génération de modèles sur le comportement du champ au cours des derniers 10 000 ans (M. Korte, communication personnelle).

Par ailleurs, les séries temporelles de déclinaison et inclinaison magnétique obtenues peuvent être analysées à des fins d'analyse statistique du comportement du CMT selon le travail déjà réalisé pour les mesures historiques du champ au cours du dernier siècle (*e.g.*, Barraclough et De Santis, 1997) ainsi que pour calculer le déplacement du pôle Nord géomagnétique (*virtual geomagnetic pole*) afin de mieux comprendre la dynamique du CMT au cours de l'Holocène.

FUTURES ÉTUDES

Les travaux futurs pourraient déterminer le rôle, encore aujourd'hui mal compris, joué par les variations du CMT et le climat de la Terre. Par exemple, des études récentes ont démontré un certain dégrée de corrélation entre les variations d'intensité du dipôle géomagnétique et des traceurs paléoclimatiques régionaux (*e.g.*, $\delta^{18}O$; cernes de croissances des arbres) au cours de l'Holocène suggérant un possible lien entre le climat et le magnétisme terrestre par l'intermédiaire du rayonnement cosmique (*e.g.*, Usoskin *et al.*, 2005; Gallet *et al.*, 2006; Knudsen et Riisager, 2009). Alors, grâce aux données paléomagnétiques obtenues dans le cadre de cette thèse, il serait possible de tester la validité de cette hypothèse qui constitue actuellement une théorie controversée à l'origine des fluctuations climatiques observées au cours de l'Holocène (*e.g.*, Usoskin et Kovaltsov, 2008; Courtillot *et al.*, 2007; Gallet *et al.*, 2006)

RÉFÉRENCES BIBLIOGRAPHIQUES

Une liste exhaustive de références est insérée à la fin de chacun des articles rédigés en anglais.

Barletta, F., St-Onge, G., Channell, J.E.T., Rochon, A., Polyak, L., Darby, D.A, 2008. High-resolution paleomagnetic secular variation and relative paleointensity records from the western Canadian Arctic: implication for Holocene stratigraphy and geomagnetic field behaviour. Canadian Journal of Earth Sciences 45: 1265-1281.

Barletta, F., St-Onge, G., Channell, J.E.T., Rochon, A., 2009a. (In press) Dating of Holocene Western Canadian Arctic sediments by matching paleomagnetic secular variation to a geomagnetic field model. Quaternary Science Reviews, doi: 10.1016/j.quascirev.2010.05.35.

Barletta, F., St-Onge, G., Stoner, J.S., Lajeunesse, P., Locat, J., 2009b. (In press) A high-resolution Holocene paleomagnetic secular variation and relative paleointensity stack from eastern Canada. Earth and Planetary Science Letters, doi: 10.1016/j.epsl.2010.07.038.

Barraclough, D.R., De Santis, A., 1997. Some possible evidence for a chaotic geomagnetic field from observational data. Physics of the Earth and Planetary Interiors 99, 207-220.

Brachfeld, S., Barletta, F., St-Onge, G., Darby, D., Ortiz, J.D, 2009. Impact of diagenesis on the environmental magnetic record from a Holocene sedimentary sequence from the Chukchi-Alaskan margin, Arctic Ocean. Global and Planetary Change 68: 100-114.

Courtillot, V., Gallet, Y., Le Mouël, J.L., Fluteau, F., and Genevey, A., 2006. Are there connections between the Earth's magnetic field and climate? Earth and Planetary Science Letters 253, 328-339.

Creer, K.M., 1981. Long-period geomagnetic secular variations since 12,000 yr BP. Nature 292: 208-212.

Gallet, Y., Genevey, A., Le Goff, M., Fluteau, F., Eshraghi, S.A., 2006. Possible impact of the Earth's magnetic field on the history of ancient civilizations. Earth and Planetary Science Letters 246, 17-26.

Jackson, A., Jonkers, A.R.T., Walker, M.R., 2000. Four centuries of geomagnetic secular variation from historical records. Philosophical Transactions of the Royal Society London A 358, 957-990.

Knudsen, M.F., Riisager, P., Donadini, F., Snowball, I., Muscheler, R., Korhonen, K., Pesonen, L.J., 2008. Variations in the geomagnetic dipole moment during the Holocene and the past 50 kyr. Earth and Planetary Science Letters 272, 319-329, doi: 10.1016/j.epsl.2008.04.048.

Knudsen, M.F., Riisager, P., 2009. Is there a link between Earth's magnetic field and low-latitude precipitation? Geology 37, 71-74, doi: 10.1130/G25238A.1.

Korte, M., Constable, C.G., 2005. Continuous geomagnetic field models for the past 7 millennia: 2. CALS7K. Geochem. Geophys. Geosyst. 6 Q02H16, doi: 10.1029/2004GC000801.

Korte, M., Genevey, A., Constable, C.G., Frank, U., Schnepp, E., 2005a. Continuous geomagnetic field models for the past 7 millennia: 1. A new global data

compilation. Geochem. Geophys. Geosyst. 6, Q02H15, doi: 10.1029/2004GC000800.

Korte, M., Constable, C.G., 2006. Centennial to millennial geomagnetic secular variation. Geophysical Journal International 167: 1-10.

Korte, M., Constable, C.G., 2006a. On the use of calibrated relative paleointensity records to improve millennial-scale geomagnetic field models. Geochem. Geophys. Geosyst. 7, Q09004, doi: 10.1029/2006GC001368.

Ledu, D., Rochon, A., de Vernal, A., St-Onge, G., 2008. Palynological evidence of Holocene climate oscillations in the Eastern Arctic: a possible shift in the Arctic Oscillation at the millennial time scale. Canadian Journal of Earth Sciences 45, 1363-1375.

Ledu, D., Rochon, A., De Vernal, A., Barletta, F., St-Onge, G. Holocene sea-ice history and climate variability along the main axis of the Northwest Passage, Canadian Arctic. Paleoceanography, doi:10.1029/2009PA001817.

Lisé-Pronovost, A., St-Onge, G., Brachfeld, S., Barletta, F., Darby, D., 2009. Paleomagnetic constraints on the Holocene stratigraphy of the Arctic Alaskan margin. Global and Planetary Change 68: 85-99.

Lund, S.P., 1996. A comparison of paleomagnetic secular variation records from North America. Journal of Geophysical Research 101, 8007-8024.

Merrill, R.T., McElhinny, M.W., McFadden, P.L., 1996. The Magnetic Field of the Earth. International Geophysics Series 63. San Diego, CA: Academic Press, 527 pp.

Snowball, I., Muscheler, R., 2007. Palaeomagnetic intensity data: an Achilles heel of solar activity reconstructions. The Holocene 17; 851.

Stern, D.P., 2002. A millennium of geomagnetism. Reviews of geophysics, 40, B1-B30.

St-Onge, G., Stoner, J.S., Hillaire-Marcel, C., 2003. Holocene paleomagnetic records from the St. Lawrence Estuary: centennial- to millennial-scale geomagnetic modulation of cosmogenic isotopes. Earth and Planetary Science Letters 209: 113-130.

Usoskin, I.G., Schuessler, M., Solanki, S.K., Mursula, K., 2005. Solar activity, cosmic rays, and Earth's temperature: A millennium-scale comparison. Journal of Geophysical Research 110, A10102, doi:10.1029/2004JA010946.

Usoskin, I.G., Kovaltsov, G.A., 2008. Cosmic rays and climate of the Earth: Possible connection. C. R. Geosciences 340, 441-450.

Verosub, K.L., Mehringer Jr., P.J., Waterstraat, P., 1986. Holocene secular variation in western North America: paleomagnetic record from Fish Lake, Harney County, Oregon. Journal of Geophysical Research B: Solid Earth, 91: 3609-3623.

ANNEXES

Tableau A.1. Position géographique des séquences sédimentaires analysées provenant de l'Ouest de l'Arctique canadien.

Carottes	Latitude (°N)	Longitude (°W)	Profondeur (m)	Longueur (m)
05	72°51.618'	158°25.26'	410	16,48
803	70°37.976'	135°52.815'	218	5,98
650	71°.18.52'	131°36.98'	246	6,08

Tableau A.2. Position géographique des séquences sédimentaires analysées provenant de l'Est canadien.

Carottes	Latitude (°N)	Longitude (°W)	Profondeur (m)	Longueur (m)
MD99-2220	48°38.32'	68°37.93'	320	51,60
42PC	49°07.193'	67°16.753'	320	7,53
36PC	48°24.031'	69°14.328'	315	6,97
35PC	46°24.5510'	58°53.6800'	380	7,59
CL04-36PC	47°40.2860'	59°59.9850'	544	7,71
37PC	48°20.0110'	61°29.9950'	408	7,90

Fig. 1A.

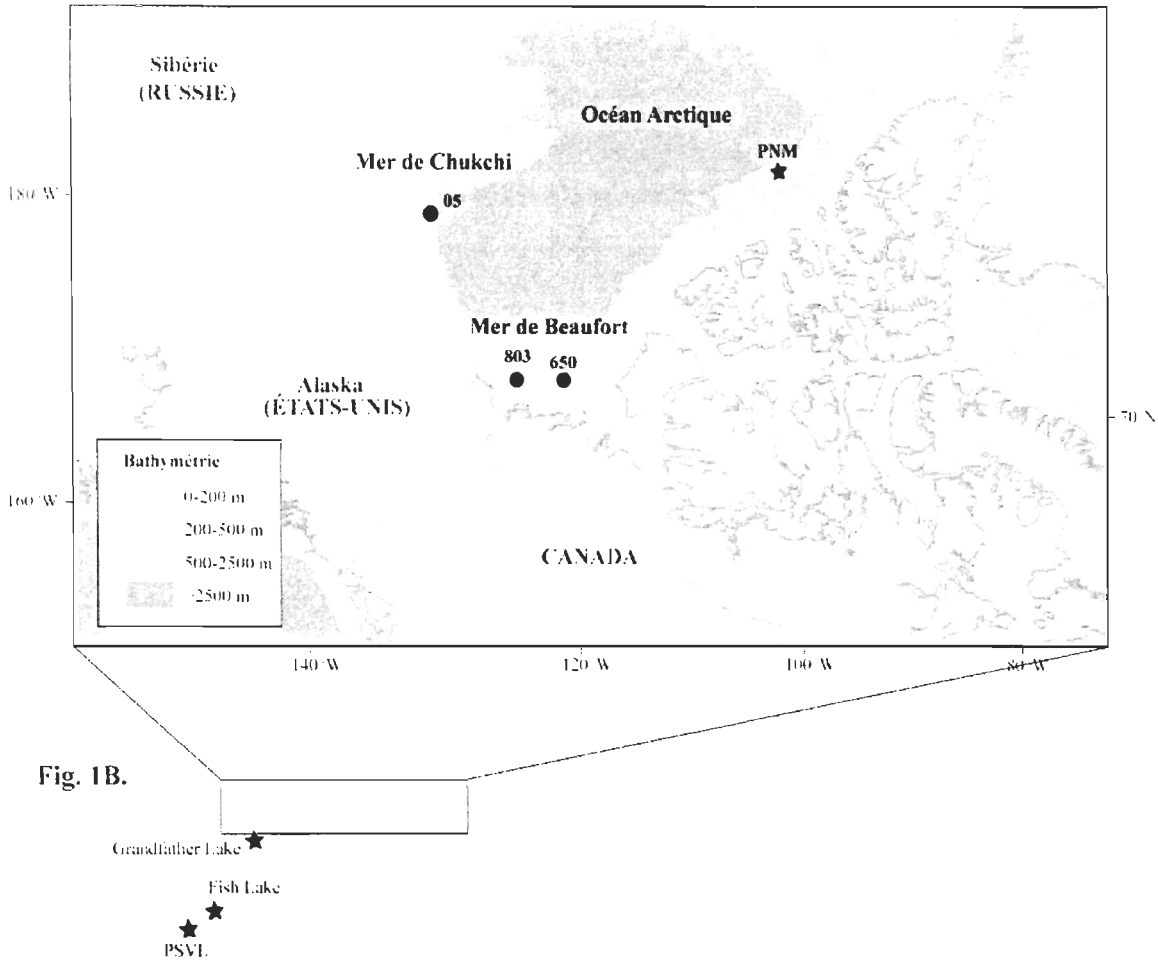
Sibérie
(RUSSIE)
Océan Arctique
Mer de Chukchi
PNM
05
Mer de Beaufort
803
650
Alaska
(ÉTATS-UNIS)
CANADA
Bathymétrie
0-200 m
200-500 m
500-2500 m
>2500 m
180 W
160 W
140 W
120 W
100 W
70 N

Fig. 1B.

Grandfather Lake
Fish Lake
PSVL

Fig. 2A.

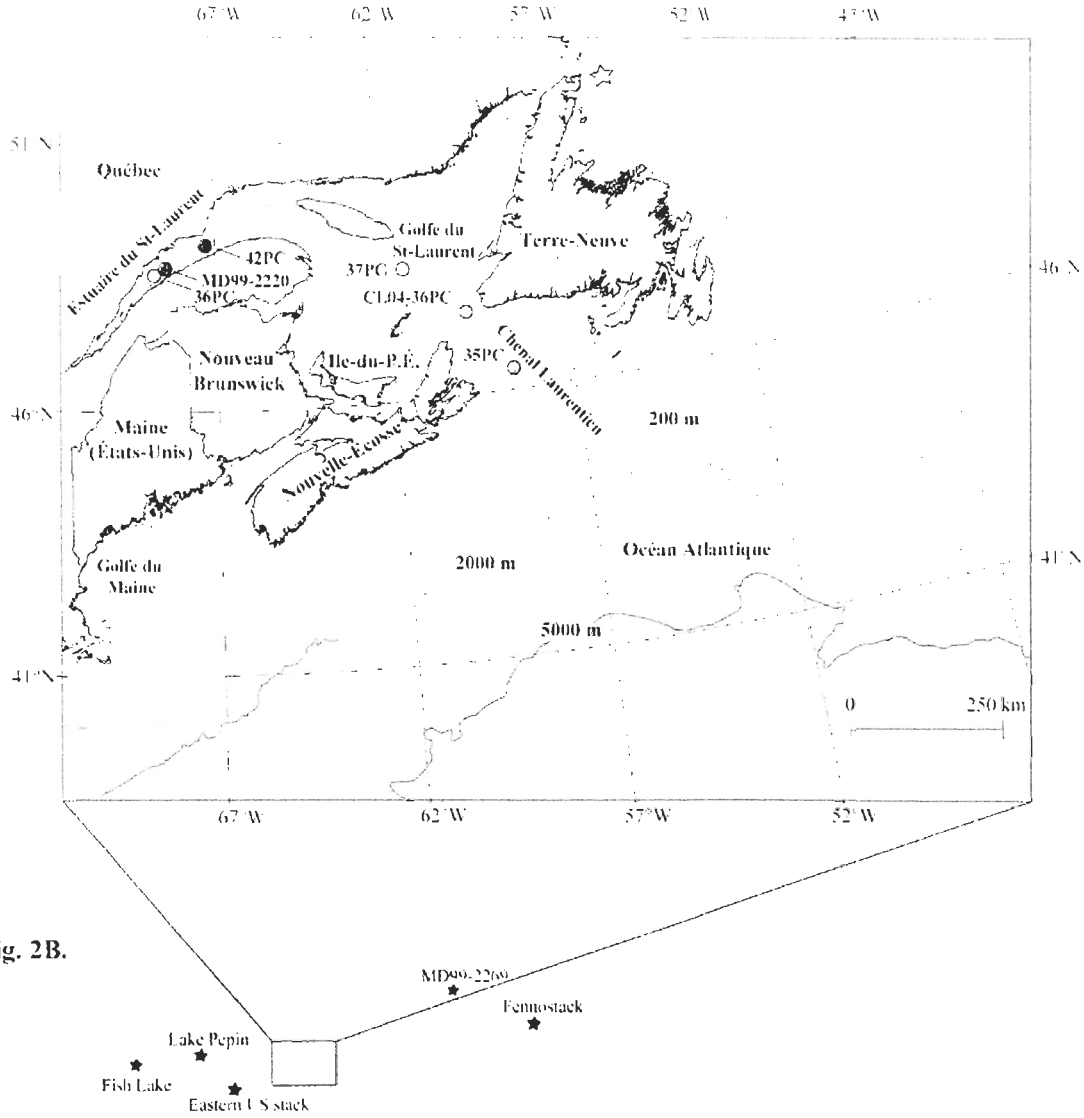
67°W
62°W
57°W
52°W
51°N
Québec
Estuaire du St-Laurent
Golfe du St-Laurent
Terre-Neuve
42PC
MD99-2220
36PC
37PC
CL04-36PC
46°N
Nouveau Brunswick
Île-du-P.É.
35PC
Chenal Laurentien
200 m
Maine (États-Unis)
Nouvelle-Écosse
Golfe du Maine
2000 m
Océan Atlantique
41°N
5000 m
0
250 km

Fig. 2B.

MD99-2269
Fennostack
Lake Pepin
Fish Lake
Eastern U.S stack